

**CHALLENGES TO QUANTUM CHROMODYNAMICS:  
ANOMALOUS SPIN, HEAVY QUARK, AND NUCLEAR PHENOMENA\***

STANLEY J. BRODSKY

Stanford Linear Accelerator Center  
Stanford University, Stanford, California 94309, USA

1. INTRODUCTION

A remarkable claim of theoretical physics is that virtually all aspects of hadron and nuclear physics can be derived from the Lagrangian density of Quantum Chromodynamics (QCD):

$$\mathcal{L}_{QCD} = -\frac{1}{2} \text{Tr} [F^{\mu\nu} F_{\mu\nu}] + \bar{\psi}(i \not{D} - m)\psi$$

$$F^{\mu\nu} = \partial^\mu A^\nu - \partial^\nu A^\mu + ig[A^\mu, A^\nu]$$

$$D^\mu = \partial^\mu + ig A^\mu$$

This elegant expression compactly describes a renormalizable theory of color-triplet spin- $\frac{1}{2}$  quark fields  $\psi$  and color-octet spin-1 gluon fields  $A^\mu$  with an exact symmetry under SU(3)-color local gauge transformations. According to QCD, the elementary degrees of freedom of hadrons and nuclei and their strong interactions are the quark and gluon quanta of these fields. The theory is, in fact, consistent with a vast array of experiments, particularly high momentum transfer phenomena, where because of the smallness of the effective coupling constant and factorization theorems for both inclusive and exclusive processes, the theory has high predictability.<sup>1</sup> (The term "exclusive" refers to reactions in which all particles are measured in the final state.)

The general structure of QCD indeed meshes remarkably well with the facts of the hadronic world, especially quark-based spectroscopy, current algebra, the approximate point-like structure of large momentum transfer inclusive reactions, and the logarithmic violation of scale invariance in deep inelastic lepton-hadron reactions. QCD has

---

\* Work supported by the Department of Energy, contract DE-AC03-76SF00515.

Invited Lectures presented at the 27th International School of Subnuclear Physics:

"The Challenging Questions"

Ettore Majorana Center for Scientific Culture

Erice, Italy, July 26-August 3, 1989

been successful in predicting the features of electron-positron and photon-photon annihilation into hadrons, including the magnitude and scaling of the cross sections, the shape of the photon structure function, the production of hadronic jets with patterns conforming to elementary quark and gluon subprocesses. The experimental measurements appear to be consistent with the basic postulates of QCD, that the charge and weak currents within hadrons are carried by fractionally-charged quarks, and that the strength of the interactions between the quarks and gluons becomes weak at short distances, consistent with asymptotic freedom.

Nevertheless in some very striking cases, the predictions of QCD appear to be in dramatic conflict with experiment:

1. The spin dependence of large angle  $pp$  elastic scattering has an extraordinarily rich structure—particularly at center-of-mass energies  $E_{CM} \simeq 5 \text{ GeV}$ . The observed behavior is quite different than the structureless predictions of perturbative QCD for exclusive processes.
2. QCD predicts a rather novel feature: instead of the traditional Glauber theory of initial and final state interactions, QCD predicts negligible absorptive corrections, i.e. the “color transparency” of high momentum transfer quasi-elastic processes in nuclei. A recent experiment at Brookhaven National Laboratory seems to confirm this prediction, at least at low energies, but the data show, that at the same energy where the anomalous spin correlations are observed in  $pp$  elastic scattering, the color transparency prediction unexpectedly fails.
3. Recent measurements by the European Muon Collaboration of the deep inelastic structure functions on a polarized proton show a number of unexpected features: a strong positive correlation of the up quark spin with the proton, a strong negative polarization of the down quark, and a significant strange quark content of the proton. The EMC data indicate that the net spin of the proton is carried by gluons and orbital angular momentum, rather than the quarks themselves.
4. The  $J/\psi$  and  $\psi'$  are supposed to be simple S-wave  $n=1$  and  $n=2$  QCD bound states of the charm and anti-charm quarks. Yet these two states have anomalously different two-body decays into vector and pseudo-scalar hadrons.
5. The hadroproduction of charm states and charmonium is supposed to be predictable from the simple fusion subprocess  $gg \rightarrow c\bar{c}$ . Recent measurements indicate that charm particles are produced at higher momentum fractions than allowed by the fusion mechanism, and they show a much more complex nuclear dependence than simple additivity in nucleon number predicted by the model.

All of these anomalies suggest that the proton itself is a much more complex object than suggested by simple non-relativistic quark models. Recent analyses of the proton distribution amplitude using QCD sum rules points to highly-nontrivial proton structure. Solutions to QCD in one-space and one-time dimension suggest that the momentum distributions of non-valence quarks in the hadrons have a non-trivial oscillatory structure. The data seems also to be suggesting that the “intrinsic” bound state structure of the proton has a non-negligible strange and charm quark content, in addition to the “extrinsic” sources of heavy quarks created in the collision itself. As we shall see in these lectures, the apparent discrepancies with experiment are not so much a failure of QCD, but rather symptoms of the complexity and richness of the theory. An important tool for analyzing this complexity is the light-cone Fock state representation of hadron wavefunctions, which provides a consistent but convenient framework for encoding the features of relativistic many-body systems in quantum field theory.

## 2. FOCK STATE EXPANSION ON THE LIGHT CONE

A key problem in the application of QCD to hadron and nuclear physics is how to determine the wave function of a relativistic multi-particle composite system. It is not possible to represent a relativistic field-theoretic bound system limited to a fixed number of constituents at a given time since the interactions create new quanta from the vacuum. Although relativistic wave functions can be represented formally in terms of the covariant Bethe-Salpeter formalism, calculations beyond ladder approximation appear intractable. Unfortunately, the Bethe-Salpeter ladder approximation is often inadequate. For example, in order to derive the Dirac equation for the electron in a static Coulomb field from the Bethe-Salpeter equation for muonium with  $m_\mu/m_e \rightarrow \infty$  one requires an infinite number of irreducible kernel contributions to the QED potential. Matrix elements of currents and the wave function normalization also require, at least formally, the consideration of an infinite sum of irreducible kernels. The relative-time dependence of the Bethe Salpeter amplitudes for states with three or more constituent fields adds severe complexities.

A different and more intuitive procedure would be to extend the Schrödinger wave function description of bound states to the relativistic domain by developing a relativistic many-body Fock expansion for the hadronic state. Formally this can be done by quantizing QCD at equal time, and calculating matrix elements from the time-ordered expansion of the  $S$ -matrix. However, the calculation of each covariant Feynman diagram with  $n$ -vertices requires the calculation of  $n!$  frame-dependent time-ordered amplitudes. Even worse, the calculation of the normalization of a bound state wave

function (or the matrix element of a charge or current operator) requires the computation of contributions from all amplitudes involving particle production from the vacuum. (Note that even after normal-ordering, the interaction Hamiltonian density for QED,  $H_I = e : \bar{\psi} \gamma_\mu \psi A^\mu :$ , contains contributions  $b^\dagger d^\dagger a^\dagger$  which create particles from the perturbative vacuum.)

Fortunately, there is a natural and consistent covariant framework, originally due to Dirac,<sup>2</sup> (quantization on the “light front”) for describing bound states in gauge theory analogous to the Fock state in non-relativistic physics. This framework is the light-cone quantization formalism in which

$$\begin{aligned} |\pi\rangle &= |q\bar{q}\rangle \psi_{q\bar{q}}^\pi + |q\bar{q}g\rangle \psi_{q\bar{q}g}^\pi + \dots \\ |p\rangle &= |qqq\rangle \psi_{qqq}^p + |qqqg\rangle \psi_{qqqg}^p + \dots \end{aligned} \tag{1}$$

Each wave function component  $\psi_n$ , etc. describes a state of fixed number of quark and gluon quanta evaluated in the interaction picture at equal light-cone “time”  $\tau = t + z/c$ . Given the  $\{\psi_n\}$ , virtually any hadronic property can be computed, including anomalous moments, form factors, structure functions for inclusive processes, distribution amplitudes for exclusive processes, etc.

The use of light-cone quantization and equal  $\tau$  wave functions, rather than equal  $t$  wave functions, is necessary for a sensible Fock state expansion. It is also convenient to use  $\tau$ -ordered light-cone perturbation theory (LCPTh) in place of covariant perturbation theory for much of the analysis of light-cone dominated processes such as deep inelastic scattering, or large- $p_\perp$  exclusive reactions.

The use of quark and gluon degrees of freedom to represent hadron dynamics seems paradoxical since free quark and gluon quanta have not been observed. Nevertheless, we can use a complete orthonormal Fock basis of free quarks and gluons, color-singlet eigenstates of the free part  $H_0^{QCD}$  of the QCD Hamiltonian to expand any hadronic state at a given time  $t$ . It is particularly advantageous to quantize the theory at a fixed light-cone time  $\tau = t + z/c$  and choose the light-cone  $A^+ = A^0 + A^z = 0$  gauge since the formulation has simple properties under Lorentz transformations, there are no ghost (negative metric) gluonic degrees of freedom, and complications due to vacuum fluctuations are minimized. Thus in  $e^+e^-$  annihilation into hadrons at high energies it is vastly simpler to use the quark and gluon Fock basis rather than the set of  $J = 1$ ,  $J_z = 1$ ,  $Q = 0$  multi-particle hadronic basis to represent the final state. Notice that the complete hadronic basis must include gluonium and other hadronic states with exotic quantum numbers. Empirically, the perturbative QCD calculations

of the final state based on jets or clusters of quarks and gluons have been shown to give a very successful representation of the observed energy and momentum distributions.

Since both the hadronic and quark-gluon bases are complete, either can be used to represent the evolution of a QCD system. For example, the proton QCD eigenstate can be defined in terms of its projections on the free quark and gluon momentum space basis to define Fock wavefunctions; the sum of squares of these quantities then defines the structure functions measured in deep inelastic scattering.

In the case of large momentum transfer exclusive reactions such as the elastic proton form factor, the state formed immediately after the hard collision is most simply described as a valence Fock state with the quarks at small relative impact parameter  $b_{\perp} \sim 1/Q$ , where  $Q = p_T$  is the momentum transfer scale. Such a state has a small color-dipole moment and thus can penetrate a nuclear medium with minimal interaction. The small impact parameter state eventually evolves to the final recoil hadron, but at high energies this occurs outside the nuclear volume. Thus quasi-elastic hard exclusive reactions are predicted to have cross sections which are additive in the number of nucleons in the nucleus. This is the phenomenon of “color transparency.” which is in striking contrast to Glauber and other calculations based on strong initial and final state absorption corrections. Alternatively, the small impact state can be represented as a coherent sum of all hadrons with the same conserved quantum numbers. At high energies, the phase coherence of the state can be maintained through the nucleus, and the coherent state can penetrate the nucleus without interaction. This is the dual representation of coherent hadrons which satisfies color transparency.

In these lectures I will discuss a number of recent developments in hadron and nuclear physics which make use of the quark/gluon light-cone Fock representation of hadronic systems. The method of discretized light-cone quantization (DLCQ)<sup>3</sup> provides a numerical method for solving gauge theories in the light-cone Fock basis. Recent results for QCD in one space and one time are presented in Section 36. The most important tool for examining the structure of hadrons is deep inelastic and elastic lepton scattering, especially experiments which use a nuclear target to filter or modify the hadronic state. I also give a brief review of what is known about proton structure in QCD. A new approach to shadowing and anti-shadowing of nuclear structure functions is also presented. The distinction between intrinsic and extrinsic contributions to the nucleon structure function is emphasized.

One of the most important challenges to the validity of the QCD description of proton interactions is the extraordinary sensitivity of high energy large angle proton-proton scattering to the spin correlations of the incident protons. A solution to this

problem based on heavy quark thresholds is described in Section 20. A prediction for a new form of quasi-stable nuclear matter is also discussed.

### 3. SPIN EFFECTS IN DEEP INELASTIC SCATTERING

As noted above, the EMC and SLAC data on polarized structure functions imply significant correlations between the spin of the target proton with the spin of the gluons and strange quarks. Thus there should be significant correlations between the target spin and spin observables in the electroproduction final state, both in the current and target fragmentation region. It is thus important to measure the spin of specific hadrons which are helicity self-analyzing through their decay products such as the  $\rho$  and the  $\Lambda$ .

The gluon distribution of a hadron is usually considered to be derived from QCD evolution of the quark structure functions beginning at a initial scale  $Q_0^2$ . In such a model there are no gluons in the hadron at a resolution scale below  $Q_0$ . The evolution is completely incoherent; i.e. each quark in the hadron radiates independently. In fact, the bound state wavefunction itself generates gluons. This is clear since one can connect the gluon distribution to the transverse part of the bound-state potential. To the extent that gluons generate the binding, they also must appear in the intrinsic gluon distribution. The diagrams in which gluons connect one quark to another are not present in the QCD evolution. The evolution contributions correspond in the bound-state equation to self-energy corrections to the quark lines at resolution scales or invariant mass larger than the scale  $Q_0$ .

It is useful to keep in mind the following simple model for the helicity parallel and helicity anti-parallel gluon distributions in the nucleon:  $G_{g/N}^+(x) = \frac{3}{2}(1-x)^4/x$  and  $G_{g/N}^-(x) = \frac{3}{2}(1-x)^6/x$ , respectively. This model is consistent with the momentum fraction carried by gluons in the proton, correct crossing behavior, dimensional counting rules at  $x \rightarrow 1$ , and Regge behavior at small  $x$ . Integrating over  $x$ , one finds that the gluon carries, on the average, 11/24 of the total nucleon  $J_z$ . It is thus consistent with experiment and the Skryme model prediction that more of the nucleon spin is carried by gluons rather than quarks.<sup>4</sup>

Recently Ivan Schmidt and I<sup>5</sup> have given model forms for the polarized and unpolarized intrinsic gluon distributions similar to the above parameterization in the nucleon which take into account coherence at low  $x$  and perturbative constraints at high  $x$ . It is expected that this should be a good characterization of the gluon distribution at the resolution scale  $Q_0^2 \simeq M_p^2$ . The leading power at  $x \sim 1$  is increased when QCD

evolution is taken into account. The change in power is

$$\Delta p_g(Q^2) = 4C_A \zeta(Q^2, Q_0^2) = \frac{1}{\pi} \int_{Q_0^2}^{Q^2} \frac{d\kappa^2}{\kappa^2} \alpha_s(\kappa^2), \quad (2)$$

where  $C_A = 3$  in QCD.<sup>6</sup> For typical values of  $Q_0 \sim 1 \text{ GeV}$ ,  $\Lambda_{\overline{MS}} \sim 0.2 \text{ GeV}$  the change in power is moderate:  $\Delta p_g(2 \text{ GeV}^2) = 0.28$ ,  $\Delta p_g(10 \text{ GeV}^2) = 0.78$ .

A recent determination of the unpolarized gluon distribution of the proton at  $Q^2 = 2 \text{ GeV}^2$  using direct photon and deep inelastic data has been given in Ref. 7. The best fit over the interval  $0.05 \leq x \leq 0.75$  assuming the form  $xG(x, Q^2 = 2 \text{ GeV}^2) = A(1-x)^{\eta_g}$  gives  $\eta_g = 3.9 \pm 0.11(+0.8 - 0.6)$ , where the errors in parenthesis allow for systematic uncertainties. This result is compatible with our model for the intrinsic gluon distribution, including the increase in power due to evolution.

The analyses of the EMC and SLAC spin-dependent structure functions as well as elastic neutrino-proton scattering imply substantial strange and anti-strange quarks in the proton, highly spin-correlated with the proton spin. The usual description of the strange sea assumes that  $s\bar{s}$  is strictly due to the simple gluon splitting process. However this implies minimal strange quark spin correlations since the strange quark and anti-quark tend to be produced with opposite helicities. Alternatively the strange sea may be “intrinsic” to the bound state equation of motion of the nucleon, and thus the strong strange spin correlation may be a non-perturbative phenomena. One expects contributions at order  $1/m_s^2$  to the strange sea from cuts of strange loops quark loops in the wavefunction with 2, 3, and 4 gluons connecting to the other quark and gluon constituents of the nucleon. Alternatively, one can regard the strange sea as a manifestation of intermediate  $K - \Lambda$  and other virtual meson-baryon pair states in the fluctuations of the proton ground state.

Experiments which examine the entire final state in electroproduction can discriminate between these extrinsic and intrinsic components to the strange sea. For example, consider events in which a strange hadron is observed at large  $z$  in the fragmentation region of the recoil jet, signifying the production and tagging of a strange quark. In the case of intrinsic strangeness, the associated  $\bar{s}$  will be in the target fragmentation region. In the case that the strange quark is created extrinsically via  $\gamma^* g \rightarrow s\bar{s}$ , both the tagged  $s$  quark and the  $\bar{s}$  hadrons will be found predominantly in the current fragmentation region.

The central focus of inelastic electroproduction is the electron-quark interaction, which at large momentum transfer can be calculated as an incoherent sum of individual quark contributions. The deep inelastic electron-proton cross section is thus given by the convolution of the electron-quark cross section times the structure functions, or equivalently the probability distributions  $G_{q/p}(x, Q^2)$ . In the "infinite momentum frame" where the proton has large momentum  $P^\mu$  and the virtual photon momentum is in the transverse direction,  $G_{q/p}(x, Q^2)$  is the probability of finding a quark  $q$  with momentum fraction  $x = Q^2/2p \cdot q$  in the proton. However in the rest frame of the target, many different physical processes occur: the photon can scatter out a quark as in the atomic physics photoelectric effect, it can hit a quark which created from a vacuum fluctuation near the proton, or the photon can first make a  $q\bar{q}$  pair, either of which can interact in the target. Thus the electron interacts with quarks which are both *intrinsic* to the proton's structure itself, or quarks which are *extrinsic*; i.e. created in the electron-proton collision itself. Much of the phenomena at small values of  $x$  such as Regge behavior, sea distributions associated with photon-gluon fusion processes, and shadowing in nuclear structure functions can be identified with the extrinsic interactions, rather than processes directly connected with the proton's intrinsic structure.

There is an amusing, though *gedanken* way to (in principle) separate the extrinsic and intrinsic contributions to the proton's structure functions. For example, suppose that one wishes to isolate the intrinsic contribution  $G_{d/p}^I(x, Q)$  to the d-quark distribution in the proton. Let us imagine that there exists another set of quarks  $\{q_o\} = u_o, d_o, s_o, c_o, \dots$  identical in all respects to the usual set of quarks but carrying zero electromagnetic and weak charges. The experimentalist could then measure the difference in scattering of electrons on protons versus electrons scattering on a new baryon with valence quarks  $|uud_o\rangle$ . This is analogous to an "empty target" subtraction. Contributions from  $q\bar{q}$  pair production in the gluonic field of the target (photon-gluon fusion) effectively cancel, so that one can then identify the difference in scattering with the intrinsic d-quark distribution of the nucleon. Because of the Pauli exclusion principle,  $d\bar{d}$  production on the proton where the  $d$  is produced in the same quantum state as the  $d$  in the nucleon is absent, but the corresponding contribution is allowed in the case of the  $|uud_o\rangle$  target. Because of this extra subtraction, the contributions associated with Reggeon exchange also cancel in the difference, and thus the intrinsic structure function  $G^I(x, Q)$  vanishes at  $x \rightarrow 0$ . The intrinsic contribu-

tion gives finite expectation values for the light-cone kinetic energy operator, “sigma” terms, and the  $J = 0$  fixed poles associated with  $\langle 1/x \rangle$ .<sup>8</sup>

## 5. EXCLUSIVE PROCESSES IN QCD

We now turn to one of the most important areas of investigation in quantum chromodynamics: few-body exclusive reactions initiated by electromagnetic initial states, such as  $e^+e^- \rightarrow H\bar{H}$ ,  $e^+e^- \rightarrow \gamma H$ , and the two-photon processes  $\gamma\gamma \rightarrow H\bar{H}$  shown in Fig. 1. The simplicity of the photon’s couplings to the quark currents and the absence of initial state hadronic interactions allows one to study the process of quark hadronization at its most basic level—the conversion of quarks into just one or two hadrons. In the low energy threshold regime the quarks interact strongly at low relative velocity to form ordinary or exotic resonances:  $q\bar{q}$ ,  $q\bar{q}g$ ,  $qq\bar{q}\bar{q}$ ,  $ggg$ , etc. At high energies, where the quarks must interact at high momentum transfer, a perturbative expansion in powers of the QCD running coupling constant becomes applicable,<sup>9</sup> leading to simple and elegant PQCD predictions. In this domain one tests not only the scaling and form of elementary quark-gluon processes, but also the structure of the hadronic wavefunctions themselves, specifically, the “distribution amplitudes”  $\phi_H(x_i, Q^2)$ , which describe the binding of quarks and gluons into hadrons. Physically,  $\phi_H(x_i, Q)$  is the probability amplitude for finding the valence quarks which carry fractional momenta  $x_i$  at impact separation  $b_i \sim 1/Q$ . The valence Fock state of a hadron is defined at a fixed light-cone time and in light-cone gauge. The  $x_i = (k^0 + k^z)/(P^0 + P^z)$  are the boost-invariant momentum fractions which satisfy  $\sum_i x_i = 1$ . Such wavefunction information is critical not only for understanding QCD from first principles, but also for a fundamental understanding of jet hadronization at the amplitude rather than probabilistic level.

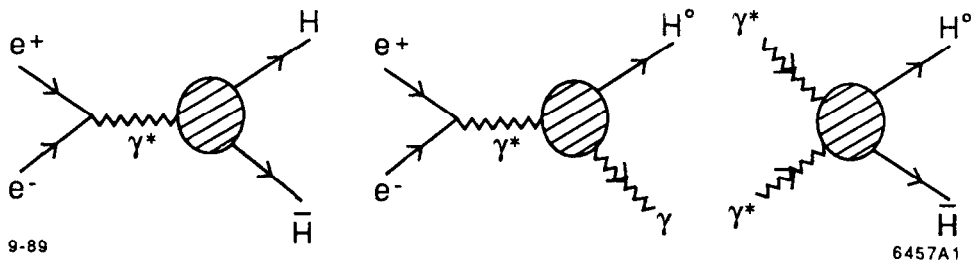


Figure 1. Exclusive processes from  $e^+e^-$  and  $\gamma\gamma$  annihilation.

At large momentum transfer all exclusive scattering reactions in QCD are charac-

terized by the fixed angle scaling law:

$$\frac{d\sigma(AB \rightarrow CD)}{dt} \simeq \frac{F(\theta_{\text{cm}})}{s^N}.$$

To first approximation the leading power is set by the sum of the minimum number of fields entering the exclusive amplitude:  $N = n_A + n_B + n_C + n_D - 2$ , where  $n = 3$  for baryons,  $n = 2$  for mesons, and  $n = 1$  for leptons and photons. This is the dimensional counting law<sup>10</sup> for the leading twist or power-law contribution. The nominal power  $N$  is modified by logarithmic corrections from the QCD running coupling constant, the logarithmic evolution of the hadronic distribution amplitudes, and in the case of hadron-hadron scattering, so-called “pinch” or multiple-scattering contributions, which lead to a small fractional change in the leading power behavior. The recent analysis of Botts and Stermann<sup>11</sup> shows that hard subprocesses dominate large momentum transfer exclusive reactions, even when pinch contributions dominate. The functional form of  $F(\theta_{\text{cm}})$  depends on the structure of the contributing quark-gluon subprocess and the shape of the hadron distribution amplitudes.

Large momentum transfer exclusive amplitudes generally involve the  $L_z = 0$  projection of the hadron’s valence Fock state wavefunction. Thus in QCD, quark helicity conservation leads to a general rule concerning the spin structure of exclusive amplitudes: the leading twist contribution to any exclusive amplitude conserves hadron helicity—the sum of the hadron helicity in the initial state equals that of the final state.

The study of time-like hadronic form factors using  $e^+e^-$  colliding beams can provide very sensitive tests of the QCD helicity selection rule. This follows because the virtual photon in  $e^+e^- \rightarrow \gamma^* \rightarrow h_A h_B$  always has spin  $\pm 1$  along the beam axis at high energies. Angular-momentum conservation implies that the virtual photon can “decay” with one of only two possible angular distributions in the center-of-momentum frame:  $(1 + \cos^2 \theta)$  for  $|\lambda_A - \lambda_B| = 1$ , and  $\sin^2 \theta$  for  $|\lambda_A - \lambda_B| = 0$ , where  $\lambda_{A,B}$  are the helicities of hadron  $h_{A,B}$ . Hadronic-helicity conservation, as required by QCD, greatly restricts the possibilities. It implies that  $\lambda_A + \lambda_B = 2\lambda_A = -2\lambda_B$ . Consequently, angular-momentum conservation requires  $|\lambda_A| = |\lambda_B| = \frac{1}{2}$  for baryons and  $|\lambda_A| = |\lambda_B| = 0$  for mesons; and the angular distributions are now completely determined:

$$\begin{aligned} \frac{d\sigma}{d\cos\theta}(e^+e^- \rightarrow B\bar{B}) &\propto 1 + \cos^2\theta(\text{baryons}), \\ \frac{d\sigma}{d\cos\theta}(e^+e^- \rightarrow M\bar{M}) &\propto \sin^2\theta(\text{mesons}). \end{aligned}$$

It should be emphasized that these predictions are far from trivial for vector mesons and for all baryons. For example, one expects distributions like  $\sin^2\theta$  for baryon pairs

in theories with a scalar or tensor gluon. Simply verifying these angular distributions would give strong evidence in favor of a vector gluon.

In the case of  $e^+e^- \rightarrow H\bar{H}$ , time-like form factors which conserve hadron helicity satisfy the dimensional counting rule:

$$F_H(Q^2) \sim 1/(Q^2)^{N_H-1}.$$

Thus at large  $s = Q^2$ , QCD predicts, modulo computable logarithms,

$$\lambda_B = -\bar{\lambda}_B = \pm \frac{1}{2}, \quad Q^4 F_1^B(Q^2) \rightarrow \text{const.}$$

for baryon pairs, and

$$\lambda_M = \bar{\lambda}_M = 0, \quad Q^2 F^M(Q^2) \rightarrow \text{const}$$

for mesons. Other form factors, such as the Pauli form factor which do not conserve hadron helicity, are suppressed by additional powers of  $1/Q^2$ . Similarly, form factors for processes in which either hadron of the pair is produced with helicity other than  $1/2$  or  $0$  are non-leading at high  $Q^2$ .

In the case of  $e^+e^-$  annihilation into vector plus pseudoscalar mesons, such as  $e^+e^- \rightarrow \rho\pi, \pi\omega$ , and  $KK^*$ , Lorentz invariance requires that the vector meson will be produced transversely polarized. Since this amplitude does not conserve hadron helicity, PQCD predicts that it will be dynamically suppressed at high momentum transfer.

We can see this in more detail as follows: The  $\gamma - \pi - \rho$  can couple through only a single form factor  $-\epsilon^{\mu\nu\tau\sigma} \epsilon_\mu^{(\gamma)} \epsilon_\nu^{(\rho)} p_\tau^{(\pi)} p_\sigma^{(\rho)} F_{\pi\rho}(s)$  — and this requires  $|\lambda_\rho| = 1$  in  $e^+e^-$  collisions. Hadronic-helicity conservation requires  $\lambda = 0$  for mesons, and thus these amplitudes are suppressed in QCD (although, not in scalar or tensor theories). Notice however that the processes  $e^+e^- \rightarrow \gamma\pi, \gamma\eta, \gamma\eta'$  are allowed by the helicity selection rule; helicity conservation applies only to the hadrons. The form factors governing these such processes are not expected to be large, e.g.  $F_{\pi\gamma}(s) \sim 2f_\pi/s$ .

The hadron helicity conservation rule has also been used to explain the observed strong suppression of  $\psi'$  decay to  $\rho\pi$  and  $KK^*$ . However, a puzzle then arises why the corresponding  $J/\psi$  decays are not suppressed. I will review this problem in Section 10.

The predictions of PQCD for the leading power behavior of exclusive amplitudes are rigorous in the asymptotic limit. Analytically, this places important constraints

on the form of the amplitude even at low momentum transfer. For example, Dubnicka and Etim<sup>12</sup> have made detailed predictions for meson and baryon form factors based on vector meson dominance considerations at low energies, and the PQCD constraints in the large space-like and time-like  $Q^2$  domains. (See Fig. 2.)

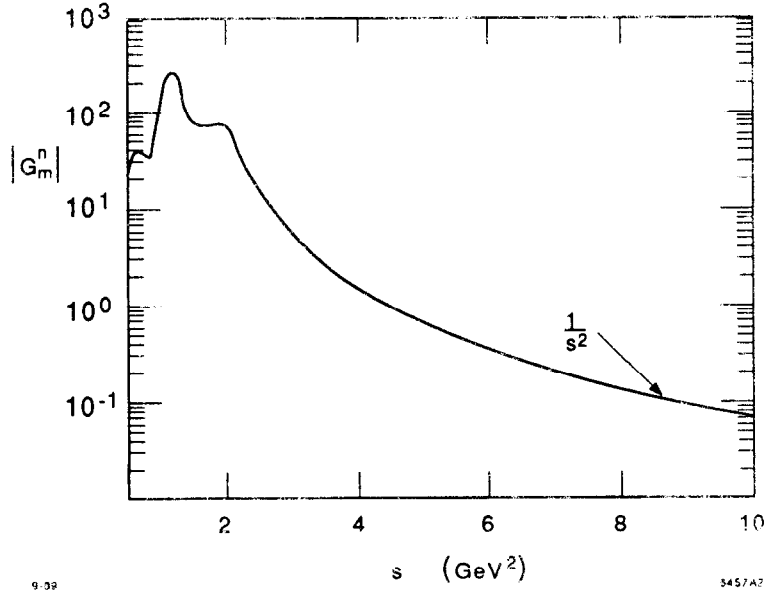


Figure 2. Prediction for the time-like magnetic form factor of the neutron using vector meson dominance and asymptotic PQCD constraints. From Ref. 12.

A central question for the phenomenology of exclusive reactions is the regime of applicability of the leading power-law predictions and the relative size of higher-twist higher power-law contributions. Thus far dimensional counting rules are all in general agreement with experiment at momentum transfers beyond a few  $GeV$ . This appears reasonable since, ignoring heavy quark production, the natural expansion scales of QCD are  $\Lambda_{\overline{MS}}$ , the light quark masses, and the intrinsic transverse momentum in the hadronic wavefunctions. An extensive review of the data is given in Ref. 9.

The recently proposed FENICE experiment at Frascati will provide the first measurements of the time-like neutron form factor and the  $e^+e^-n/\bar{n}$  to  $p\bar{p}$  ratio. A high-luminosity “Tau-Charm Factory” would allow the exploration of a large array of exclusive channels such as  $e^+e^-$  or  $\gamma\gamma \rightarrow p\bar{p}$ ,  $n\bar{n}$ ,  $\Lambda\bar{\Lambda}$ ,  $\pi^+\pi^-$ ,  $K\bar{K}$ ,  $N\bar{N}^*$ ,  $\pi\rho$ ,  $\gamma\pi^0$ , etc., both on and off the charmonium resonances. Many of these channels have not yet been studied experimentally, and measurements will only become practical at luminosities of  $10^{33} \text{ cm}^{-2} \text{ sec}^{-1}$  or greater. At such intensities, corresponding to approximately  $10^8 \mu^+\mu^-$  per year, one can also study *nuclear* final states such as  $e^+e^- \rightarrow \bar{d}np$ . It is

very important to measure the ratio of the neutron and proton form factors to high precision, and to check the angular distribution of the baryon pairs to test the predicted dominance of the helicity conserving Dirac form factor  $F_1$  over the Pauli form factor at large time-like  $Q^2$ .

Since exclusive channels have highly constrained final states of minimal complexity, they are generally distinctive and background-free. In each exclusive channel one tests not only the scaling and helicity structure of the quark and gluon processes, but also features of the distribution amplitude, the most basic measure of a hadron in terms of its valence quark degrees of freedom.

A more detailed review of the two-photon predictions applicable to high luminosity  $e^+e^-$  colliders are given in Section 15 and Ref. 13.

## 6. FACTORIZATION THEOREM FOR EXCLUSIVE PROCESSES

The predictions of QCD for the leading twist contribution to exclusive  $e^+e^-$  and  $\gamma\gamma$  annihilation amplitudes have the general form:

$$M(e^+e^- \rightarrow H\bar{H}) = \int_0^1 \Pi dx_i T_H(x_i, \alpha_s(Q^2)) \phi_H(x, Q) \phi_{\bar{H}}(x, Q).$$

The hard-scattering amplitude  $T_H(e^+e^- \rightarrow q\bar{q}q\bar{q})$  is computed by replacing each hadron with its collinear valence quarks. By definition, the internal integrations in  $T_H$  are restricted to transverse momentum greater than an intermediate scale  $\tilde{Q}$ ; it is thus free of infrared or collinear divergences and it can be expanded systematically in powers of  $\alpha_s(\tilde{Q}^2)$ . The distribution amplitudes are gauge-invariant wavefunctions obtained by integrating the valence Fock State wavefunctions over transverse momentum up to the scale  $\tilde{Q}$ . As in the case of the factorization theorem for inclusive reactions, it is convenient to choose the intermediate renormalization scale  $\tilde{Q}$  to be of order  $Q$  in order to minimize large higher order terms.

The distribution amplitude  $\phi_H(x, Q)$  satisfies an evolution equation in  $\log Q^2$  which sums all logarithms from the collinear integration regime. The solution has the form

$$\phi_H(x_i, Q) = \sum_n a_n^H C_n(x_i) \log^{-\gamma_n} Q^2$$

where the  $C_n$  are known polynomials, the fractional numbers  $\gamma_n$  are computed anomalous dimensions, and the  $a_n^H$  are determined from an initial condition or non-perturbative

input for  $\phi_H(x_i, Q_0)$ . The results for meson pair production are rigorous in the sense that they are proved to all orders in perturbation theory. In the case of baryon pair production, one can use an all-orders resummation to show that the soft region of integration where  $x \sim 1$  is, in fact, Sudakov suppressed.

## 7. ELECTROMAGNETIC FORM FACTORS OF BARYONS

Applying factorization, any helicity-conserving baryon form factor at large space-like or time-like  $Q^2$  has the form: (see Fig. 3)

$$F_B(Q^2) = \int_0^1 [dy] \int_0^1 [dx] \phi_B^\dagger(y_j, Q) T_H(x_i, y_j, Q) \phi_B(x_i, Q),$$

where to leading order in  $\alpha_s(Q^2)$ ,  $T_H$  is computed from  $3q + \gamma^* \rightarrow 3q$  tree graph amplitudes:

$$T_H = \left[ \frac{\alpha_s(Q^2)}{Q^2} \right]^2 f(x_i, y_j)$$

and

$$\phi_B(x_i, Q) = \int [d^2 k_\perp] \psi_V(x_i, \vec{k}_\perp) \theta(k_\perp^2 < Q^2)$$

is the valence three-quark wavefunction evaluated at quark impact separation  $b_\perp \sim \mathcal{O}(Q^{-1})$ . Since  $\phi_B$  only depends logarithmically on  $Q^2$  in QCD, the main dynamical dependence of  $F_B(Q^2)$  is the power behavior  $(Q^2)^{-2}$  derived from the scaling behavior of the elementary propagators in  $T_H$ .

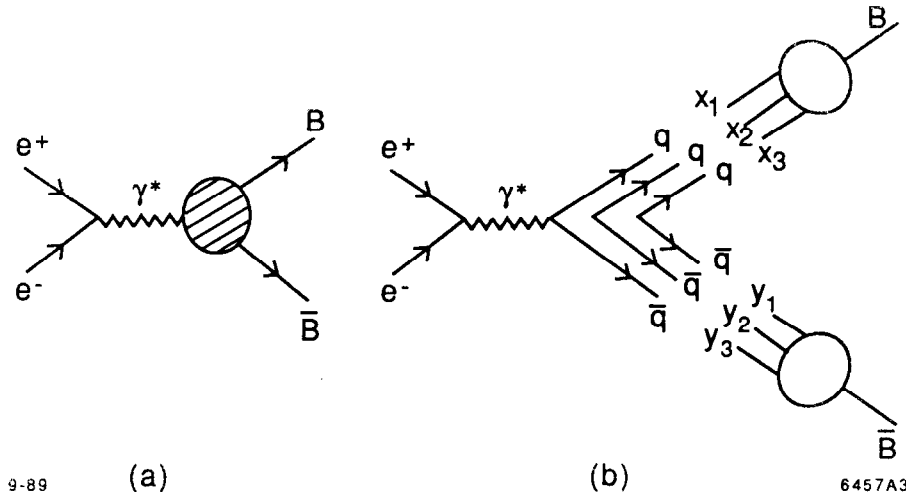


Figure 3. Calculation of the time-like baryon form factor from PQCD factorization.

More explicitly, the proton's magnetic form factor has the form:<sup>14</sup>

$$G_M(Q^2) = \left[ \frac{\alpha_s(Q^2)}{Q^2} \right]^2 \sum_{n,m} a_{nm} \left( \log \frac{Q^2}{\Lambda^2} \right)^{-\gamma_n - \gamma_m} \\ \times \left[ 1 + \mathcal{O}(\alpha_s(Q)) + \mathcal{O}\left(\frac{1}{Q}\right) \right].$$

The first factor, in agreement with the quark counting rule, is due to the hard scattering of the three valence quarks from the initial to final nucleon direction. Higher Fock states lead to form factor contributions of successively higher order in  $1/Q^2$ . The logarithmic corrections derive from an evolution equation for the nucleon distribution amplitude. The  $\gamma_n$  are the computed anomalous dimensions, reflecting the short distance scaling of three-quark composite operators. The results hold for any baryon to baryon vector or axial vector transition amplitude that conserves the baryon helicity. Helicity non-conserving form factors should fall as an additional power of  $1/Q^2$ .<sup>15</sup> Measurements<sup>16</sup> of the transition form factor to the  $J = 3/2$   $N(1520)$  nucleon resonance are consistent with  $J_z = \pm 1/2$  dominance, as predicted by the helicity conservation rule.<sup>15</sup> A review of the data on spin effects in electron nucleon scattering in the resonance region is given in Ref. 16. The FENICE experiment and a Tau-Charm factory could provide measurements on the whole range of baryon pair production processes, including hyperon production, isobar production, etc.

An essential question for the interpretation of such experiments is the scale of momentum transfer where leading-twist PQCD contributions dominate exclusive amplitudes.

The perturbative scaling regime of the meson form factor and  $\gamma\gamma \rightarrow M\bar{M}$  amplitudes is primarily controlled by the virtuality of the hardest quark propagator— if the quark is far off-shell, multiple gluon exchange contributions involving soft gluon insertions are suppressed by inverse powers of the quark propagator. Thus non-leading twist contributions are suppressed by powers of  $\mu^2 / \langle (1-x)Q^2 \rangle$ , where  $\mu^2$  is a typical hadronic scale. Physically, there is not sufficient time to exchange soft gluons or gluonium. Thus the perturbative analysis is valid as long as the single gluon exchange propagator can be approximated by inverse power behavior  $D(k^2) \propto 1/k^2$ . The gluon virtuality  $\langle (1-x)(1-y)Q^2 \rangle$  thus needs to be larger than a small multiple of  $\Lambda_{\overline{MS}}^2$ . This allows the PQCD predictions to start to be valid at  $Q^2$  of order a few  $GeV^2$ , which is consistent with data.

However, the normalization of the leading twist predictions may be strongly affected by higher corrections in  $\alpha_s(Q^2)$ . A similar situation occurs in time-like inclusive

reactions, such as massive pair production, where large  $K$  factors occur. Thus at this time normalization predictions for exclusive amplitudes cannot be considered decisive tests of PQCD.<sup>9</sup>

The predictions for the leading twist contributions to the magnitude of the proton form factor are sensitive to the  $x \sim 1$  dependence of the proton distribution amplitude,<sup>17</sup> particularly if one assumes the validity of the strongly asymmetric QCD sum rule forms for distribution amplitude. Chernyak, et al.<sup>18</sup> have found, however, that their QCD sum rule predictions are not significantly changed when higher moments of the distribution amplitude are included. In the analysis of Ref. 19 it was argued that only a small fraction of the proton and pion form factor normalization at experimentally accessible momentum transfer comes from regions of integration in which all the propagators are hard. However, a new analysis by Dziembowski, et al.<sup>20</sup> shows that the QCD sum rule distribution amplitudes of Chernyak, et al.<sup>21</sup> together with the perturbative QCD prediction gives contributions to the form factors which agree with the measured normalization of the pion form factor at  $Q^2 > 4 \text{ GeV}^2$  and proton form factor  $Q^2 > 20 \text{ GeV}^2$  to within a factor of two. In this calculation the virtuality of the exchanged gluon is restricted to  $|k^2| > 0.25 \text{ GeV}^2$ . The authors assume  $\alpha_s = 0.3$  and that the underlying wavefunctions fall off exponentially at the  $x \simeq 1$  endpoints. Another model of the proton distribution amplitude with di-quark clustering<sup>22</sup> chosen to satisfy the QCD sum rule moments come even closer. Considering the uncertainty in the magnitude of the higher order corrections, one cannot expect better agreement between the QCD predictions and experiment.

Measurements of rare exclusive processes are essential for testing the PQCD predictions and for placing constraints on hadron wavefunctions. However, the relative importance of non-perturbative contributions to form factors clearly remains an important issue. Models can be constructed in which non-perturbative effects persist to high  $Q$ .<sup>19</sup> In other models, which are explicitly rotationally invariant,<sup>23</sup> such effects vanish rapidly as  $Q$  increases.<sup>24,25,26,27</sup> The resolution of such uncertainties will require better understanding of the non-perturbative wave-function and the role played by Sudakov form factors in the end-point region. In the case of elastic hadron-hadron scattering amplitudes, the recent analysis of Botts and Serman<sup>11</sup> shows that, because of Sudakov suppression, even pinch contributions are dominated by hard gluon exchange subprocesses.

If the QCD sum rule results are correct, then hadrons have highly structured momentum-space valence wavefunctions. In the case of mesons, the results from both the lattice calculations and QCD sum rules show that the pion and other pseudo-scalar

mesons have a dip structure at zero relative velocity their distribution amplitude— the light quarks in hadrons are highly relativistic. This gives further indication that while nonrelativistic potential models are useful for enumerating the spectrum of hadrons (because they express the relevant degrees of freedom), they may not be reliable in predicting wavefunction structure.

## 8. SUPPRESSION OF FINAL STATE INTERACTIONS

In general, one expects exclusive amplitudes to be complicated by strong hadronic final state interactions. For example, the intermediate process  $e^+e^- \rightarrow p\bar{p}$  shown in Fig. 4 leads by charged pion exchange to a contribution to neutron pair production  $e^+e^- \rightarrow n\bar{n}$ . Such final-state interactions corrections to the time-like neutron form factor correspond to higher Fock contributions of the neutron wavefunction. By dimensional power counting, such terms are suppressed at large  $Q^2$  by at least two powers of  $1/Q^2$ . Thus final state interactions are dynamically suppressed in the high momentum transfer domain.

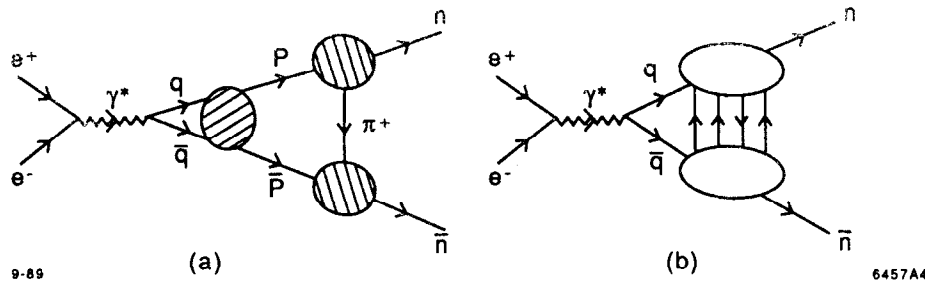


Figure 4. Illustration of a final-state interaction correction to the time-like neutron form factor. As shown in (b), the meson exchange contributions correspond to higher Fock components in the neutron wavefunction and are suppressed at high  $Q^2$ .

Because of the absence of meson exchange and other final state interactions, the perturbative QCD predictions for the time-like baryon form factors are relatively uncomplicated, and directly reflect the coupling of the virtual photon to the quark current. For example, in the case of the ratio of nucleon magnetic form factors  $G_M^n(Q^2)/G_M^p(Q^2)$ , the ratio of quark charges  $e_d/e_u = -1/2$  is the controlling factor. Various model wavefunctions have been proposed to describe the nucleon distribution amplitudes. In the case of the QCD sum rule wavefunction calculated by Chernyak, Ogloblin, and Zhitnitskii, the neutron to proton form factor ratio is predicted to be -0.47 because of the strong dominance at large light-cone momentum fraction  $x$  of the  $u$  quark which has its helicity aligned with of the helicity of the proton. An alternative model given

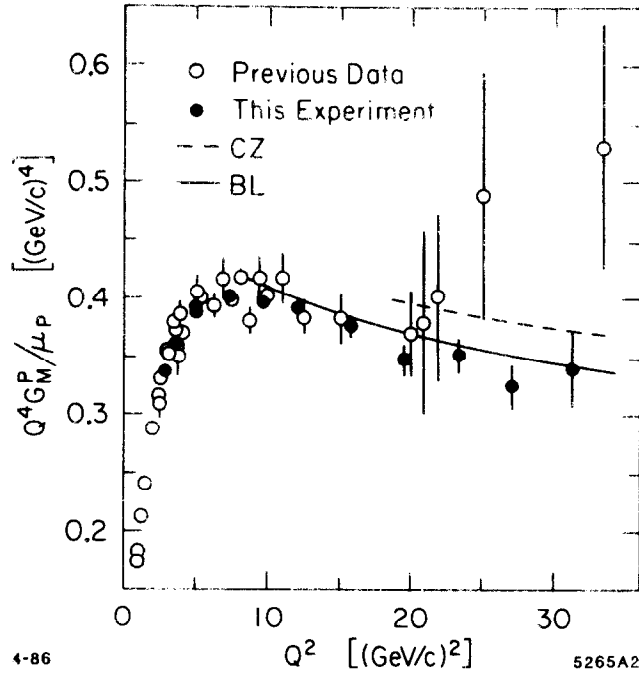


Figure 5. Comparison of the scaling behavior of the proton magnetic form factor with the theoretical predictions of Refs. 14 and 21. The slow fall-off is mainly due to the QCD running coupling constant. The CZ predictions<sup>21</sup> are normalized in sign and magnitude. The data are from Ref. 28.

by Gary and Stefanis gives a much smaller ratio:  $-0.10$ . Both the COZ and GS model forms for  $\phi_p(x_i, Q)$  taken together with the PQCD factorization formula can account for the magnitude and sign of the proton form factor at large space-like  $Q^2$ :  $Q^4 G_M^p(Q^2) = 0.95 \text{ GeV}^4$  for COZ and  $1.18 \text{ GeV}^4$  for GS. (See Fig. 5.) Experimentally  $Q^4 G_M^p(Q^2) \approx 1.0 \text{ GeV}^4$  for  $10 < Q^2 < 30 \text{ GeV}^2$ . These QCD sum rule predictions assume a constant value for the effective running coupling constant,  $\alpha_s(\tilde{Q}^2) = 0.3$ . The validity of such predictions for the absolute normalization of form factors is thus in considerable doubt, particularly because of the many uncertainties from higher order corrections. Still it should be noted that the predictions of the general magnitude and sign is non-trivial. For example, a “non-relativistic” nucleon distribution amplitude proportional to  $\delta(x_1 - 1/3)\delta(x_2 - 1/3)$  gives  $Q^4 G_M^p(Q^2) = -0.3 \times 10^{-2}$ .

In the case of the inverse process,  $\bar{p}p \rightarrow e^+e^-$ , initial state interactions are suppressed. It is interesting to consider the consequences of this PQCD prediction if the  $\bar{p}p$  annihilation occurs inside a nucleus, as in the quasi-elastic reaction  $\bar{p}A \rightarrow e^+e^-(A-1)$ . The absence of initial state interactions implies that the reaction rate for exclusive annihilation in the nucleus will be additive in the number of protons  $Z$ . This is the prediction of “color transparency.”<sup>29</sup> In general, this novel feature of large momentum quasi-elastic processes in nuclei is a consequence of the small color dipole moment of

the hadronic state entering the exclusive amplitude. Even in the case of hadronic scattering such as  $pp \rightarrow p\bar{p}$  where pinch contributions are important, one can show<sup>11</sup> that the impact separation of the quarks entering the subprocess is small, almost of order  $1/Q$  so that color transparency is a universal feature of the PQCD predictions.

An important test of color transparency was recently made at BNL through measurements of the nuclear dependence of quasi-elastic large angle  $pp$  scattering in nuclei. Conventional analysis of the absorptive initial and final state interactions predict that only  $\sim 15\%$  of the protons are effective scatters in large nuclei. The results for various energies up to  $E_{\text{cm}} = 5 \text{ GeV}$  show that the effective fraction of protons  $Z_{\text{eff}}/Z$  rises monotonically with momentum transfer to about 0.5, as predicted by PQCD color transparency, contrary to the conventional Glauber analyses. However, at  $E_{\text{cm}} \sim 5 \text{ GeV}$ , normal absorption was observed, contrary to the PQCD predictions. This unexpected and anomalous behavior, as well as the sharp features observed in the spin correlation  $A_{NN}$  seen in large angle  $pp$  scattering at the same energy could be due to a resonance or threshold enhancement at the threshold for open charm production.<sup>30</sup> Further discussion is given in Section 20.

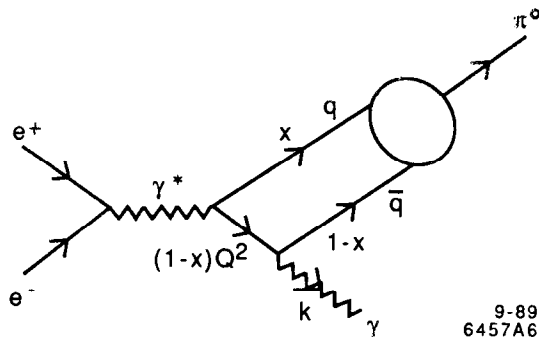


Figure 6. Illustration of the leading PQCD contribution to the  $\gamma^* \rightarrow \pi^0 \gamma$  time-like form factor.

## 9. THE $\gamma\pi_0$ TRANSITION FORM FACTOR

The most elementary exclusive amplitude in QCD is the photon-meson transition form factor  $F_{\gamma\pi^0}(Q^2)$ , since it involves only one hadronic state. As seen from the structure of the diagram in Fig. 6 that the leading behavior of  $F_{\gamma\pi^0}(Q^2)$  at large  $Q^2$  is simply  $1/Q^2$ , reflecting the elementary scaling of the quark propagator at large virtuality. This scaling tests PQCD in exclusive processes in as basic a way as Bjorken scaling in deep inelastic lepton-hadron scattering tests the short distance behavior of QCD in inclusive reactions.

One can easily show that the asymptotic behavior of the transition form factor has the simple form

$$F_{\gamma\pi^0} \propto \frac{1}{Q^2} \int_0^1 \frac{dx}{1-x} \phi_\pi(x, Q)$$

Thus

$$R(e^+e^- \rightarrow \gamma\pi^0) \propto \alpha \left| \int_0^1 \frac{dx}{1-x} \phi_\pi(x, Q) \right|^2 \sim 10^{-4}$$

at  $Q^2 = 10 \text{ GeV}^2$ . Detailed predictions are given in Ref. 9. Furthermore, the ratio of the pion form factor to the square of the  $F_{\gamma\pi^0}$  transition form factor is directly proportional to  $\alpha_s(Q^2)$ , independent of the pion distribution amplitude. Thus measurements of this ratio at time-like  $Q^2$  will give a new rigorous measure of the running QCD coupling constant.

Higher order corrections to  $F_{\gamma\pi^0}$  from diagrams in which the quark propagator is interrupted by soft gluons are power-law suppressed. If the gluon carries high momentum of order  $Q$ , the corrections are higher order in  $\alpha_s(Q^2)$ . Unlike the meson and baryon form factors, there are no potentially soft gluon propagators in  $T_H$  for this process.

The scaling behavior of the PQCD prediction has recently been checked for the space-like  $\gamma\eta$  and  $\gamma\eta'$  transition form factors. This amplitude was obtained from measurements of tagged two-photon processes  $\gamma^*\gamma \rightarrow \eta$  and  $\eta'$  by the *TPC/γγ* collaboration at PEP. The results, shown in Fig. 13, in Section 15, provide a highly significant test of the PQCD analysis. Similarly, the time-like  $\gamma^* \rightarrow \gamma\pi^0$  measurement would be one of the most fundamental measurements possible at a high luminosity  $e^+e^-$  collider.

## 10. EXCLUSIVE CHARMONIUM DECAYS

The  $J/\psi$  decays into isospin-zero final states through the intermediate three-gluon channel. If PQCD is applicable, then the leading contributions to the decay amplitudes preserve hadron helicity. Thus as in the continuum decays, baryon pairs are predicted to have a  $1+v^2 \cos^2 \theta_{\text{cm}}$  distribution with opposite helicities  $\lambda = -\bar{\lambda} = \pm \frac{1}{2}$ , and mesons with a  $\sin^2 \theta_{\text{cm}}$  distribution and helicity zero.

The calculation of the decay of the  $J/\psi$  to baryon pairs is obtained simply by (1) constructing the hard scattering amplitude  $T_H$  for  $c\bar{c} \rightarrow ggg \rightarrow (q\bar{q})(q\bar{q})(q\bar{q})$  where the final  $qqq$  and  $\bar{q}\bar{q}\bar{q}$  are collinear with the produced baryon and anti-baryon respectively, and (2) convoluting  $T_H$  with  $\phi_B(x_i, \tilde{Q})$  and  $\phi_{\bar{B}}(y_i, \tilde{Q})$ . (See Fig. 7.) The scale  $\tilde{Q}$  is set

by the characteristic momentum transfers in the decay. The  $J/\psi$  itself enters through its wavefunction at the origin which is fixed by its leptonic decay. Assuming a mean value  $\alpha_s = 0.3$ , one predicts  $\Gamma(J/\psi \rightarrow p\bar{p}) = 0.34 \text{ KeV}$  for the recent QCD sum rule distribution amplitude proposed by Chernyak, Ogloblin, and Zhitnitskii. The QCD sum rule form obtained by King and Sachrajda predicts  $\Gamma(J/\psi \rightarrow p\bar{p}) = 0.73 \text{ KeV}$ . Both models for the distribution amplitude together with the PQCD factorization for exclusive amplitudes can account for the magnitude and sign as well as the scaling of the proton form factor at large space-like  $Q^2$ . In contrast a non-relativistic ansatz for the distribution amplitude centered at  $x_i = 1/3$  gives a much smaller rate:  $\Gamma = 0.4 \times 10^{-3} \text{ KeV}$ . The measured rate is  $0.15 \text{ KeV}$ . (Note that the PQCD prediction depends on  $\alpha_s$  to the sixth power. Thus if the mean value of  $\alpha_s = 0.26$ , one finds agreement with the calculated rate for  $J/\psi \rightarrow p\bar{p}$  using the COZ proton distribution amplitude.) The predicted angular distribution  $1 + \cos^2 \theta$  is consistent with published data.<sup>31</sup> This is important evidence favoring a vector gluon, since scalar- or tensor-gluon theories would predict a distribution of  $\sin^2 \theta + O(\alpha_s)$ .

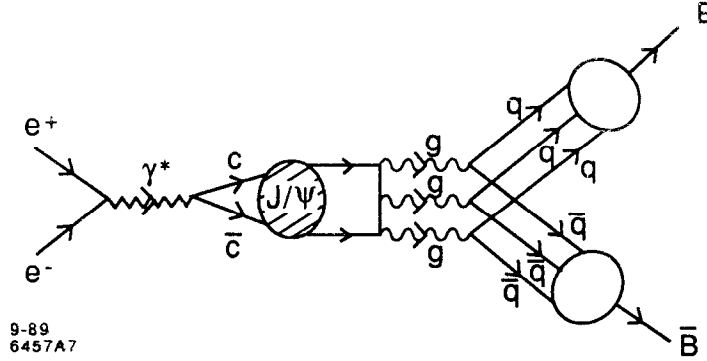


Figure 7. Illustration of the leading PQCD contribution for  $J/\psi$  decay to baryon pairs.

Dimensional-counting rules can also be checked by comparing the  $\psi$  and  $\psi'$  rates into  $p\bar{p}$ , normalized by the total rates into light-quark hadrons so as to remove dependence upon the heavy-quark wave functions. Theory predicts that the ratio of branching fractions for the  $p\bar{p}$  decays of the  $\psi$  and  $\psi'$  is

$$\frac{B(\psi' \rightarrow p\bar{p})}{B(\psi \rightarrow p\bar{p})} \sim Q_{e^+e^-} \left( \frac{M_\psi}{M_{\psi'}} \right)^8,$$

where  $Q_{e^+e^-}$  is the ratio of branching fractions into  $e^+e^-$ :

$$Q_{e^+e^-} \equiv \frac{B(\psi' \rightarrow e^+e^-)}{B(J/\psi \rightarrow e^+e^-)} = 0.135 \pm 0.023$$

Existing data suggest a ratio  $(M_{\psi'}/M_{\psi})^n$  with  $n = 6 \pm 3$ , in good agreement with QCD. One can also use the data for  $\psi \rightarrow p\bar{p}, \Lambda\bar{\Lambda}, \Xi\bar{\Xi}$ , etc. to estimate the relative magnitudes of the quark distribution amplitudes for baryons. Correcting for phase space, one obtains  $\phi_p \sim 1.04(13)\phi_n \sim 0.82(5)\phi_{\Xi} \sim 1.08(8)\phi_{\Sigma} \sim 1.14(5)\phi_{\Lambda}$  by assuming similar functional dependence on the quark momentum fractions  $x_i$  for each case.

As is well known, the decay  $\psi \rightarrow \pi^+\pi^-$  must be electromagnetic if  $G$ -parity is conserved by the strong interactions. To leading order in  $\alpha_s$ , the decay is through a virtual photon (i.e.  $\psi \rightarrow \gamma^* \rightarrow \pi^+\pi^-$ ) and the rate is determined by the pion's electromagnetic form factor:

$$\frac{\Gamma(\psi \rightarrow \pi^+\pi^-)}{\Gamma(\psi \rightarrow \mu^+\mu^-)} = \frac{1}{4}[F_{\pi}(s)]^2[1 + O(\alpha_s(s))],$$

where  $s = (3.1 \text{ GeV})^2$ . Taking  $F_{\pi}(s) \simeq (1 - s/m_{\rho}^2)^{-1}$  gives a rate  $\Gamma(\psi \rightarrow \pi^+\pi^-) \sim 0.0011\Gamma(\psi \rightarrow \mu^+\mu^-)$ , which compares well with the measured ratio 0.0015(7). This indicates that there is indeed little asymmetry in the pion's wave function.

The same analysis applied to  $\psi \rightarrow K^+K^-$  suggests that the kaon's wave function is nearly symmetric about  $x = \frac{1}{2}$ . The ratio  $\Gamma(\psi \rightarrow K^+K^-)/\Gamma(\psi \rightarrow \pi^+\pi^-)$  is  $2 \pm 1$ , which agrees with the ratio  $(f_K/f_{\pi})^4 \sim 2$  expected if  $\pi$  and  $K$  have similar quark distribution amplitudes. This conclusion is further supported by measurements of  $\psi \rightarrow K_L K_S$  which vanishes completely if the  $K$  distribution amplitudes are symmetric; experimentally the limit is  $\Gamma(\psi \rightarrow K_L K_S)/\Gamma(\psi \rightarrow K^+K^-) \lesssim \frac{1}{2}$ .

It is important to test these PQCD and QCD sum rule predictions for the whole array of baryon pairs at both the  $J/\psi$  and  $\psi'$ . These decays give a direct measurement on the relative normalization of moments of the baryon distribution amplitudes. A particularly interesting quantity is the ratio  $\Gamma(J/\psi \rightarrow p\bar{p})/\Gamma(J/\psi \rightarrow n\bar{n})$ . Including the electromagnetic one-photon intermediate state contribution, one then obtains the prediction  $\Gamma(J/\psi \rightarrow p\bar{p})/\Gamma(J/\psi \rightarrow n\bar{n}) = 1.16$ . The present measurements<sup>32</sup> give  $BR(J/\psi \rightarrow p\bar{p}) = 0.22 \pm 0.02\%$  and  $BR(J/\psi \rightarrow n\bar{n}) = 0.18 \pm 0.09\%$ . An important part of the QCD prediction is the electromagnetic decay amplitude controlled by the ratio of time-like form factors near the  $J/\psi$ . Using the QCD sum rule distribution amplitudes obtained by Chernyak and Zhitnitskii, one predicts

$$M_{J/\psi}^4 G_M^p(Q^2 = M_{J/\psi}^2) = 1.1 \text{ GeV}^4$$

$$M_{J/\psi}^4 G_M^n(Q^2 = M_{J/\psi}^2) = -0.55 \text{ GeV}^4,$$

which can be directly checked by measurements off resonance.

## 11. THE $\pi$ - $\rho$ PUZZLE

We have emphasized that a central prediction of perturbative QCD for exclusive processes is hadron helicity conservation: to leading order in  $1/Q$ , the total helicity of hadrons in the initial state must equal the total helicity of hadrons in the final state. This selection rule is independent of any photon or lepton spin appearing in the process. The result follows from (a) neglecting quark mass terms, (b) the vector coupling of gauge particles, and (c) the dominance of valence Fock states with zero angular momentum projection.<sup>15</sup> The result is true in each order of perturbation theory in  $\alpha_s$ .

Hadron helicity conservation appears relevant to a puzzling anomaly in the exclusive decays  $J/\psi$  and  $\psi' \rightarrow \rho\pi, K^*\bar{K}$  and possibly other Vector-Pseudoscalar (VP) combinations. One expects the  $J/\psi$  and  $\psi'$  mesons to decay to hadrons via three gluons or, occasionally, via a single direct photon. In either case the decay proceeds via  $|\Psi(0)|^2$ , where  $\Psi(0)$  is the wave function at the origin in the nonrelativistic quark model for  $c\bar{c}$ . Thus it is reasonable to expect on the basis of perturbative QCD that for any final hadronic state  $h$  that the branching fractions scale like the branching fractions into  $e^+e^-$ :

$$Q_h \equiv \frac{B(\psi' \rightarrow h)}{B(J/\psi \rightarrow h)} \cong Q_{e^+e^-}$$

Usually this is true, as is well documented in Ref. 33 for  $p\bar{p}\pi^0$ ,  $2\pi^+2\pi^-\pi^0$ ,  $\pi^+\pi^-\omega$ , and  $3\pi^+3\pi^-\pi^0$ , hadronic channels. The startling exceptions occur for  $\rho\pi$  and  $K^*\bar{K}$  where the present experimental limits<sup>33</sup> are  $Q_{\rho\pi} < 0.0063$  and  $Q_{K^*\bar{K}} < 0.0027$ .

Perturbative QCD quark helicity conservation implies<sup>15</sup>  $Q_{\rho\pi} \equiv [B(\psi' \rightarrow \rho\pi)/B(J/\psi \rightarrow \rho\pi)] \leq Q_{e^+e^-} [M_{J/\psi}/M_{\psi'}]^6$ . This result includes a form factor suppression proportional to  $[M_{J/\psi}/M_{\psi'}]^4$  and an additional two powers of the mass ratio due to helicity flip. However, this suppression is not nearly large enough to account for the data.

From the standpoint of perturbative QCD, the observed suppression of  $\psi' \rightarrow VP$  is to be expected; it is the  $J/\psi$  that is anomalous.<sup>34</sup> The  $\psi'$  obeys the perturbative QCD theorem that total hadron helicity is conserved in high-momentum transfer exclusive processes. The general validity of the QCD helicity conservation theorem at charmonium energies is of course open to question. An alternative model<sup>35</sup> based on nonperturbative exponential vertex functions, has recently been proposed to account for the anomalous exclusive decays of the  $J/\psi$ . However, helicity conservation has

received important confirmation in  $J/\psi \rightarrow p\bar{p}$  where the angular distribution is known experimentally to follow  $[1 + \cos^2 \theta]$  rather than  $\sin^2 \theta$  for helicity flip, so the decays  $J/\psi \rightarrow \pi\rho$ , and  $K\bar{K}$  seem truly exceptional.

The helicity conservation theorem follows from the assumption of short-range point-like interactions among the constituents in a hard subprocess. One way in which the theorem might fail for  $J/\psi \rightarrow \text{gluons} \rightarrow \pi\rho$  is if the intermediate gluons resonate to form a gluonium state  $\mathcal{O}$ . (See Fig. 8.) If such a state exists, has a mass near that of the  $J/\psi$ , and is relatively stable, then the subprocess for  $J/\psi \rightarrow \pi\rho$  occurs over large distances and the helicity conservation theorem need no longer apply. This would also explain why the  $J/\psi$  decays into  $\pi\rho$  and not the  $\psi'$ .

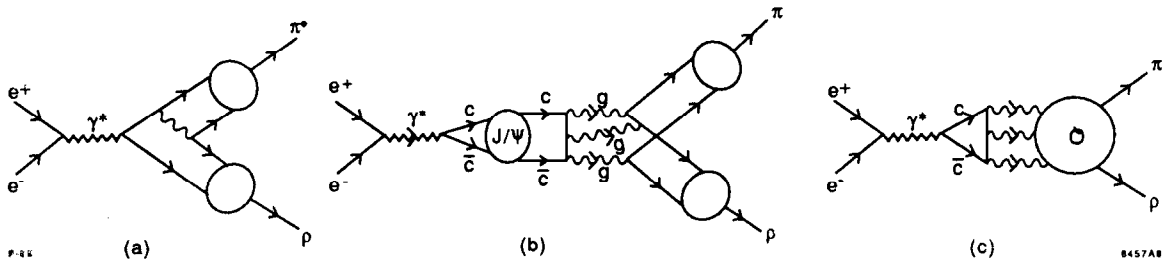


Figure 8. Illustration of QCD contributions for  $J/\psi \rightarrow \rho\pi$ . A non-perturbative contribution due to a gluonium resonance is shown in (c).

Tuan, Lepage, and I<sup>34</sup> have thus proposed, following Hou and Soni,<sup>36</sup> that the enhancement of  $J/\psi \rightarrow K^*\bar{K}$  and  $J/\psi \rightarrow \rho\pi$  decay modes is caused by a quantum mechanical mixing of the  $J/\psi$  with a  $J^{PC} = 1^{--}$  vector gluonium state  $\mathcal{O}$  which causes the breakdown of the QCD helicity theorem. The decay width for  $J/\psi \rightarrow \rho\pi(K^*\bar{K})$  via the sequence  $J/\psi \rightarrow \mathcal{O} \rightarrow \rho\pi(K^*\bar{K})$  must be substantially larger than the decay width for the (non-pole) continuum process  $J/\psi \rightarrow 3 \text{ gluons} \rightarrow \rho\pi(K^*\bar{K})$ . In the other channels (such as  $p\bar{p}$ ,  $p\bar{p}\pi^0$ ,  $2\pi^+2\pi^-\pi^0$ , etc.), the branching ratios of the  $\mathcal{O}$  must be so small that the continuum contribution governed by the QCD theorem dominates over that of the  $\mathcal{O}$  pole. For the case of the  $\psi'$  the contribution of the  $\mathcal{O}$  pole must always be inappreciable in comparison with the continuum process where the QCD theorem holds. The experimental limits on  $Q_{\rho\pi}$  and  $Q_{K^*\bar{K}}$  are now substantially more stringent than when Hou and Soni made their estimates of  $M_{\mathcal{O}}$ ,  $\Gamma_{\mathcal{O} \rightarrow \rho\pi}$  and  $\Gamma_{\mathcal{O} \rightarrow K^*\bar{K}}$  in 1982.

A gluonium state of this type was first postulated by Freund and Nambu<sup>37</sup> based on  $OZI$  dynamics soon after the discovery of the  $J/\psi$  and  $\psi'$  mesons. In fact, Freund and Nambu predicted that the  $\mathcal{O}$  would decay primarily into  $\rho\pi$  and  $K^*\bar{K}$ , with severe suppression of decays into other modes like  $e^+e^-$  as required for the solution of the puzzle.

Branching fractions for final states  $h$  which can proceed only through the intermediate gluonium state have the ratio:

$$Q_h = Q_{e^+e^-} \frac{(M_{J/\psi} - M_{\mathcal{O}})^2 + \frac{1}{4} \Gamma_{\mathcal{O}}^2}{(M_{\psi'} - M_{\mathcal{O}})^2 + \frac{1}{4} \Gamma_{\mathcal{O}}^2}$$

It is assumed that the coupling of the  $J/\psi$  and  $\psi'$  to the gluonium state scales as the  $e^+e^-$  coupling. The value of  $Q_h$  is small if the  $\mathcal{O}$  is close in mass to the  $J/\psi$ . Thus one requires  $(M_{J/\psi} - M_{\mathcal{O}})^2 + \frac{1}{4} \Gamma_{\mathcal{O}}^2 \lesssim 2.6 Q_h \text{ GeV}^2$ . The experimental limit for  $Q_{K^*\bar{K}}$  then implies  $[(M_{J/\psi} - M_{\mathcal{O}})^2 + \frac{1}{4} \Gamma_{\mathcal{O}}^2]^{1/2} \lesssim 80 \text{ MeV}$ . This implies  $|M_{J/\psi} - M_{\mathcal{O}}| < 80 \text{ MeV}$  and  $\Gamma_{\mathcal{O}} < 160 \text{ MeV}$ . Typical allowed values are  $M_{\mathcal{O}} = 3.0 \text{ GeV}$ ,  $\Gamma_{\mathcal{O}} = 140 \text{ MeV}$  or  $M_{\mathcal{O}} = 3.15 \text{ GeV}$ ,  $\Gamma_{\mathcal{O}} = 140 \text{ MeV}$ . Notice that the gluonium state could be either lighter or heavier than the  $J/\psi$ . The branching ratio of the  $\mathcal{O}$  into a given channel must exceed that of the  $J/\psi$ .

It is not necessarily obvious that a  $J^{PC} = 1^{--}$  gluonium state with these parameters would necessarily have been found in experiments to date. One must remember that though  $\mathcal{O} \rightarrow \rho\pi$  and  $\mathcal{O} \rightarrow K^*\bar{K}$  are important modes of decay, at a mass of order 3.1 GeV many other modes (albeit less important) are available. Hence, a total width  $\Gamma_{\mathcal{O}} \cong 100$  to 150 MeV is quite conceivable. Because of the proximity of  $M_{\mathcal{O}}$  to  $M_{J/\psi}$ , the most important signatures for an  $\mathcal{O}$  search via exclusive modes  $J/\psi \rightarrow K^*\bar{K}h$ ,  $J/\psi \rightarrow \rho\pi h$ ;  $h = \pi\pi, \eta, \eta'$ , are no longer available by phase-space considerations. However, the search could still be carried out using  $\psi' \rightarrow K^*\bar{K}h$ ,  $\psi' \rightarrow \rho\pi h$ ; with  $h = \pi\pi$ , and  $\eta$ . Another way to search for  $\mathcal{O}$  in particular, and the three-gluon bound states in general, is via the inclusive reaction  $\psi' \rightarrow (\pi\pi) + X$ , where the  $\pi\pi$  pair is an iso-singlet. The three-gluon bound states such as  $\mathcal{O}$  should show up as peaks in the missing mass (i.e. mass of  $X$ ) distribution.

The most direct way to search for the  $\mathcal{O}$  is to scan  $\bar{p}p$  or  $e^+e^-$  annihilation at  $\sqrt{s}$  within  $\sim 100 \text{ MeV}$  of the  $J/\psi$ , triggering on vector/pseudoscalar decays such as  $\pi\rho$  or  $\bar{K}K^*$ .

The fact that the  $\rho\pi$  and  $K^*\bar{K}$  channels are strongly suppressed in  $\psi'$  decays but not in  $J/\psi$  decays clearly implies dynamics beyond the standard charmonium analysis. The hypothesis of a three-gluon state  $\mathcal{O}$  with mass within  $\cong 100 \text{ MeV}$  of the  $J/\psi$  mass provides a natural, perhaps even compelling, explanation of this anomaly. If this description is correct, then the  $\psi'$  and  $J/\psi$  hadronic decays not only confirm hadron helicity conservation (at the  $\psi'$  momentum scale), but they also provide a signal for bound gluonic matter in QCD.

A major problem, however, for the gluonium explanation of the  $\rho\pi$  puzzle, is the relatively large decay rate recently reported for  $J/\psi \rightarrow \omega\pi^0$ . The published branching ratio is  $0.048 \pm 0.007\%$  approximately three times larger than the  $\pi^+\pi^-$  rate. Both of these  $I = 1$  decays are evidently due to electromagnetic decays, but there is no sign of suppression due to hadron helicity conservation. One possibility is that there are additional  $q\bar{q}g$   $I = 1$  resonances in the 3 GeV mass range which contribute to the  $\omega\pi$  channel. In any event it will be very important to compare these branching ratios at the  $\psi'$  and off resonance.

## 12. TIME-LIKE COMPTON PROCESSES

The high luminosity of a Tau Charm factory can allow the study of the basic Compton amplitude  $M(\gamma^* \rightarrow \pi^+\pi^-\gamma)$  and the related Compton processes. The interference of this amplitude with contributions from diagrams where the photon is emitted from the initial electron or positron will produce a large front-back asymmetry in the  $e^+e^- \rightarrow \pi^+\pi^-\gamma$  process. (See Fig. 9.) We can estimate the event rate from  $R(e^+e^- \rightarrow \pi^+\pi^-\gamma) \sim (\alpha/\pi)F_\pi^2(Q^2) \sim 10^{-4}$  to  $10^{-5}$  which corresponds to  $10^4$  to  $10^3$  events per year at  $10^{33} \text{ cm}^{-2} \text{ sec}^{-1}$  luminosity.

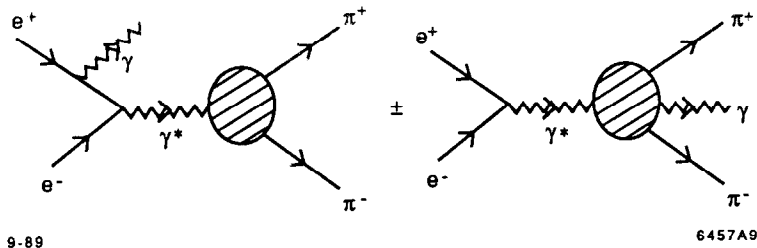


Figure 9. Interfering coherent amplitudes contributing to  $e^+e^- \rightarrow \gamma\pi^+\pi^-$ . This process measures the crossed pion Compton amplitude.

The Compton amplitude on a pion has thus far been studied only in the  $\gamma\gamma \rightarrow \pi^+\pi^-$  reaction. The available Mark II and TPC/ $\gamma\gamma$  data is in reasonable agreement with the leading twist QCD predictions. The QCD analysis predicts simple crossing of the large-angle  $\gamma\gamma \rightarrow \pi^+\pi^-$  amplitude to the  $\gamma^* \rightarrow \pi^+\pi^-\gamma$  amplitude. Extensive predictions are also now available for off-shell photons using PQCD factorization. A critical feature of the predictions is the presence of local two-photon couplings which lead to a dependence on photon mass  $Q$  much less severe than that predicted by vector meson dominance.

### 13. MULTI-HADRON PRODUCTION

A high luminosity  $e^+e^-$  facility could be used for the study of four-baryon exclusive final states and the search for new types of di-baryon states such as the  $H$ , the postulated  $\Lambda\Lambda$  resonance suggested by Jaffe and others. (See Fig. 10.)

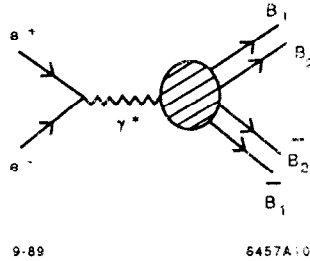


Figure 10. Production of four-baryon states in  $e^+e^-$  annihilation.

Dimensional counting predicts that the cross section for the production of  $N_M$  mesons,  $N_B$  baryons and  $N_{\bar{B}}$  antibaryons at different fixed center of mass solid angle  $\Delta\Omega$  scales as  $\Delta\sigma \propto s^{-2-N_M-2N_B-2N_{\bar{B}}}$ . Thus we can estimate  $R_{e^+e^- \rightarrow B_1 B_2 \bar{B}_1 \bar{B}_2} \sim |F_{B_1}(Q^2/4)F_{B_2}(Q^2/4)|^2$ . The argument of the baryon form factor is  $Q^2/4$  since each baryon is produced with half the available momentum. At  $s = Q^2 = 16 \text{ GeV}^2$ , this corresponds to an annihilation ratio  $R \sim 10^{-4}$ . The production of the  $np\bar{d}$  nuclear final state is further reduced by the probability that the nucleons fuse in a restricted phase space, and thus is suppressed by an additional power of  $1/Q^2$ .

The above estimates are consistent with the "reduced amplitude" formalism for exclusive nuclear processes which has been successful predicting the scaling behavior of the deuteron form factor and the deuteron photo-disintegration cross section at fixed  $\theta_{\text{cm}}$ .

One can thus envision having sufficient luminosity at a  $e^+e^-$  collider to search for the  $H$  di-lambda in the missing mass distribution in the reaction  $e^+e^- \rightarrow \overline{\Lambda\Lambda}X$ . This method can be extended to search for exotic resonances in the  $\Lambda p$ ,  $\Sigma p$  di-baryon systems. The rate for four-meson exclusive channels is considerably larger, and affords the possibility of studying the interactions of di-meson systems such as  $K^+K^+$ . In each case the study of multi-hadron exclusive channels can allow the study of the scattering length and range of hadron-hadron final state interactions.

## 14. HEAVY QUARK EXCLUSIVE STATES AND FORM FACTOR ZEROS IN QCD

The exclusive pair production of heavy hadrons  $|Q_1\bar{Q}_2\rangle$ ,  $|Q_1Q_2Q_3\rangle$  consisting of higher generation quarks ( $Q_i = t, b, c$ , and possibly  $s$ ) can be reliably predicted within the framework of perturbative QCD, since the required wavefunction input is essentially determined from nonrelativistic considerations.<sup>38</sup> The results can be applied to  $e^+e^-$  annihilation,  $\gamma\gamma$  annihilation, and W and Z decay into higher generation pairs. The normalization, angular dependence and helicity structure can be predicted away from threshold, allowing a detailed study of the basic elements of heavy quark hadronization.

It is interesting to test the predictions of QCD factorization for time-like meson form factors for the production of heavy meson pairs, such as  $e^+e^- \rightarrow D\bar{D}$  and  $e^+e^- \rightarrow D_s\bar{D}_s$ .

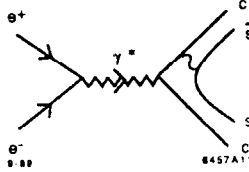


Figure 11. Illustration of the dominant hard scattering diagram for  $D_s\bar{D}_s$  pair production in QCD.

A particularly striking feature of the QCD predictions is the existence of a zero in the form factor and  $e^+e^-$  annihilation cross section for zero-helicity hadron pair production close to the specific time-like value  $q^2/4M_H^2 = m_h/2m_\ell$  where  $m_h$  and  $m_\ell$  are the heavier and lighter quark masses, respectively. This zero reflects the destructive interference between the spin-dependent and spin-independent (Coulomb exchange) couplings of the exchanged gluon shown in Fig. 11; it is thus a novel feature of the gauge theory. In fact, all pseudoscalar meson form factors are predicted in QCD to reverse sign from space-like to time-like asymptotic momentum transfer because of their essentially monopole form. For  $m_h > 2m_\ell$  the form factor zero occurs in the physical region.

In the case of  $e^+e^- \rightarrow D_s\bar{D}_s$  the amplitude vanishes and changes sign at  $Q^2/4M_{D_s}^2 \approx m_c/2m_s$ . Since background terms are expected to be monotonic, an amplitude zero must occur somewhere above threshold in  $e^+e^- \rightarrow D_s\bar{D}_s$ . (See Fig. 12.) The

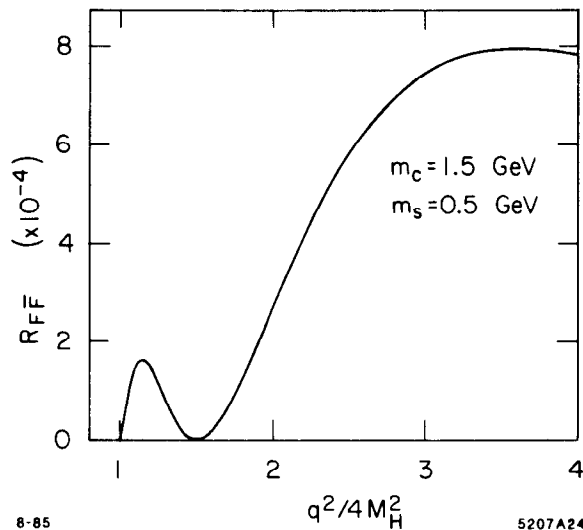


Figure 12. Perturbative QCD prediction<sup>38</sup> for  $R(e^+e^- \rightarrow D_s\bar{D}_s)$ . The normalization depends on assumptions for the  $D_s$  wavefunction.

absolute rate near threshold for this process depends on the wavefunction parameters, particularly the mean square relative velocity of the constituents. We estimate  $R(D_s\bar{D}_s) < 10^{-4}$ .

To leading order in  $1/q^2$ , the production amplitude for hadron pair production is given by the factorized form

$$M_{H\bar{H}} = \int [dx_i] \int [dy_j] \phi_H^\dagger(x_i, \tilde{q}^2) \phi_{\bar{H}}^\dagger(y_j, \tilde{q}^2) T_H(x_i, y_j; \tilde{q}^2, \theta_{CM})$$

where  $[dx_i] = \delta(\sum_{k=1}^n x_k - 1) \prod_{k=1}^n dx_k$  and  $n = 2, 3$  is the number of quarks in the valence Fock state. The scale  $\tilde{q}^2$  is set from higher order calculations, but it reflects the minimum momentum transfer in the process. The main dynamical dependence of the form factor is controlled by the hard scattering amplitude  $T_H$  which is computed by replacing each hadron by collinear constituents  $P_i^\mu = x_i P_H^\mu$ . Since the collinear divergences are summed in  $\phi_H$ ,  $T_H$  can be systematically computed as a perturbation expansion in  $\alpha_s(q^2)$ .

The distribution amplitude required for heavy hadron production  $\phi_H(x_i, q^2)$  is computed as an integral of the valence light-cone Fock wavefunction up to the scale  $Q^2$ . For the case of heavy quark bound states, one can assume that the constituents are sufficiently non-relativistic that gluon emission, higher Fock states, and retardation of the effective potential can be neglected. The quark distributions are then controlled by a simple nonrelativistic wavefunction, which can be taken in the model form:

$$\psi_M(x_i, \vec{k}_{\perp i}) = \frac{C}{x_1^2 x_2^2 \left[ M_H^2 - \frac{\vec{k}_{\perp 1}^2 + m_1^2}{x_1} - \frac{\vec{k}_{\perp 2}^2 + m_2^2}{x_2} \right]^2}$$

This form is chosen since it coincides with the usual Schrödinger-Coulomb wavefunction in the nonrelativistic limit for hydrogenic atoms and has the correct large momentum behavior induced from the spin-independent gluon couplings. The wavefunction is peaked at the mass ratio  $x_i = m_i/M_H$ :

$$\left(x_i - \frac{m_i}{M_H}\right)^2 \sim \frac{\langle k_z^2 \rangle}{M_H^2}$$

where  $\langle k_z^2 \rangle$  is evaluated in the rest frame. Normalizing the wavefunction to unit probability gives

$$C^2 = 128\pi (\langle v^2 \rangle)^{5/2} m_r^5 (m_1 + m_2)$$

where  $\langle v^2 \rangle$  is the mean square relative velocity and  $m_r = m_1 m_2 / (m_1 + m_2)$  is the reduced mass. The corresponding distribution amplitude is

$$\begin{aligned} \phi(x_i) &= \frac{C}{16\pi^2} \frac{1}{[x_1 x_2 M_H^2 - x_2 m_1^2 - x_1 m_2^2]} \\ &\cong \frac{1}{\sqrt{2\pi}} \frac{\gamma^{3/2}}{M_H^{1/2}} \delta\left(x_1 - \frac{m_1}{m_1 + m_2}\right). \end{aligned}$$

It is easy to see from the structure of  $T_H$  for  $e^+e^- \rightarrow M\bar{M}$  that the spectator quark pair is produced with momentum transfer squared  $q^2 x_s y_s = 4m_s^2$ . Thus heavy hadron pair production is dominated by diagrams in which the primary coupling of the virtual photon is to the heavier quark pair. The perturbative predictions are thus expected to be accurate even near threshold to leading order in  $\alpha_s(4m_\ell^2)$  where  $m_\ell$  is the mass of lighter quark in the meson.

The leading order  $e^+e^-$  production helicity amplitudes for higher generation meson ( $\lambda = 0, \pm 1$ ) and baryon ( $\lambda = \pm 1/2, \pm 3/2$ ) pairs are computed in Ref. 38 as a function of  $q^2$  and the quark masses. The analysis is simplified by using the peaked form of the distribution amplitude, Eq. (6). In the case of meson pairs the (unpolarized)  $e^+e^-$

annihilation cross section has the general form<sup>\*</sup>

$$\begin{aligned}
4\pi \frac{d\sigma}{d\Omega} (e^+e^- \rightarrow M_\lambda \bar{M}_{\bar{\lambda}}) &= \frac{3}{4} \beta \sigma_{e^+e^- \rightarrow \mu^+\mu^-} \left[ \frac{1}{2} \beta^2 \sin^2 \theta \right. \\
&\times \left[ |F_{0,0}(q^2)|^2 + \frac{1}{(1-\beta^2)^2} \left\{ (3-2\beta^2+3\beta^4)|F_{1,1}(q^2)|^2 \right. \right. \\
&\left. \left. - 4(1+\beta^2) \operatorname{Re}(F_{1,1}(q^2)F_{0,1}^*(q^2)) + 4|F_{0,1}(q^2)|^2 \right\} \right] \\
&\left. + \frac{3\beta^2}{2(1-\beta^2)} (1+\cos^2 \theta) |F_{0,1}(q^2)|^2 \right]
\end{aligned}$$

where  $q^2 = s = 4M_H^2 \bar{q}^2$  and the meson velocity is  $\beta = 1 - \frac{4M_H^2}{q^2}$ . The production form factors have the general form

$$F_{\lambda\bar{\lambda}} = \frac{\langle v^2 \rangle^2}{(\bar{q}^2)^2} (A_{\lambda\bar{\lambda}} + \bar{q}^2 B_{\lambda\bar{\lambda}})$$

where A and B reflect the Coulomb-like and transverse gluon couplings, respectively. The results to leading order in  $\alpha_s$  are given in Ref. 38. In general A and B have a slow logarithmic dependence due to the  $q^2$ -evolution of the distribution amplitudes. The form factor zero for the case of pseudoscalar pair production reflects the numerator structure of the  $T_H$  amplitude.

$$\text{Numerator} \sim e_1 \left( \bar{q}^2 - \frac{m_1^2}{4M_H^2} \frac{1}{x_2 y_1} - \frac{m_2^2}{4M_H^2} \frac{x_1}{x_2^2 y_2} \right)$$

For the peaked wavefunction,

$$F_{0,0}^M(q^2) \propto \frac{1}{(\bar{q}^2)^2} \left\{ e_1 \left( \bar{q}^2 - \frac{m_1}{2m_2} \right) + e_2 \left( \bar{q}^2 - \frac{m_2}{2m_1} \right) \frac{m_2^2}{m_1^2} \right\}$$

If  $m_1$  is much greater than  $m_2$  then the  $e_1$  is dominant and changes sign at  $q^2/4M_H^2 = m_1/2m_2$ . The contribution of the  $e_2$  term and higher order contributions are small

---

\*  $F_{\lambda\bar{\lambda}}(q^2)$  is the form factor for the production of two mesons which have both spin and helicity ( $Z$ -component of spin) as  $\lambda$  and  $\bar{\lambda}$  respectively. There are two Lorentz and gauge invariant form factors of vector pair production. However, one of them turns out to be the same as the form factor of pseudoscalar plus vector production multiplied by  $M_H$ . Therefore the differential cross section for the production of two mesons with spin 0 or 1 can be represented in terms of three independent form factors.

and nearly constant in the region where the  $e_1$  term changes sign; such contributions can displace slightly but not remove the form factor zero. These results also hold in quantum electrodynamics; e.g., pair production of muonium ( $\mu - e$ ) atoms in  $e_+e_-$  annihilation. Gauge theory predicts a zero at  $\bar{q}^2 = m_\mu/2m_e$ .

These explicit results for form factors also show that the onset of the leading power-law scaling of a form factor is controlled by the ratio of the A and B terms; i.e., when the transverse contributions exceed the Coulomb mass-dominated contributions. The Coulomb contribution to the form factor can also be computed directly from the convolution of the initial and final wavefunctions. Thus, contrary to the claim of Ref. 19 there are no extra factors of  $\alpha_s(q^2)$  which suppress the “hard” versus nonperturbative contributions.

The form factors for the heavy hadrons are normalized by the constraint that the Coulomb contribution to the form factor equals the total hadronic charge at  $q^2 = 0$ . Further, by the correspondence principle, the form factor should agree with the standard non-relativistic calculation at small momentum transfer. All of these constraints are satisfied by the form

$$F_{0,0}^M(q^2) = e_1 \frac{16\gamma^4}{(q^2 + \gamma^2)^2} \left( \frac{M_H^2}{m_2^2} \right)^2 \left( 1 - \frac{q^2}{4M_H^2} \frac{2m_2}{m_1} \right) + 1 \leftrightarrow 2 .$$

At large  $q^2$  the form factor can also be written as

$$F_{(0,0)}^M = e_1 \frac{16\pi\alpha_s f_M^2}{9q^2} \left( \frac{M_H^2}{m_2^2} \right) + (1 \leftrightarrow 2) , \quad \frac{f_M}{2\sqrt{3}} = \int_0^1 dx \phi(x, Q)$$

where  $f_M = (6\gamma^3/\pi M_H)^{1/2}$  is the meson decay constant. Detailed results for  $F\bar{F}$  and  $B_c\bar{B}_c$  production are give in Ref. 38.

At low relative velocity of the hadron pair one also expects resonance contributions to the form factors. For these heavy systems such resonances could be related to  $q\bar{q}q\bar{q}$  bound states. From Watson’s theorem, one expects any resonance structure to introduce a final-state phase factor, but not destroy the zero of the underlying QCD prediction.

Analogous calculations of the baryon form factor, retaining the constituent mass structure have also been done. The numerator structure for spin 1/2 baryons has the

form

$$A + B\bar{q}^2 + c\bar{q}^4 .$$

Thus it is possible to have two form factor zeros; e.g., at space-like and time-like values of  $q^2$ .

Although the measurements are difficult and require large luminosity, the observation of the striking zero structure predicted by QCD would provide a unique test of the theory and its applicability to exclusive processes. The onset of leading power behavior is controlled simply by the mass parameters of the theory.

## 15. EXCLUSIVE $\gamma\gamma$ REACTIONS

A number of interesting  $\gamma\gamma$  annihilation processes could be studied advantageously at a high intensity  $e^+e^-$  collider. Such two-photon reactions have a number of unique features which are important for testing QCD:<sup>39</sup>

1. Any even charge conjugation hadronic state can be created in the annihilation of two photons—an initial state of minimum complexity. Because  $\gamma\gamma$  annihilation is complete, there are no spectator hadrons to confuse resonance analyses. Thus, one has a clean environment for identifying the exotic color-singlet even  $C$  composites of quarks and gluons  $|q\bar{q}\rangle$ ,  $|gg\rangle$ ,  $|ggg\rangle$ ,  $|q\bar{q}g\rangle$ ,  $|qq\bar{q}\bar{q}\rangle$ , ... which are expected to be present in the few GeV mass range. (Because of mixing, the actual mass eigenstates of QCD may be complicated admixtures of the various Fock components.)
2. The mass and polarization of each of the incident virtual photons can be continuously varied, allowing highly detailed tests of theory. Because a spin-one state cannot couple to two on-shell photons, a  $J = 1$  resonance can be uniquely identified by the onset of its production with increasing photon mass.<sup>40</sup>
3. Two-photon physics plays an especially important role in probing dynamical mechanisms. In the low momentum transfer domain,  $\gamma\gamma$  reactions such as the total annihilation cross section and exclusive vector meson pair production can give important insights into the nature of diffractive reactions in QCD. Photons in QCD couple directly to the quark currents at any resolution scale. Predictions for high momentum transfer  $\gamma\gamma$  reactions, including the photon structure functions,  $F_2^\gamma(x, Q^2)$  and  $F_L^\gamma(x, Q^2)$ , high  $p_T$  jet production, and exclusive channels are thus much more specific than corresponding hadron-induced reactions. The point-like coupling of the annihilating photons leads to a host of special features which differ markedly with predictions based on vector meson dominance models.

4. Exclusive  $\gamma\gamma$  processes provide a window for viewing the wavefunctions of hadrons in terms of their quark and gluon degrees of freedom. In the case of  $\gamma\gamma$  annihilation into hadron pairs, the angular distribution of the production cross section directly reflects the shape of the distribution amplitude (valence wavefunction) of each hadron.

A simple, but still very important example,<sup>14</sup> is the  $Q^2$ -dependence of the reaction  $\gamma^*\gamma \rightarrow M$  where  $M$  is a pseudoscalar meson such as the  $\eta$ . The invariant amplitude contains only one form factor:

$$M_{\mu\nu} = \epsilon_{\mu\nu\sigma\tau} p_\eta^\sigma q^\tau F_{\gamma\eta}(Q^2).$$

It is easy to see from power counting at large  $Q^2$  that the dominant amplitude (in light-cone gauge) gives  $F_{\gamma\eta}(Q^2) \sim 1/Q^2$  and arises from diagrams which have the minimum path carrying  $Q^2$ : i.e., diagrams in which there is only a single quark propagator between the two photons. The coefficient of  $1/Q^2$  involves only the two-particle  $q\bar{q}$  distribution amplitude  $\phi(x, Q)$ , which evolves logarithmically on  $Q$ . Higher particle number Fock states give higher power-law falloff contributions to the exclusive amplitude.

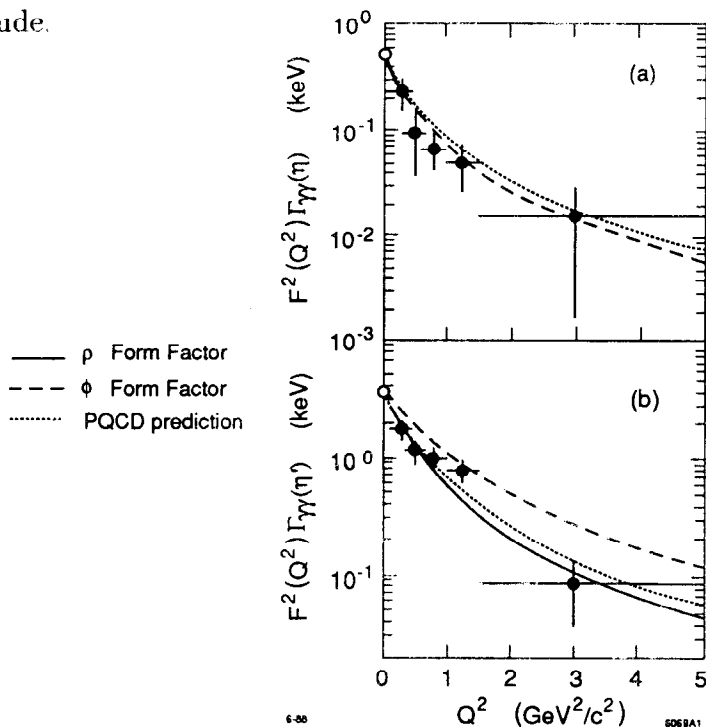


Figure 13. Comparison of TPC/ $\gamma\gamma$  data<sup>41</sup> for the  $\gamma - \eta$  and  $\gamma - \eta'$  transition form factors with the QCD leading twist prediction of Ref. 42. The VMD predictions are also shown

The TPC/ $\gamma\gamma$  data<sup>41</sup> shown in Fig. 13 are in striking agreement with the predicted QCD power: a fit to the data gives  $F_{\gamma\eta}(Q^2) \sim (1/Q^2)^n$  with  $n = 1.05 \pm 0.15$ . Data

for the  $\eta'$  from Pluto and the TPC/ $\gamma\gamma$  experiments give similar results, consistent with scale-free behavior of the QCD quark propagator and the point coupling to the quark current for both the real and virtual photons. In the case of deep inelastic lepton scattering, the observation of Bjorken scaling tests the same scaling of the quark Compton amplitude when both photons are virtual.

The QCD power law prediction,  $F_{\gamma\eta}(Q^2) \sim 1/Q^2$ , is consistent with dimensional counting<sup>10</sup> and also emerges from current algebra arguments (when both photons are very virtual).<sup>43</sup> On the other hand, the  $1/Q^2$  falloff is also expected in vector meson dominance models. The QCD and VDM predictions can be readily discriminated by studying  $\gamma^*\gamma^* \rightarrow \eta$ . In VMD one expects a product of form factors; in QCD, the fall-off of the amplitude is still  $1/Q^2$  where  $Q^2$  is a linear combination of  $Q_1^2$  and  $Q_2^2$ . It is clearly very important to test this essential feature of QCD.

We also note that photon-photon collisions provide a way to measure the running coupling constant in an exclusive channel, independent of the form of hadronic distribution amplitudes.<sup>42</sup> The photon-meson transition form factors  $F_{\gamma \rightarrow M}(Q^2)$ ,  $M = \pi^0, \eta^0, f$ , etc., are measurable in tagged  $e\gamma \rightarrow e'M$  reactions. QCD predicts

$$\alpha_s(Q^2) = \frac{1}{4\pi} \frac{F_\pi(Q^2)}{Q^2 |F_{\pi\gamma}(Q^2)|^2}$$

where to leading order the pion distribution amplitude enters both numerator and denominator in the same manner.

Exclusive two-body processes  $\gamma\gamma \rightarrow H\bar{H}$  at large  $s = W_{\gamma\gamma}^2 = (q_1 + q_2)^2$  and fixed  $\theta_{\text{cm}}^{\gamma\gamma}$  provide a particularly important laboratory for testing QCD, since the large momentum-transfer behavior, helicity structure, and often even the absolute normalization can be rigorously predicted.<sup>42,44</sup> The angular dependence of some of the  $\gamma\gamma \rightarrow H\bar{H}$  cross sections reflects the shape of the hadron distribution amplitudes  $\phi_H(x_i, Q)$ . The  $\gamma\gamma \rightarrow H\bar{H}$  amplitude can be written as a factorized form

$$\mathcal{M}_{\lambda\lambda'}(W_{\gamma\gamma}, \theta_{\text{cm}}) = \int_0^1 [dy_i] \phi_H^*(x_i, Q) \phi_H^*(y_i, Q) T_{\lambda\lambda'}(x, y; W_{\gamma\gamma}, \theta_{\text{cm}})$$

where  $T_{\lambda\lambda'}$  is the hard scattering helicity amplitude. To leading order  $T \propto \alpha(\alpha_s/W_{\gamma\gamma}^2)^n$  and  $d\sigma/dt \sim W_{\gamma\gamma}^{-(2n+2)} f(\theta_{\text{cm}})$  where  $n = 1$  for meson and  $n = 2$  for baryon pairs.

Lowest order predictions for pseudo-scalar and vector-meson pairs for each helicity amplitude are given in Ref. 42. In each case the helicities of the hadron pairs are equal and opposite to leading order in  $1/W^2$ . The normalization and angular dependence of

the leading order predictions for  $\gamma\gamma$  annihilation into charged meson pairs are almost model independent; i.e., they are insensitive to the precise form of the meson distribution amplitude. If the meson distribution amplitudes is symmetric in  $x$  and  $(1-x)$ , then the same quantity

$$\int_0^1 dx \frac{\phi_\pi(x, Q)}{(1-x)}$$

controls the  $x$ -integration for both  $F_\pi(Q^2)$  and to high accuracy  $M(\gamma\gamma \rightarrow \pi^+\pi^-)$ . Thus for charged pion pairs one obtains the relation:

$$\frac{\frac{d\sigma}{dt}(\gamma\gamma \rightarrow \pi^+\pi^-)}{\frac{d\sigma}{dt}(\gamma\gamma \rightarrow \mu^+\mu^-)} \cong \frac{4|F_\pi(s)|^2}{1 - \cos^4 \theta_{\text{cm}}}$$

Note that in the case of charged kaon pairs, the asymmetry of the distribution amplitude may give a small correction to this relation.

The scaling behavior, angular behavior, and normalization of the  $\gamma\gamma$  exclusive pair production reactions are nontrivial predictions of QCD. Mark II meson pair data and PEP4/PEP9 data<sup>45</sup> for separated  $\pi^+\pi^-$  and  $K^+K^-$  production in the range  $1.6 < W_{\gamma\gamma} < 3.2$  GeV near  $90^\circ$  are in satisfactory agreement with the normalization and energy dependence predicted by QCD (see Fig. 14). In the case of  $\pi^0\pi^0$  production, the  $\cos^2 \theta_{\text{cm}}$  dependence of the cross section can be inverted to determine the  $x$ -dependence of the pion distribution amplitude.

The wavefunction of hadrons containing light and heavy quarks such as the K, D-meson are likely to be asymmetric due to the disparity of the quark masses. In a gauge theory one expects that the wavefunction is maximum when the quarks have zero relative velocity; this corresponds to  $x_i \propto m_{i\perp}$  where  $m_{\perp}^2 = k_{\perp}^2 + m^2$ . An explicit model for the skewing of the meson distribution amplitudes based on QCD sum rules is given by Benayoun and Chernyak.<sup>46</sup> These authors also apply their model to two-photon exclusive processes such as  $\gamma\gamma \rightarrow K^+K^-$  and obtain some modification compared to the strictly symmetric distribution amplitudes. If the same conventions are used to label the quark lines, the calculations of Benayoun and Chernyak are in complete agreement with those of Ref. 42.

The one-loop corrections to the hard scattering amplitude for meson pairs have been calculated by Nizic.<sup>47</sup> The QCD predictions for mesons containing admixtures of the  $|gg\rangle$  Fock state is given by Atkinson, Sucher, and Tsokos.<sup>44</sup>

The perturbative QCD analysis has been extended to baryon-pair production in comprehensive analyses by Farrar, et al.<sup>48,44</sup> and by Gunion, et al.<sup>44</sup> Predictions are

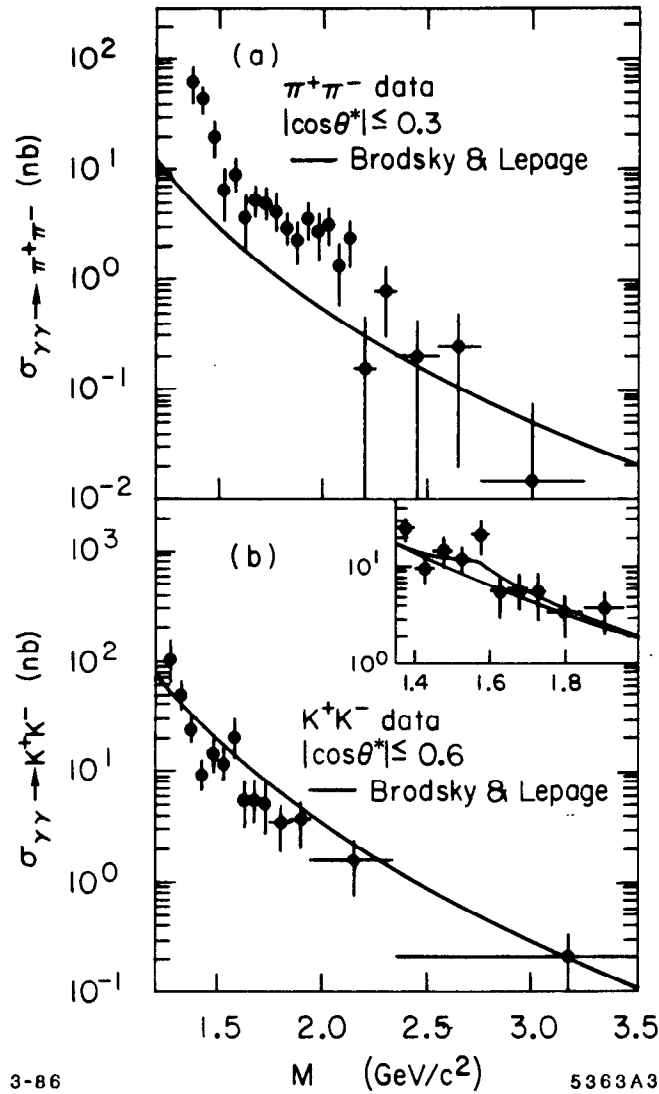


Figure 14. Comparison of  $\gamma\gamma \rightarrow \pi^+\pi^-$  and  $\gamma\gamma \rightarrow K^+K^-$  meson pair production data with the parameter-free perturbative QCD prediction of Ref. 42. The theory predicts the normalization and scaling of the cross sections. The data are from the TPC/ $\gamma\gamma$  collaboration.<sup>45</sup>

given for the “sideways” Compton process  $\gamma\gamma \rightarrow p\bar{p}$ ,  $\Delta\bar{\Delta}$  pair production, and the entire decuplet set of baryon pair states. The arduous calculation of 280  $\gamma\gamma \rightarrow qq\bar{q}\bar{q}$  diagrams in  $T_H$  required for calculating  $\gamma\gamma \rightarrow B\bar{B}$  is greatly simplified by using two-component spinor techniques. The doubly charged  $\Delta$  pair is predicted to have a fairly small normalization. Experimentally such resonance pairs may be difficult to identify under the continuum background.

The normalization and angular distribution of the QCD predictions for proton-antiproton production depend in detail on the form of the nucleon distribution amplitude, and thus provide severe tests of the model form derived by Chernyak, Ogloblin, and Zhitnitskii<sup>18</sup> from QCD sum rules.

The region of applicability of the leading power-law predictions for  $\gamma\gamma \rightarrow p\bar{p}$  re-

quires that one be beyond resonance or threshold effects. It presumably is set by the scale where  $Q^4 G_M(Q^2)$  is roughly constant; i.e.,  $Q^2 > 3 \text{ GeV}^2$ . Measurements of baryon pairs should be sufficiently far from threshold for quantitative tests of the PQCD predictions.<sup>49</sup>

The QCD predictions for  $\gamma\gamma \rightarrow H\bar{H}$  can be extended to the case of one or two virtual photons, for measurements in which one or both electrons are tagged. Because of the direct coupling of the photons to the quarks, the  $Q_1^2$  and  $Q_2^2$  dependence of the  $\gamma\gamma \rightarrow H\bar{H}$  amplitude for transversely polarized photons is minimal at  $W^2$  large and fixed  $\theta_{\text{cm}}$ , since the off-shell quark and gluon propagators in  $T_H$  already transfer hard momenta; i.e., the  $2\gamma$  coupling is effectively local for  $Q_1^2, Q_2^2 \ll p_T^2$ . The  $\gamma^*\gamma^* \rightarrow \bar{B}B$  and  $M\bar{M}$  amplitudes for off-shell photons have been calculated by Millers and Gunion.<sup>44</sup> In each case, the predictions show strong sensitivity to the form of the respective baryon and meson distribution amplitudes.

## 16. HIGHER TWIST EFFECTS

One of the most elusive topics in PQCD has been the unambiguous identification of higher-twist effects in inclusive reaction. A signal for a dynamical higher-twist amplitude has been seen in pion-induced Drell-Yan reactions, where a  $1/Q^2$  component to the pion structure function  $F_L^\pi(x_1, Q^2)$  coupling to longitudinal photons dominates the cross section at large  $x_1$ . In addition, a Rice-Fermilab experiment studying pion-induced di-jet production has found evidence for the directly-coupled pion higher-twist subprocess  $\pi g \rightarrow q\bar{q}$  which has the unusual property that there is no jet of hadrons left in the beam direction.

In the case of inclusive quark jet fragmentation,  $e^+e^- \rightarrow \pi X$ , PQCD predicts analogous anomalous behavior in the jet distribution at large  $z = E_\pi/Q$ . In the analysis one must take into account the subprocess  $\gamma^* \rightarrow \pi q\bar{q}$  illustrated in Fig. 15 where the pion is produced directly at short distances, in addition to the standard leading twist process where the pion is produced from jet fragmentation. The net result is a prediction at large  $z$  of the form

$$\frac{d\sigma(e^+e^- \rightarrow \pi X)}{dz^d \cos \theta} = A(1-z)^2(1 + \cos^2 \theta) + B \frac{\sin^2 \theta}{Q^2}.$$

Although the corresponding  $B$  term has been observed in the Drell-Yan reaction, it has never been seen unambiguously in jet fragmentation. A range of  $e^+e^-$  energies would be advantageous in identifying the  $1/Q^2$  dependence of the direct pion contributions.

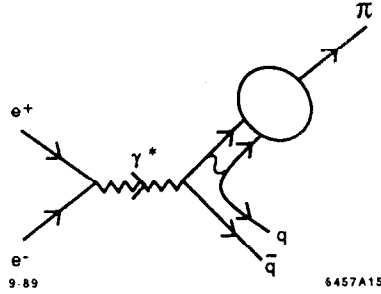


Figure 15. Higher-twist contribution to jet fragmentation in  $e^+e^- \rightarrow \pi X$ . The pion couples through its distribution amplitude  $\phi_\pi(x, Q)$ .

## 17. TAUONIUM AND THRESHOLD $\tau^+\tau^-$ PRODUCTION

In principle,  $J^P = 1^-$  QED bound states of  $\tau^+\tau^-$  could be produced as very narrow resonances below threshold in  $e^+e^-$  annihilation.<sup>50</sup> Unfortunately the observation of even the lowest ortho-tauonium state at a measurable level would require much higher incident energy resolution than presently possible. The higher  $n$  excitations are suppressed by a factor  $1/n^3$ , so radiative decay signals would not be produced at a practical rate. Worse, the  $\tau$  will decay weakly before radiative transitions can occur.

The continuum production of the  $\tau^+\tau^-$  near threshold is strongly modified by final-state QED interactions.<sup>51</sup> The leading order correction to the Born term at threshold has the form  $(1 + \alpha f(v))$  where  $v = (1 - 4M_\tau^2/s)$  and

$$f(v) = \frac{\pi}{2v} - \frac{3+v}{4} \left( \frac{\pi}{2} - \frac{3}{4\pi} \right).$$

The singular factor in  $1/v$  cancels the phase-space factor in the Born cross section, giving a non-zero rate for production at threshold. The analogous effect is well-known in QCD for threshold charm production, and has been taken into account in the duality formulas which relate charm hadron production to the mass of the charm quark.<sup>52</sup> It would be interesting to check the threshold production of  $e^+e^- \rightarrow \tau^+\tau^-$  and verify this interesting feature of  $\tau$  electrodynamics.

Let us now return to the question of the normalization of exclusive amplitudes in QCD. It should be emphasized that because of the uncertain magnitude of corrections of higher order in  $\alpha_s(Q^2)$ , comparisons with the normalization of experiment with model predictions could be misleading. Nevertheless, in this section it shall be assumed that the leading order normalization is at least approximately accurate. If the higher order corrections are indeed small, then the normalization of the proton form factor at large  $Q^2$  is a non-trivial test of the distribution amplitude shape; for example, if the proton wave function has a non-relativistic shape peaked at  $x_i \sim 1/3$  then one obtains the wrong sign for the nucleon form factor. Furthermore symmetrical distribution amplitudes predict a very small magnitude for  $Q^4 G_M^p(Q^2)$  at large  $Q^2$ .

The phenomenology of hadron wavefunctions in QCD is now just beginning. Constraints on the baryon and meson distribution amplitudes have been recently obtained using QCD sum rules and lattice gauge theory. The results are expressed in terms of gauge-invariant moments  $\langle x_j^m \rangle = \int \Pi dx_i x_j^m \phi(x_i, \mu)$  of the hadron's distribution amplitude. A particularly important challenge is the construction of the baryon distribution amplitude. In the case of the proton form factor, the constants  $a_{nm}$  in the QCD prediction for  $G_M$  must be computed from moments of the nucleon's distribution amplitude  $\phi(x_i, Q)$ . There are now extensive theoretical efforts to compute this nonperturbative input directly from QCD. The QCD sum rule analysis of Chernyak et al.<sup>21,18</sup> provides constraints on the first 12 moments of  $\phi(x, Q)$ . Using as a basis the polynomials which are eigenstates of the nucleon evolution equation, one gets a model representation of the nucleon distribution amplitude, as well as its evolution with the momentum transfer scale. The moments of the proton distribution amplitude computed by Chernyak et al., have now been confirmed in an independent analysis by Sachrajda and King.<sup>53</sup>

A three-dimensional "snapshot" of the proton's  $uud$  wavefunction at equal light cone time as deduced from QCD sum rules at  $\mu \sim 1$  GeV by Chernyak et al.<sup>18</sup> and King and Sachrajda<sup>53</sup> is shown in Fig. 16. The QCD sum rule analysis predicts a surprising feature: strong flavor asymmetry in the nucleon's momentum distribution. The computed moments of the distribution amplitude imply that 65% of the proton's momentum in its 3-quark valence state is carried by the u-quark which has the same helicity as the parent hadron.

Dziembowski and Mankiewicz<sup>26</sup> have recently shown that the asymmetric form of the CZ distribution amplitude can result from a rotationally-invariant CM wave

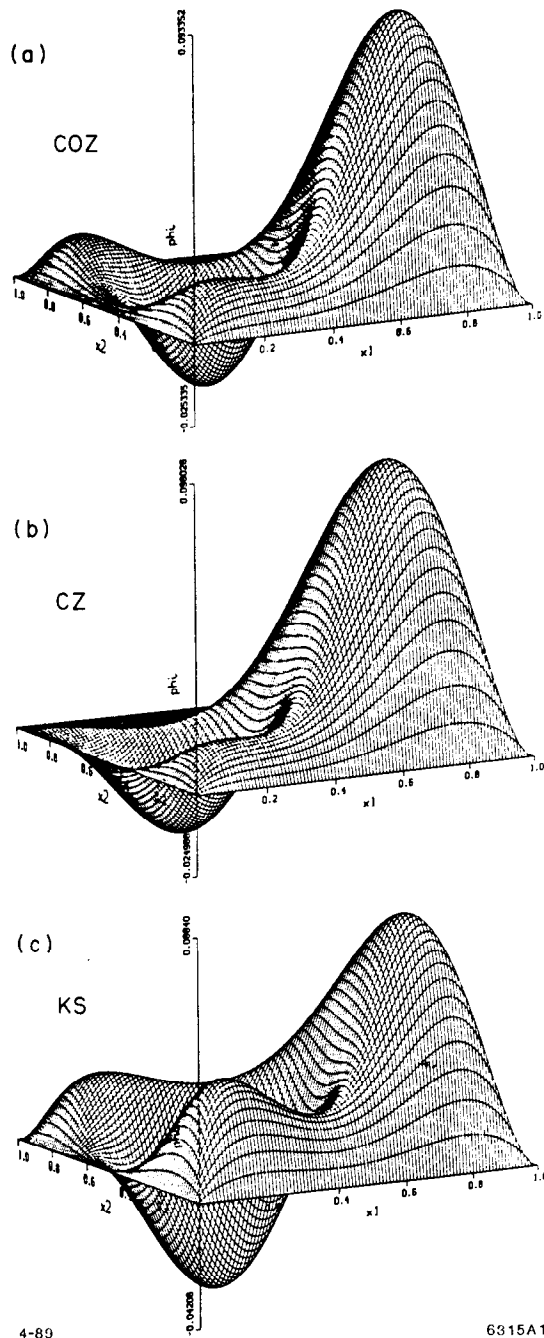


Figure 16 The proton distribution amplitude  $\phi_p(x_i, \mu)$  determined at the scale  $\mu \sim 1$  GeV from QCD sum rules.

function transformed to the light cone using free quark dynamics. They find that one can simultaneously fit low energy phenomena (charge radii, magnetic moments, etc.), the measured high momentum transfer hadron form factors, and the CZ distribution amplitudes with a self-consistent ansatz for the quark wave functions. Thus for the first time one has a somewhat complete model for the relativistic three-quark structure of the hadrons. In the model the transverse size of the valence wave function is not found to be significantly smaller than the mean radius of the proton averaged over all Fock states as argued in Ref. 54. Dziembowski et al. also find that the pertur-

bative QCD contribution to the form factors in their model dominates over the soft contribution (obtained by convoluting the non-perturbative wave functions) at a scale  $Q/N \approx 1$  GeV, where  $N$  is the number of valence constituents. (This criterion was also derived in Ref. 55.)

Gari and Stefanis<sup>56</sup> have developed a model for the nucleon form factors which incorporates the CZ distribution amplitude predictions at high  $Q^2$  together with VMD constraints at low  $Q^2$ . Their analysis predicts sizeable values for the neutron electric form factor at intermediate values of  $Q^2$ .

A detailed phenomenological analysis of the nucleon form factors for different shapes of the distribution amplitudes has been given by Ji, Sill, and Lombard-Nelsen.<sup>57</sup> Their results show that the CZ wave function is consistent with the sign and magnitude of the proton form factor at large  $Q^2$  as recently measured by the American University/SLAC collaboration<sup>28</sup> (see Fig. 17).

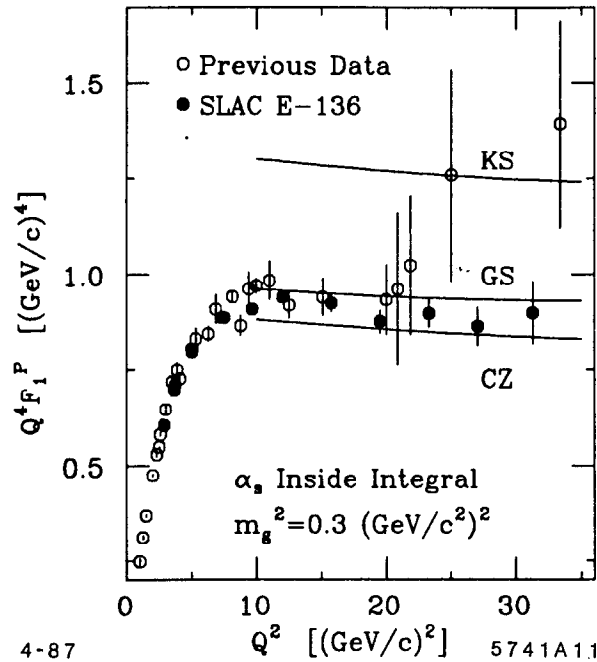


Figure 17. Predictions for the normalization and sign of the proton form factor at high  $Q^2$  using perturbative QCD factorization and QCD sum rule predictions for the proton distribution amplitude (from Ref. 57.) The predictions use forms given by Chernyak and Zhitnitskii, King and Sachrajda,<sup>53</sup> and Gari and Stefanis.<sup>56</sup>

It should be stressed that the magnitude of the proton form factor is sensitive to the  $x \sim 1$  dependence of the proton distribution amplitude, where non-perturbative effects could be important.<sup>17</sup> The asymmetry of the distribution amplitude emphasizes contributions from the large  $x$  region. Since non-leading corrections are expected when the quark propagator scale  $Q^2(1-x)$  is small, in principle relatively large momentum

transfer is required to clearly test the perturbative QCD predictions. Chernyak et al.<sup>18</sup> have studied this effect in some detail and claim that their QCD sum rule predictions are not significantly changed when higher moments of the distribution amplitude are included.

It is important to notice that the perturbative scaling regime of the meson form factor is controlled by the virtuality of the quark propagator. When the quark is far off-shell, multiple gluon exchange contributions involving soft gluon insertions are suppressed by inverse powers of the quark propagator; there is not sufficient time to exchange soft gluons or gluonium. Thus the perturbative analysis is valid as long as the single gluon exchange propagator has inverse power behavior. There is thus no reason to require that the gluon be far off-shell, as in the analysis of Ref. 19.

The moments of distribution amplitudes can also be computed using lattice gauge theory.<sup>58</sup> In the case of the pion distribution amplitudes, there is good agreement of the lattice gauge theory computations of Martinelli and Sachrajda<sup>59</sup> with the QCD sum rule results. This check has strengthened confidence in the reliability of the QCD sum rule method, although the shape of the meson distribution amplitudes are unexpectedly structured: the pion distribution amplitude is broad and has a dip at  $x = 1/2$ . The QCD sum rule meson distributions, combined with the perturbative QCD factorization predictions, account well for the scaling, normalization of the pion form factor and  $\gamma\gamma \rightarrow M^+M^-$  cross sections.

In the case of the baryon, the asymmetric three-quark distributions are consistent with the normalization of the baryon form factor at large  $Q^2$  and also the branching ratio for  $J/\psi \rightarrow p\bar{p}$ . The data for large angle Compton scattering  $\gamma p \rightarrow \gamma p$  are also well described.<sup>44</sup> However, a very recent lattice calculation of the lowest two moments by Martinelli and Sachrajda<sup>59</sup> does not show skewing of the average fraction of momentum of the valence quarks in the proton. This lattice result is in contradiction to the predictions of the QCD sum rules and does cast some doubt on the validity of the model of the proton distribution proposed by Chernyak et al.<sup>18</sup> The lattice calculation is performed in the quenched approximation with Wilson fermions and requires an extrapolation to the chiral limit.

The contribution of soft momentum exchange to the hadron form factors is a potentially serious complication when one uses the QCD sum rule model distribution amplitudes. In the analysis of Ref. 19 it was argued that only about 1% of the proton form factor comes from regions of integration in which all the propagators are hard. A new analysis by Dziembowski et al.<sup>20</sup> shows that the QCD sum rule<sup>21</sup> distribution

amplitudes of Chernyak et al.<sup>21</sup> together with the perturbative QCD prediction gives contributions to the form factors which agree with the measured normalization of the pion form factor at  $Q^2 > 4 \text{ GeV}^2$  and proton form factor  $Q^2 > 20 \text{ GeV}^2$  to within a factor of two. In the calculation the virtuality of the exchanged gluon is restricted to  $|k^2| > 0.25 \text{ GeV}^2$ . The authors assume  $\alpha_s = 0.3$  and that the underlying wavefunctions fall off exponentially at the  $x \simeq 1$  endpoints. Another model of the proton distribution amplitude with diquark clustering<sup>22</sup> chosen to satisfy the QCD sum rule moments come even closer. Considering the uncertainty in the magnitude of the higher order corrections, one really cannot expect better agreement between the QCD predictions and experiment.

The relative importance of non-perturbative contributions to form factors is also an issue. Unfortunately, there is little that can be said until we have a deeper understanding of the end-point behavior of hadronic wavefunctions, and of the role played by Sudakov form factors in the end-point region. Models have been constructed in which non-perturbative effects persist to high  $Q$ .<sup>19</sup> Other models have been constructed in which such effects vanish rapidly as  $Q$  increases.<sup>24,25,26</sup>

If the QCD sum rule results are correct then, the light hadrons are highly structured oscillating momentum-space valence wavefunctions. In the case of mesons, the results from both the lattice calculations and QCD sum rules show that the light quarks are highly relativistic. This gives further indication that while nonrelativistic potential models are useful for enumerating the spectrum of hadrons (because they express the relevant degrees of freedom), they may not be reliable in predicting wavefunction structure.

## 19. A TEST OF COLOR TRANSPARENCY

A striking feature of the QCD description of exclusive processes is “color transparency:” The only part of the hadronic wavefunction that scatters at large momentum transfer is its valence Fock state where the quarks are at small relative impact separation. Such a fluctuation has a small color-dipole moment and thus has negligible interactions with other hadrons. Since such a state stays small over a distance proportional to its energy, this implies that quasi-elastic hadron-nucleon scattering at large momentum transfer as illustrated in Fig. 18 can occur additively on all of the nucleons in a nucleus with minimal attenuation due to elastic or inelastic final state interactions in the nucleus, i.e. the nucleus becomes “transparent.” By contrast, in conventional Glauber scattering, one predicts strong, nearly energy-independent initial and final

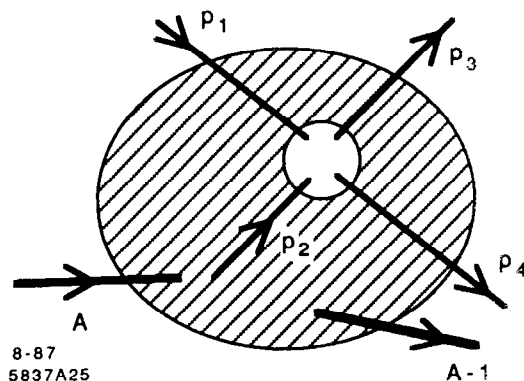
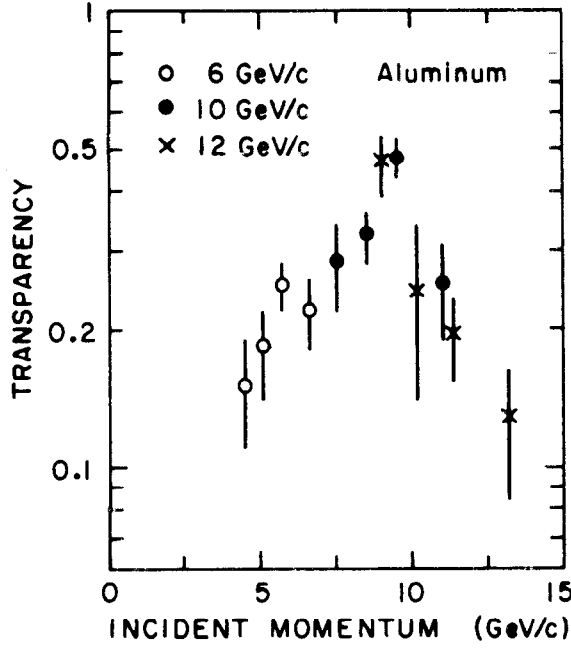


Figure 18. Quasi-elastic  $pp$  scattering inside a nuclear target. Normally one expects such processes to be attenuated by elastic and inelastic interactions of the incident proton and the final state interaction of the scattered proton. Perturbative QCD predicts minimal attenuation; i.e. “color transparency,” at large momentum transfer.<sup>29</sup>

state attenuation. A detailed discussion of the time and energy scales required for the validity of the PQCD prediction is given in by Farrar et al. and Mueller in Ref. 29.

A recent experiment<sup>60</sup> at BNL measuring quasi-elastic  $pp \rightarrow pp$  scattering at  $\theta_{cm} = 90^\circ$  in various nuclei appears to confirm the color transparency prediction—at least for  $p_{lab}$  up to 10 GeV/c (see Fig. 19). Descriptions of elastic scattering which involve soft hadronic wavefunctions cannot account for the data. However, at higher energies,  $p_{lab} \sim 12$  GeV/c, normal attenuation is observed in the BNL experiment. This is the same kinematical region  $E_{cm} \sim 5$  GeV where the large spin correlation in  $A_{NN}$  are observed.<sup>61</sup> I shall argue that both features may be signaling new  $s$ -channel physics associated with the onset of charmed hadron production.<sup>30</sup> Clearly, much more testing of the color transparency phenomena is required, particularly in quasi-elastic lepton-proton scattering, Compton scattering, antiproton-proton scattering, etc. The cleanest test of the PQCD prediction is to check for minimal attenuation in large momentum transfer lepton-proton scattering in nuclei since there are no complications from pinch singularities or resonance interference effects.

One can also understand the origin of color transparency as a consequence of the PQCD prediction that soft initial-state corrections to reactions such as  $\bar{p}p \rightarrow \bar{\ell}\ell$  are suppressed at high lepton pair mass. This is a remarkable consequence of gauge theory and is quite contrary to normal treatments of initial interactions based on Glauber theory. This novel effect can be studied in quasielastic  $\bar{p}A \rightarrow \bar{\ell}\ell (A-1)$  reaction, in which there are no extra hadrons produced and the produced leptons are coplanar with the beam. (The nucleus  $(A-1)$  can be left excited). Since PQCD predicts the absence of initial-state elastic and inelastic interactions, the number of such events should be strictly additive in the number  $Z$  of protons in the nucleus, every proton in



3-88

5970A10

Figure 19. Measurements of the transparency ratio

$$T = \frac{Z_{eff}}{Z} = \frac{d\sigma}{dt}[pA \rightarrow p(A-1)] / \frac{d\sigma}{dt}[pA \rightarrow pp]$$

near  $90^\circ$  on Aluminum.<sup>60</sup> Conventional theory predicts that  $T$  should be small and roughly constant in energy. Perturbative QCD<sup>29</sup> predicts a monotonic rise to  $T = 1$ .

the nucleus is equally available for short-distance annihilation. In traditional Glauber theory only the surface protons can participate because of the strong absorption of the  $\bar{p}$  as it traverses the nucleus.

The above description is the ideal result for large  $s$ . QCD predicts that additivity is approached monotonically with increasing energy, corresponding to two effects: a) the effective transverse size of the  $\bar{p}$  wavefunction is  $b_\perp \sim 1/\sqrt{s}$ , and b) the formation time for the  $\bar{p}$  is sufficiently long, such that the Fock state stays small during transit of the nucleus.

The color transparency phenomena is also important to test in purely hadronic quasiexclusive antiproton-nuclear reactions. For large  $p_T$  one predicts

$$\frac{d\sigma}{dt dy} (\bar{p}A \rightarrow \pi^+\pi^- + (A-1)) \simeq \sum_{p \in A} G_{p/A}(y) \frac{d\sigma}{dt} (\bar{p}p \rightarrow \pi^+\pi^-) ,$$

where  $G_{p/A}(y)$  is the probability distribution to find the proton in the nucleus with

light-cone momentum fraction  $y = (p^0 + p^z)/(p_A^0 + p_A^z)$ , and

$$\frac{d\sigma}{dt}(\bar{p}p \rightarrow \pi^+\pi^-) \simeq \left(\frac{1}{p_T^2}\right)^8 f(\cos\theta_{\text{cm}}).$$

The distribution  $G_{p/A}(y)$  can also be measured in  $eA \rightarrow ep(A-1)$  quasiexclusive reactions. A remarkable feature of the above prediction is that there are no corrections required from initial-state absorption of the  $\bar{p}$  as it traverses the nucleus, nor final-state interactions of the outgoing pions. Again the basic point is that the only part of hadron wavefunctions which is involved in the large  $p_T$  reaction is  $\psi_H(b_\perp \sim \mathcal{O}(1/p_T))$ , i.e. the amplitude where all the valence quarks are at small relative impact parameter. These configurations correspond to small color singlet states which, because of color cancellations, have negligible hadronic interactions in the target. Measurements of these reactions thus test a fundamental feature of the Fock state description of large  $p_T$  exclusive reactions.

Another interesting feature which can be probed in such reactions is the behavior of  $G_{p/A}(y)$  for  $y$  well away from the Fermi distribution peak at  $y \sim m_N/M_A$ . For  $y \rightarrow 1$  spectator counting rules<sup>62</sup> predict  $G_{p/A}(y) \sim (1-y)^{2N_s-1} = (1-y)^{6A-7}$  where  $N_s = 3(A-1)$  is the number of quark spectators required to “stop” ( $y_i \rightarrow 0$ ) as  $y \rightarrow 1$ . This simple formula has been quite successful in accounting for distributions measured in the forward fragmentation of nuclei at the BEVALAC.<sup>63</sup> Color transparency can also be studied by measuring quasiexclusive  $J/\psi$  production by anti-protons in a nuclear target  $\bar{p}A \rightarrow J/\psi(A-1)$  where the nucleus is left in a ground or excited state, but extra hadrons are not created (see Fig. 20). The cross section involves a convolution of the  $\bar{p}p \rightarrow J/\psi$  subprocess cross section with the distribution  $G_{p/A}(y)$  where  $y = (p^0 + p^3)/(p_A^0 + p_A^3)$  is the boost-invariant light-cone fraction for protons in the nucleus. This distribution can be determined from quasiexclusive lepton-nucleon scattering  $\ell A \rightarrow \ell p(A-1)$ .

In first approximation  $\bar{p}p \rightarrow J/\psi$  involves  $qqq + \bar{q}\bar{q}\bar{q}$  annihilation into three charmed quarks. The transverse momentum integrations are controlled by the charm mass scale and thus only the Fock state of the incident antiproton which contains three antiquarks at small impact separation can annihilate. Again it follows that this state has a relatively small color dipole moment, and thus it should have a longer than usual mean-free path in nuclear matter; i.e. color transparency. Unlike traditional expectations, QCD predicts that the  $\bar{p}p$  annihilation into charmonium is not restricted to the front surface of the nucleus. The exact nuclear dependence depends on the formation time for the physical  $\bar{p}$  to couple to the small  $\bar{q}\bar{q}\bar{q}$  configuration,  $\tau_F \propto E_p$ .

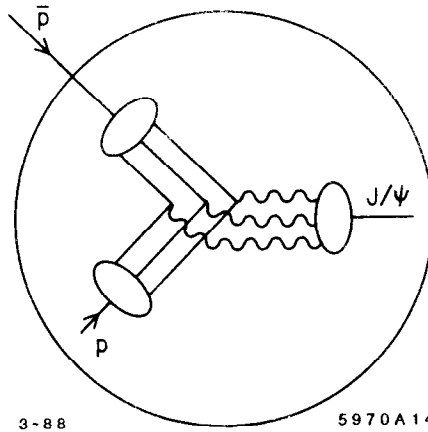


Figure 20. Schematic representation of quasielastic charmonium production in  $\bar{p}A$  reactions.

It may be possible to study the effect of finite formation time by varying the beam energy,  $E_p$ , and using the Fermi-motion of the nucleon to stay at the  $J/\psi$  resonance. Since the  $J/\psi$  is produced at nonrelativistic velocities in this low energy experiment, it is formed inside the nucleus. The  $A$ -dependence of the quasiexclusive reaction can thus be used to determine the  $J/\psi$ -nucleon cross section at low energies. For a normal hadronic reaction  $\bar{p}A \rightarrow HX$ , we expect  $A_{\text{eff}} \sim A^{1/3}$ , corresponding to absorption in the initial and final state. In the case of  $\bar{p}A \rightarrow J/\psi^X$  one expects  $A_{\text{eff}}$  much closer to  $A^1$  if color transparency is fully effective and  $\sigma(J/\psi^N)$  is small.

## 20. SPIN CORRELATIONS IN PROTON-PROTON SCATTERING

One of the most serious challenges to quantum chromodynamics is the behavior of the spin-spin correlation asymmetry  $A_{NN} = \frac{[d\sigma(\uparrow\uparrow) - d\sigma(\uparrow\downarrow)]}{[d\sigma(\uparrow\uparrow) + d\sigma(\uparrow\downarrow)]}$  measured in large momentum transfer  $pp$  elastic scattering (see Fig. 21). At  $p_{\text{lab}} = 11.75$  GeV/c and  $\theta_{\text{cm}} = \pi/2$ ,  $A_{NN}$  rises to  $\simeq 60\%$ , corresponding to four times more probability for protons to scatter with their incident spins both normal to the scattering plane and parallel, rather than normal and opposite.

The polarized cross section shows a striking energy and angular dependence not expected from the slowly-changing perturbative QCD predictions. However, the unpolarized data is in first approximation consistent with the fixed angle scaling law  $s^{10} d\sigma/dt(pp \rightarrow pp) = f(\theta_{CM})$  expected from the perturbative analysis (see Fig. 22). The onset of new structure<sup>64</sup> at  $s \simeq 23$  GeV<sup>2</sup> is a sign of new degrees of freedom in the two-baryon system. In this section, I will discuss a possible explanation<sup>30</sup> for (1) the observed spin correlations, (2) the deviations from fixed-angle scaling laws, and (3) the anomalous energy dependence of absorptive corrections to quasielastic  $pp$  scattering in nuclear targets, in terms of a simple model based on two  $J = L = S = 1$

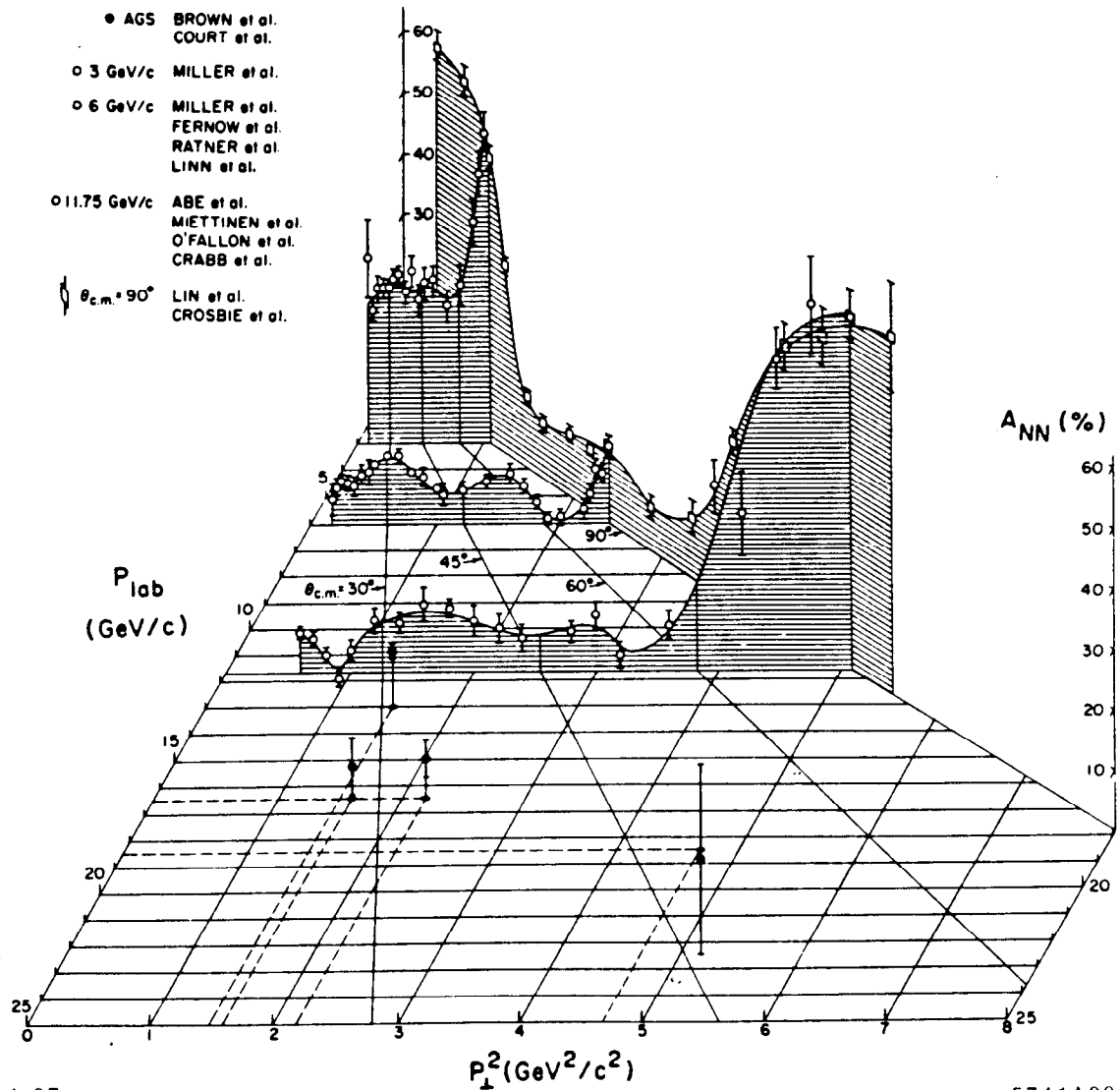


Figure 21. The spin-spin correlation  $A_{NN}$  for elastic  $pp$  scattering with beam and target protons polarized normal to the scattering plane.<sup>65</sup>  $A_{NN} = 60\%$  implies that it is four times more probable for the protons to scatter with spins parallel rather than antiparallel.

broad resonances (or threshold enhancements) interfering with a perturbative QCD quark-interchange background amplitude. The structures in the  $pp \rightarrow pp$  amplitude may be associated with the onset of strange and charmed thresholds. The fact that the produced quark and anti-quark have opposite parity explains why the  $L = 1$  channel is involved. If the charm threshold explanation is correct, large angle  $pp$  elastic scattering would have been virtually featureless for  $p_{lab} \geq 5$  GeV/c, had it not been for the onset of heavy flavor production. As a further illustration of the threshold effect, one can see the effect in  $A_{NN}$  due to a narrow  ${}^3F_3^p p$  resonance at  $\sqrt{s} = 2.17$  GeV ( $p_{lab} = 1.26$  GeV/c) associated with the  $p\Delta$  threshold.

The perturbative QCD analysis<sup>66</sup> of exclusive amplitudes assumes that large momentum transfer exclusive scattering reactions are controlled by short distance quark-

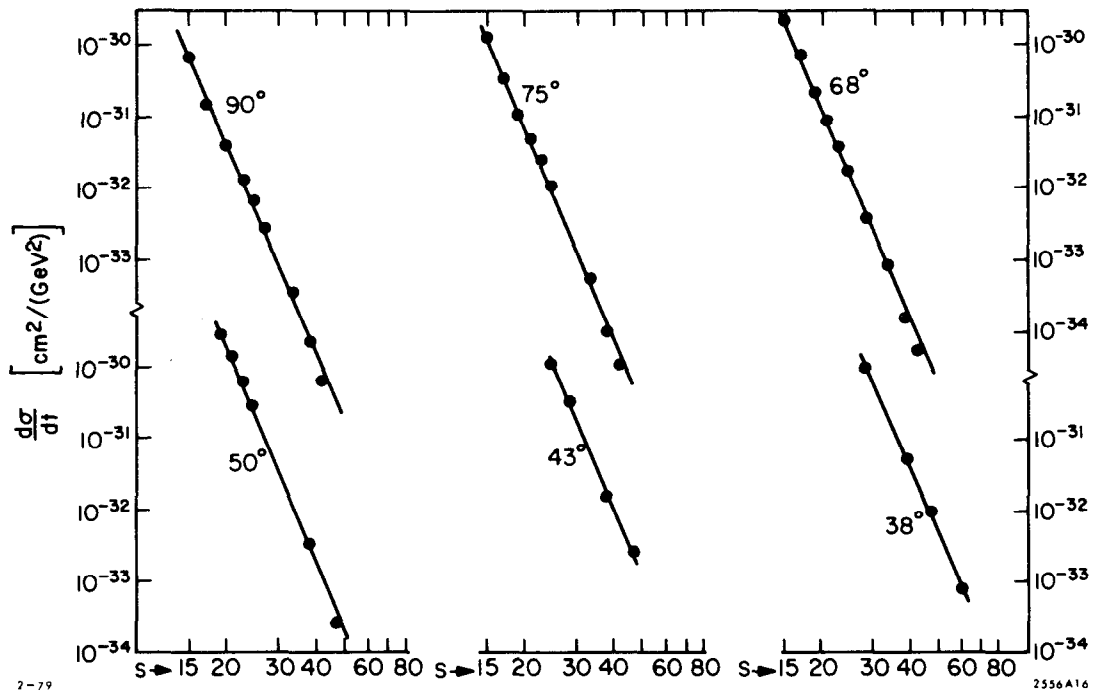


Figure 22. Test of fixed  $\theta_{CM}$  scaling for elastic  $pp$  scattering. The data compilation is from Landshoff and Polkinghorne.

gluon subprocesses, and that corrections from quark masses and intrinsic transverse momenta can be ignored. The main predictions are fixed-angle scaling laws<sup>10</sup> (with small corrections due to evolution of the distribution amplitudes, the running coupling constant, and pinch singularities), hadron helicity conservation,<sup>15</sup> and the novel phenomenon, “color transparency.”<sup>29</sup>

As discussed in Section 9, a test of color transparency in large momentum transfer quasielastic  $pp$  scattering at  $\theta_{cm} \simeq \pi/2$  has recently been carried out at BNL using several nuclear targets (C, Al, Pb).<sup>60</sup> The attenuation at  $p_{lab} = 10$  GeV/c in the various nuclear targets was observed to be in fact much less than that predicted by traditional Glauber theory (see Fig. 19). This appears to support the color transparency prediction.

The expectation from perturbative QCD is that the transparency effect should become even more apparent as the momentum transfer rises. Nevertheless, at  $p_{lab} = 12$  GeV/c, normal attenuation was observed. One can explain this surprising result if the scattering at  $p_{lab} = 12$  GeV/c ( $\sqrt{s} = 4.93$  GeV), is dominated by an  $s$ -channel  $B=2$  resonance (or resonance-like structure) with mass near 5 GeV, since unlike a hard-scattering reaction, a resonance couples to the fully-interacting large-scale structure of the proton. If the resonance has spin  $S = 1$ , this can also explain the large spin correlation  $A_{NN}$  measured nearly at the same momentum,  $p_{lab} = 11.75$  GeV/c. Conversely, in the momentum range  $p_{lab} = 5$  to 10 GeV/c one predicts that the per-

turbative hard-scattering amplitude is dominant at large angles. The experimental observation of diminished attenuation at  $p_{lab} = 10$  GeV/c thus provides support for the QCD description of exclusive reactions and color transparency.

What could cause a resonance at  $\sqrt{s} = 5$  GeV, more than 3 GeV beyond the  $pp$  threshold? There are a number of possibilities: (a) a multigluonic excitation such as  $|qqqqqqggg\rangle$ , (b) a “hidden color” color singlet  $|qqqqqq\rangle$  excitation,<sup>67</sup> or (c) a “hidden flavor”  $|qqqqqqQ\bar{Q}\rangle$  excitation, which is the most interesting possibility, since it naturally explains the spin-parity of the resonance or threshold enhancement, and it leads to many testable consequences.

As in QED, where final state interactions give large enhancement factors for attractive channels in which  $Z\alpha/v_{rel}$  is large, one expects resonances or threshold enhancements in QCD in color-singlet channels at heavy quark production thresholds since all the produced quarks have similar velocities.<sup>68</sup> One thus can expect resonant behavior at  $M^* = 2.55$  GeV and  $M^* = 5.08$  GeV, corresponding to the threshold values for open strangeness:  $pp \rightarrow \Lambda K^+ p$ , and open charm:  $pp \rightarrow \Lambda_c D^0 p$ , respectively. In any case, the structure at 5 GeV is highly inelastic: its branching ratio to the proton-proton channel is  $B^{pp} \simeq 1.5\%$ .

A model for this phenomenon is given in Ref. 30. In order not to over complicate the phenomenology; the simplest Breit–Wigner parameterization of the resonances was used. There has not been an attempt to optimize the parameters of the model to obtain a best fit. It is possible that what is identified a single resonance is actually a cluster of resonances.

The background component of the model is the perturbative QCD amplitude. Although complete calculations are not yet available, many features of the QCD predictions are understood, including the approximate  $s^{-4}$  scaling of the  $pp \rightarrow pp$  amplitude at fixed  $\theta_{cm}$  and the dominance of those amplitudes that conserve hadron helicity.<sup>15</sup> Furthermore, recent data comparing different exclusive two-body scattering channels from BNL<sup>69</sup> show that quark interchange amplitudes<sup>70</sup> dominate quark annihilation or gluon exchange contributions. Assuming the usual symmetries, there are five independent  $pp$  helicity amplitudes:  $\phi_1 = M(++ , ++)$ ,  $\phi_2 = M(-- , ++)$ ,  $\phi_3 = M(+-, +-)$ ,  $\phi_4 = M(-+, +-)$ ,  $\phi_5 = M(++ , +-)$ . The helicity amplitudes for quark interchange have a definite relationship:<sup>71</sup>

$$\begin{aligned} \phi_1(\text{PQCD}) &= 2\phi_3(\text{PQCD}) = -2\phi_4(\text{PQCD}) \\ &= 4\pi C F(t)F(u) \left[ \frac{t - m_d^2}{u - m_d^2} + (u \leftrightarrow t) \right] e^{i\delta} \end{aligned}$$

The hadron helicity non-conserving amplitudes,  $\phi_2(\text{PQCD})$  and  $\phi_5(\text{PQCD})$  are zero. This form is consistent with the nominal power-law dependence predicted by perturbative QCD and also gives a good representation of the angular distribution over a broad range of energies.<sup>72</sup> Here  $F(t)$  is the helicity conserving proton form factor, taken as the standard dipole form:  $F(t) = (1 - t/m_d^2)^{-2}$ , with  $m_d^2 = 0.71 \text{ GeV}^2$ . As shown in Ref. 71, the PQCD-quark-interchange structure alone predicts  $A_{NN} \simeq 1/3$ , nearly independent of energy and angle.

Because of the rapid fixed-angle  $s^{-4}$  falloff of the perturbative QCD amplitude, even a very weakly-coupled resonance can have a sizeable effect at large momentum transfer. The large empirical values for  $A_{NN}$  suggest a resonant  $pp \rightarrow pp$  amplitude with  $J = L = S = 1$  since this gives  $A_{NN} = 1$  (in absence of background) and a smooth angular distribution. Because of the Pauli principle, an  $S = 1$  di-proton resonances must have odd parity and thus odd orbital angular momentum. The the two non-zero helicity amplitudes for a  $J = L = S = 1$  resonance can be parameterized in Breit-Wigner form:

$$\phi_3(\text{resonance}) = 12\pi \frac{\sqrt{s}}{p_{\text{cm}}} d_{1,1}^1(\theta_{\text{cm}}) \frac{\frac{1}{2} \Gamma^{pp}(s)}{M^* - E_{\text{cm}} - \frac{i}{2} \Gamma} ,$$

$$\phi_4(\text{resonance}) = -12\pi \frac{\sqrt{s}}{p_{\text{cm}}} d_{-1,1}^1(\theta_{\text{cm}}) \frac{\frac{1}{2} \Gamma^{pp}(s)}{M^* - E_{\text{cm}} - \frac{i}{2} \Gamma} .$$

(The  ${}^3F_3$  resonance amplitudes have the same form with  $d_{\pm 1,1}^3$  replacing  $d_{\pm 1,1}^1$ .) As in the case of a narrow resonance like the  $Z^0$ , the partial width into nucleon pairs is proportional to the square of the time-like proton form factor:  $\Gamma^{pp}(s)/\Gamma = B^{pp}|F(s)|^2/|F(M^{*2})|^2$ , corresponding to the formation of two protons at this invariant energy. The resonant amplitudes then die away by one inverse power of  $(E_{\text{cm}} - M^*)$  relative to the dominant PQCD amplitudes. (In this sense, they are higher twist contributions relative to the leading twist perturbative QCD amplitudes.) The model is thus very simple: each  $pp$  helicity amplitude  $\phi_i$  is the coherent sum of PQCD plus resonance components:  $\phi = \phi(\text{PQCD}) + \Sigma\phi(\text{resonance})$ . Because of pinch singularities and higher-order corrections, the hard QCD amplitudes are expected to have a nontrivial phase;<sup>73</sup> the model allows for a constant phase  $\delta$  in  $\phi(\text{PQCD})$ . Because of the absence of the  $\phi_5$  helicity-flip amplitude, the model predicts zero single spin asymmetry  $A_N$ . This is consistent with the large angle data at  $p_{\text{lab}} = 11.75 \text{ GeV}/c$ .<sup>74</sup>

At low transverse momentum,  $p_T \leq 1.5 \text{ GeV}$ , the power-law fall-off of  $\phi(\text{PQCD})$  in  $s$  disagrees with the more slowly falling large-angle data, and one has little guidance

from basic theory. The main interest in this low-energy region is to illustrate the effects of resonances and threshold effects on  $A_{NN}$ . In order to keep the model tractable, one can extend the background quark interchange and the resonance amplitudes at low energies using the same forms as above but replacing the dipole form factor by a phenomenological form  $F(t) \propto e^{-1/2\beta\sqrt{|t|}}$ . A kinematic factor of  $\sqrt{s}/2p_{\text{cm}}$  is included in the background amplitude. The value  $\beta = 0.85 \text{ GeV}^{-1}$  then gives a good fit to  $d\sigma/dt$  at  $\theta_{\text{cm}} = \pi/2$  for  $p_{\text{lab}} \leq 5.5 \text{ GeV}/c$ .<sup>75</sup> The normalizations are chosen to maintain continuity of the amplitudes.

The predictions of the model and comparison with experiment are shown in Figs. 23–28. The following parameters are chosen:  $C = 2.9 \times 10^3$ ,  $\delta = -1$  for the normalization and phase of  $\phi(\text{PQCD})$ . The mass, width and  $pp$  branching ratio for the three resonances are  $M_d^* = 2.17 \text{ GeV}$ ,  $\Gamma_d = 0.04 \text{ GeV}$ ,  $B_d^{pp} = 1$ ;  $M_s^* = 2.55 \text{ GeV}$ ,  $\Gamma_s = 1.6 \text{ GeV}$ ,  $B_s^{pp} = 0.65$ ; and  $M_c^* = 5.08 \text{ GeV}$ ,  $\Gamma_c = 1.0 \text{ GeV}$ ,  $B_c^{pp} = 0.0155$ , respectively. As shown in Figs. 23 and 24, the deviations from the simple scaling predicted by the PQCD amplitudes are readily accounted for by the resonance structures. The cusp which appears in Fig. 24 marks the change in regime below  $p_{\text{lab}} = 5.5 \text{ GeV}/c$  where PQCD becomes inapplicable. It is interesting to note that in this energy region normal attenuation of quasielastic  $pp$  scattering is observed.<sup>60</sup> The angular distribution (normalized to the data at  $\theta_{\text{cm}} = \pi/2$ ) is predicted to broaden relative to the steeper perturbative QCD form, when the resonance dominates. As shown in Fig. 25 this is consistent with experiment, comparing data at  $p_{\text{lab}} = 7.1$  and  $12.1 \text{ GeV}/c$ .

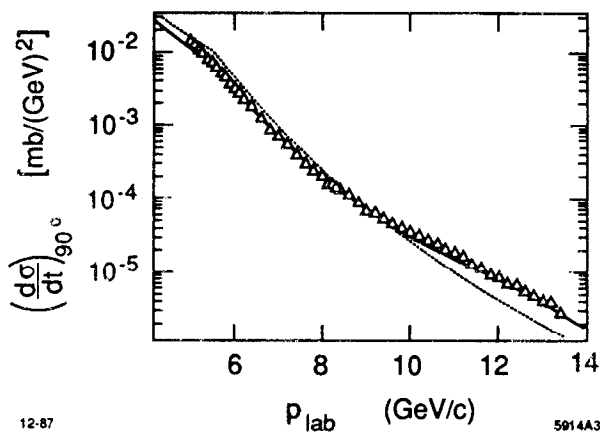


Figure 23. Prediction (solid curve) for  $d\sigma/dt(pp \rightarrow pp)$  at  $\theta_{\text{cm}} = \pi/2$  compared with the data of Akerlof et al.<sup>75</sup> The dotted line is the background PQCD prediction.

The most striking test of the model is its prediction for the spin correlation  $A_{NN}$  shown in Fig. 26. The rise of  $A_{NN}$  to  $\simeq 60\%$  at  $p_{\text{lab}} = 11.75 \text{ GeV}/c$  is correctly reproduced by the high energy  $J=1$  resonance interfering with  $\phi(\text{PQCD})$ . The narrow

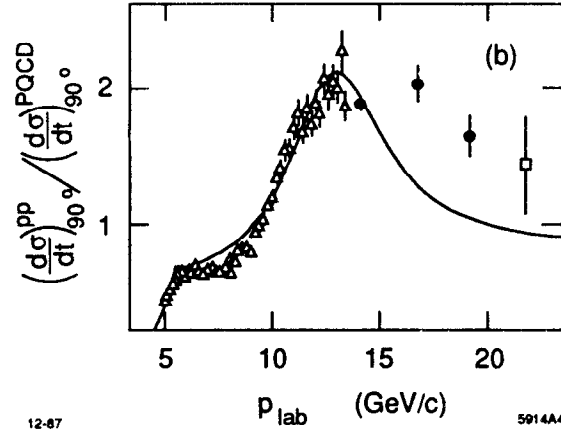


Figure 24. Ratio of  $d\sigma/dt(pp \rightarrow pp)$  at  $\theta_{cm} = \pi/2$  to the PQCD prediction. The data<sup>75</sup> are from Akerlof et al. (open triangles), Allaby et al. (solid dots) and Cocconi et al. (open square). The cusp at  $p_{lab} = 5.5$  GeV/c indicates the change of regime from PQCD.

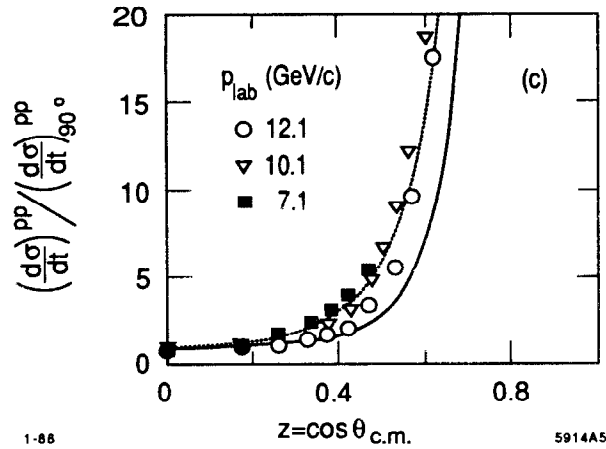


Figure 25. The  $pp \rightarrow pp$  angular distribution normalized at  $\theta_{cm} = \pi/2$ . The data are from the compilation given in Sivers et al., Ref. 69. The solid and dotted lines are predictions for  $p_{lab} = 12.1$  and  $7.1$  GeV/c, respectively, showing the broadening near resonance.

peak which appears in the data of Fig. 26 corresponds to the onset of the  $pp \rightarrow p\Delta(1232)$  channel which can be interpreted as a  $uuuuddq\bar{q}$  resonant state. Because of spin-color statistics one expects in this case a higher orbital momentum state, such as a  $pp^3 F_3$  resonance. The model is also consistent with the recent high-energy data point for  $A_{NN}$  at  $p_{lab} = 18.5$  GeV/c and  $p_T^2 = 4.7$  GeV<sup>2</sup> (see Fig. 27). The data show a dramatic decrease of  $A_{NN}$  to zero or negative values. This is explained in the model by the destructive interference effects above the resonance region. The same effect accounts for the depression of  $A_{NN}$  for  $p_{lab} \approx 6$  GeV/c shown in Fig. 26. The comparison of the angular dependence of  $A_{NN}$  with data at  $p_{lab} = 11.75$  GeV/c is shown in Fig. 28. The agreement with the data<sup>76</sup> for the longitudinal spin correlation  $A_{LL}$  at the same  $p_{lab}$  is somewhat worse.

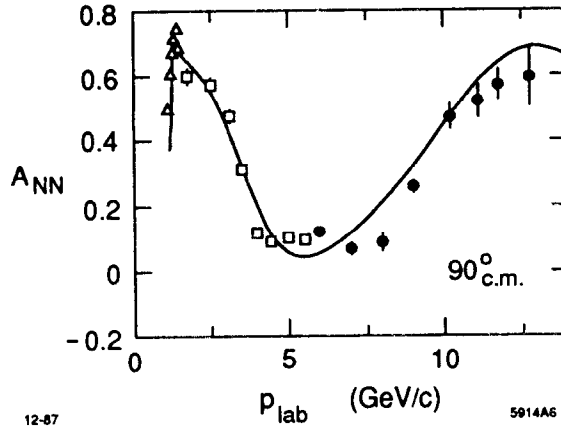


Figure 26.  $A_{NN}$  as a function of  $p_{lab}$  at  $\theta_{cm} = \pi/2$ . The data<sup>75</sup> are from Crosbie et al. (solid dots), Lin et al. (open squares) and Bhatia et al. (open triangles). The peak at  $p_{lab} = 1.26$  GeV/c corresponds to the  $p\Delta$  threshold. The data are well reproduced by the interference of the broad resonant structures at the strange ( $p_{lab} = 2.35$  GeV/c) and charm ( $p_{lab} = 12.8$  GeV/c) thresholds, interfering with a PQCD background. The value of  $A_{NN}$  from PQCD alone is  $1/3$ .

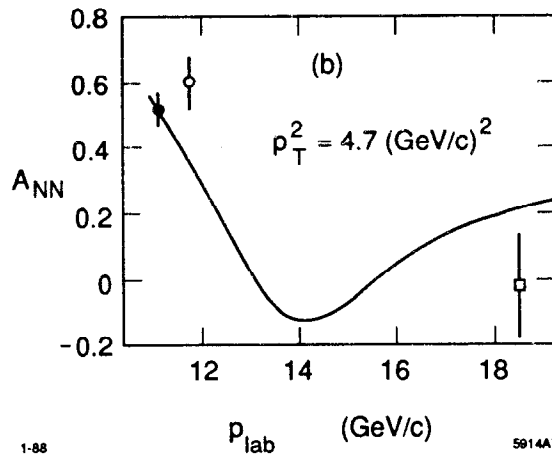


Figure 27.  $A_{NN}$  at fixed  $p_T^2 = (4.7 \text{ GeV/c})^2$ . The data point<sup>75</sup> at  $p_{lab} = 18.5$  GeV/c is from Court et al.

The simple model discussed here shows that many features can be naturally explained with only a few ingredients: a perturbative QCD background plus resonant amplitudes associated with rapid changes of the inelastic  $pp$  cross section. The model provides a good description of the  $s$  and  $t$  dependence of the differential cross section, including its “oscillatory” dependence<sup>77</sup> in  $s$  at fixed  $\theta_{cm}$ , and the broadening of the angular distribution near the resonances. Most important, it gives a consistent explanation for the striking behavior of both the spin-spin correlations and the anomalous energy dependence of the attenuation of quasielastic  $pp$  scattering in nuclei. It is predicted that color transparency should reappear at higher energies ( $p_{lab} \geq 16$  GeV/c), and also at smaller angles ( $\theta_{cm} \approx 60^\circ$ ) at  $p_{lab} = 12$  GeV/c where the perturbative QCD amplitude dominates. If the  $J=1$  resonance structures in  $A_{NN}$  are indeed associated

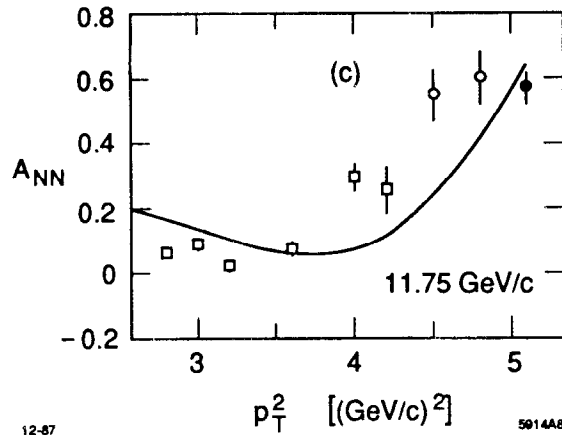


Figure 28.  $A_{NN}$  as a function of transverse momentum. The data<sup>65</sup> are from Crabb et al. (open circles) and O'Fallon et al. (open squares). Diffractive contributions should be included for  $p_T^2 \leq 3 \text{ GeV}^2$ .

with heavy quark degrees of freedom, then the model predicts inelastic  $pp$  cross sections of the order of  $1 \text{ mb}$  and  $1 \mu\text{b}$  for the production of strange and charmed hadrons near their respective thresholds.<sup>78</sup> Thus a crucial test of the heavy quark hypothesis for explaining  $A_{NN}$ , rather than hidden color or gluonic excitations, is the observation of significant charm hadron production at  $p_{lab} \geq 12 \text{ GeV}/c$ .

Recently Ralston and Pire<sup>73</sup> have proposed that the oscillations of the  $pp$  elastic cross section and the apparent breakdown of color transparency are associated with the dominance of the Landshoff pinch contributions at  $\sqrt{s} \sim 5 \text{ GeV}$ . The oscillating behavior of  $d\sigma/dt$  is due to the energy dependence of the relative phase between the pinch and hard-scattering contributions. They assume color transparency will disappear whenever the pinch contributions are dominant since such contributions could couple to wavefunctions of large transverse size. The large spin correlation in  $A_{NN}$  is not readily explained in the Ralston-Pire model. Furthermore, the recent analysis by Botts and Sterman<sup>11</sup> suggests that the pinch contributions should satisfy color transparency. In any event, more data and analysis are needed to discriminate between models.

## 21. HEAVY QUARK THRESHOLD PHENOMENA

As we have discussed in the previous section, one of the most interesting anomalies in hadron physics is the remarkable behavior of the spin-spin correlation  $A_{NN}$  for  $pp \rightarrow pp$  elastic scattering at  $\theta_{cm} = 90^\circ$ : as  $\sqrt{s}$  crosses  $5 \text{ GeV}$  the ratio of cross sections for protons scattering with their incident spins parallel and normal to the scattering plane to scattering with their spins anti-parallel changes rapidly from approximately 2:1 to 4:1.<sup>79</sup> As de Teramond and I have discussed,<sup>30</sup> this behavior can be understood

as the consequence of a strong threshold enhancement at the open-charm threshold for  $pp \rightarrow \Lambda_c Dp$  at  $\sqrt{s} = 5.08 \text{ GeV}$

Strong final-state interactions are expected at the threshold for new flavor production, since at threshold, all the quarks in the final state have nearly zero relative velocity. The dominant enhancement in the  $pp \rightarrow pp$  amplitude is expected in the partial wave  $J = L = S = 1$ , which matches the quantum numbers of the  $J = 1$   $S$ -wave eight-quark system  $qqqqq(c\bar{c})_{S=1}$  at threshold, since the  $c$  and  $\bar{c}$  have opposite parity. Even though the charm production rate is small, of order of  $1\mu b$ , it can have a large effect on the elastic  $pp \rightarrow pp$  amplitude at  $90^\circ$  since the competing perturbative QCD hard-scattering amplitude at large momentum transfer is also very small at  $\sqrt{s} = 5 \text{ GeV}$ .

In the following sections we discuss the production of hidden charm below threshold in hadronic and nuclear collisions.<sup>80</sup> Consider the reaction  $pd \rightarrow (c\bar{c})He^3$  where the charmonium state is produced nearly at rest. At the threshold for charm production, the incident nuclei will be nearly stopped (in the center-of-mass frame) and will fuse into a compound nucleus (the  $He^3$ ) because of the strong attractive nuclear force. The charmonium state will be attracted to the nucleus by the QCD gluonic van der Waals force. One thus expects strong final state interactions near threshold. In fact, we shall argue that the  $c\bar{c}$  system will bind to the  $He^3$  nucleus. It is thus likely that a new type of exotic nuclear bound state will be formed: charmonium bound to nuclear matter. Such a state should be observable at a distinct  $pd$  energy, spread by the width of the charmonium state, and it will decay to unique signatures such as  $pd \rightarrow He^3\gamma\gamma$ . The binding energy in the nucleus gives a measure of the charmonium's interactions with ordinary hadrons and nuclei; its decays will measure hadron-nucleus interactions and test color transparency starting from a unique initial state condition.

## 22. THE QCD VAN DER WAALS INTERACTION

In quantum chromodynamics, a heavy quarkonium  $Q\bar{Q}$  state such as the  $\eta_c$  interacts with a nucleon or nucleus through multiple gluon exchange. This is the QCD analogue of the attractive QED van der Waals potential. Unlike QED, the potential cannot have an inverse power-law at large distances because of the absence of zero mass gluonium states.<sup>81</sup> Since the  $(Q\bar{Q})$  and nucleons have no quarks in common, the quark interchange (or equivalently the effective meson exchange) potential should be negligible. Since there is no Pauli blocking, the effective quarkonium-nuclear interaction will not have a short-range repulsion.

The QCD van der Waals interaction is the simplest example of a nuclear force in QCD. In this paper we shall show that this potential is sufficiently strong to bind quarkonium states such as the  $\eta_c$  and  $\eta_b$  to nuclear matter. The signal for such states will be narrow peaks in energy in the production cross section.

On general grounds one expects that the effective non-relativistic potential between heavy quarkonium and nucleons can be parameterized by a Yukawa form

$$V_{(Q\bar{Q})A} = -\frac{\alpha e^{-\mu r}}{r}. \quad (1)$$

Since the gluons have spin-one, the interaction is vector-like. This implies a rich spectrum of quarkonium-nucleus bound states with spin-orbit and spin-spin hyperfine splitting.

Thus far lattice gauge theory and other non-perturbative methods have not determined the range or magnitude of the gluonic potential between hadrons. However, we can obtain some constraint on the  $J = 1$  flavor singlet interactions of hadrons by identifying the potential with the magnitude of the term linear in  $s$  in the meson-nucleon or meson-nucleus scattering amplitude. One can identify pomeron exchange with the eikonalization of the two-gluon exchange potential.<sup>82</sup>

To obtain a specific parameterization we shall make use of the phenomenological model of pomeron interactions developed by Donnachie and Landshoff.<sup>83</sup> These authors note that in order to account for the additive quark rule for total cross sections, the pomeron must have a somewhat local structure; its couplings are analogous to that of a heavy photon. The short-range character of the pomeron reflects the fact that the minimum gluonium mass which can be exchanged in the  $t$ -channel is of order several  $GeV$ . Interference terms between amplitudes involving different quarks can then be neglected.

The Donnachie-Landshoff formalism leads to an  $s$ -independent Chou-Yang parameterization of the meson-nucleon and meson-nucleus cross sections at small  $t$ :

$$\frac{d\sigma}{dt}(MA \rightarrow MA) = \frac{[2\beta F_M(t)]^2 [3A\beta F_A(t)]^2}{4\pi}. \quad (2)$$

Here  $\beta = 1.85 GeV^{-1}$  is the pomeron-quark coupling constant, and  $A$  is the nucleon number of the nucleus. To first approximation the form factors can be identified with the helicity-zero meson and nuclear electromagnetic form factors. We assume that  $\beta$  is independent of the meson type and nucleus.

Equation (2) gives a reasonable parameterization of the  $s$ -independent elastic hadron-hadron and hadron-nucleus scattering cross sections from very low to very high energies. Ignoring corrections due to eikonalization, we can identify the cross section at  $s \gg |t|$  with that due to the vector Yukawa potential

$$\frac{d\sigma}{dt}(MA \rightarrow MA) = \frac{4\pi\alpha^2}{(-t + \mu^2)^2}. \quad (3)$$

We calculate the effective coupling  $\alpha$  and the range  $\mu$  from  $(d\sigma/dt)^{1/2}$  and its slope at  $t = 0$ . Thus  $\mu^{-2} = |dF_A(t)/dt|_{t=0} = \langle R_A^2 \rangle / 6$  and  $\alpha = 3A\beta^2\mu^2/2\pi$ . For meson  $He^3$  scattering, one finds  $\alpha \simeq 0.3$  and  $\mu \simeq 250 \text{ MeV}$  reflecting the smearing of the local interaction over the nuclear volume. The radius of the charmonium system is somewhat smaller than that of the light mesons, so we expect that the pomeron coupling to the  $\eta_c$  will be reduced from the above values; the actual reduction is however model dependent since it is sensitive to the intrinsic momentum scale of the gluonic exchange potential. There are also uncertainties in the extrapolation of pomeron values to the Van der Waals couplings. For simplicity we will take  $\alpha = 0.3$  as a standard value, but note that the actual coupling in QCD may be somewhat different.

In the case of  $\eta_c$  nucleus interactions, the QCD van der Waals potential is effectively the only QCD interaction. In the threshold regime the  $\eta_c$  is non-relativistic, and an effective-potential Schrödinger equation of motion is applicable. To first approximation we will treat the  $\eta_c$  as a stable particle. The effective potential is then real since higher energy intermediate states from charmonium or nuclear excitations should not be important.

We compute the binding energy using the variational wavefunction  $\psi(r) = \sqrt{(\gamma^3/\pi)} \exp(-\gamma r)$ . The condition for binding by the Yukawa potential with this wavefunction is  $\alpha m_{red} > \mu$ . This condition is not met for charmonium-proton or charmonium-deuterium systems. However, the binding of the  $\eta_c$  to a heavy nucleus increases rapidly with  $A$ , since the potential strength is linear in  $A$ , and the kinetic energy  $\langle \vec{p}^2/2m_{red} \rangle$  decreases faster than the square of the nuclear size. If the width of the  $c\bar{c}$  is much smaller than its binding energy, the charmonium state lives sufficiently long that it can be considered stable for the purposes of calculating its binding to the nucleus.<sup>85</sup> For  $\eta_c He^3$  and  $\alpha = 0.3$  the computed binding energy is  $\sim 20 \text{ MeV}$ , and for  $\eta_c He^4$  the binding energy is over  $100 \text{ MeV}$ . The predicted binding energies are large even though the QCD van der Waals potential is relatively weak compared to the one-pion-exchange Yukawa potential; this is due to the absence of Pauli blocking or a repulsive short-range potential for heavy quarks in the nucleus. Table I gives a list of

computed binding energies for the  $c\bar{c}$  and  $b\bar{b}$  nuclear systems. A two-parameter variational wavefunction of the form  $(e^{-\alpha_1 r} - e^{-\alpha_2 r})/r$  gives essentially the same results. Our results also have implications for the binding of strange hadrons to nuclei.<sup>85</sup> However, the strong mixing of the  $\eta$  with non-strange quarks makes the interpretation of such states more complicated.

### 23. SEARCHING FOR $c\bar{c}$ NUCLEAR-BOUND STATES

It is clear that the production cross section for charm production near threshold in nuclei will be very small. We estimate rates in Section 25. However the signals for bound  $c\bar{c}$  to nuclei are very distinct. The most practical measurement could be the inclusive process  $pd \rightarrow He^3 X$ , where the missing mass  $M_X$  is constrained close to the charmonium mass. (See Fig. 29.) Since the decay of the bound  $c\bar{c}$  is isotropic in the center-of-mass, but backgrounds are peaked forward, the most favorable signal-to-noise is at backward  $He^3$  cm angles. If the  $\eta_c$  is bound to the  $He^3$ , a peak will be found at a distinct value of incident  $pd$  energy:  $\sqrt{s} = M_{\eta_c} + M_{He^3} - \epsilon$ , spread by the intrinsic width of the  $\eta_c$ . Here  $\epsilon$  is the  $\eta_c$ -nucleus binding energy predicted from the Schrödinger equation.

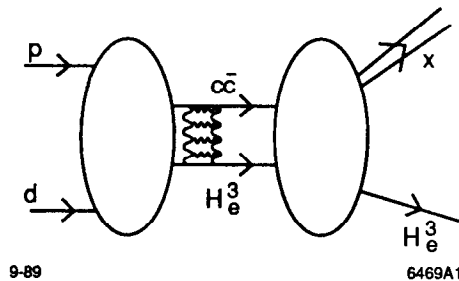


Figure 29. Formation of the  $(c\bar{c}) - He^3$  bound state in the process  $pd \rightarrow He^3 X$ .

The momentum distribution of the outgoing nucleus in the center-of-mass frame is given by  $dN/d^3p = |\psi(\vec{p})|^2$ . Thus the momentum distribution gives a direct measure of the  $c\bar{c}$ -nuclear wavefunction. The width of the momentum distribution is given by the wavefunction parameter  $\gamma$ , which is tabulated in Table I. The kinematics for several different reactions are given in Table II. From the uncertainty principle we expect that the final state momentum  $\vec{p}$  is related inversely to the uncertainty in the  $c\bar{c}$  position when it decays. By measuring the binding energy and recoil momentum distribution in  $\vec{p}$ , one determines the Schrödinger wavefunction, which then can be easily inverted to give the quarkonium-nuclear potential.

Table I

$A$	$\langle R_A^2 \rangle^{1/2}$	$\mu$	$\alpha$	$(c\bar{c})$			$(b\bar{b})$		
				$m_{red}$	$\gamma$	$\langle H \rangle$	$m_{red}$	$\gamma$	$\langle H \rangle$
1	3.9	0.529	0.458	0.715		$> 0$	0.85		$> 0$
2	10.7	0.229	0.172	1.15		$> 0$	1.563	0.18	-0.0012
3	9.5	0.26	0.327	1.45	0.40	-0.019	2.16	0.65	-0.050
	9.9	0.25	0.301		0.37	-0.015		0.60	-0.040
4	8.2	0.299	0.585	1.66	0.92	-0.143	2.66	1.52	-0.303
	8.4	0.292	0.557		0.87	-0.127		1.45	-0.271
	8.7	0.282	0.519		0.81	-0.107		1.35	-0.232
6	11.2	0.22	0.470	1.95	0.89	-0.128	3.50	1.63	-0.293
9	11.2	0.22	0.705	2.20	1.53	-0.407	4.42	3.11	-0.951
12	12.0	0.204	0.819	2.36	1.92	-0.637	5.09	4.16	-1.546
16	13.4	0.183	0.876	2.49	2.17	-0.805	5.74	5.0	-2.046

Binding energies  $\epsilon = |\langle H \rangle|$  of the  $\eta_c$  and  $\eta_b$  to various nuclei, in  $GeV$ . Here  $\gamma$  (in  $GeV$ ) is the range parameter of the variational wavefunction, and  $\mu$  (in  $GeV$ ) and  $\alpha$  are the parameters of the Yukawa potential. The data for  $\langle R_A^2 \rangle^{1/2}$  (in  $GeV^{-1}$ ) are from Ref. 86. We have assumed  $M_{\eta_b} = 9.34 GeV$ .<sup>87</sup>

Table II

Process	$M_1$	$M_2$	$M_A$	$\epsilon$	$\sqrt{s}$	$p_{cm}$	$p_1^{lab}$
$\gamma He^3 \rightarrow (He^3 \eta_c)$	0	2.808	2.808	0.020	5.77	2.20	4.52
$pd \rightarrow (He^3 \eta_c)$	0.938	1.876	2.808	0.020	5.77	2.48	7.64
$\bar{p}He^4 \rightarrow (H^3 \eta_c)$	0.938	3.728	2.808	0.020	5.77	1.48	2.30
$\gamma He^4 \rightarrow (He^4 \eta_c)$	0	3.728	3.728	0.120	6.59	2.24	3.96
$nHe^3 \rightarrow (He^4 \eta_c)$	0.938	2.808	3.728	0.120	6.59	2.60	6.09
$dd \rightarrow (He^4 \eta_c)$	1.876	1.876	3.728	0.120	6.59	2.71	9.51

Kinematics for the production of  $\eta_c$ -nucleus bound states. All quantities are given in GeV.

Energy conservation in the center of mass implies

$$E_{cm} = E_X + E_A \simeq M_X + M_A + \frac{\vec{p}^2}{2M_r'} \quad (4)$$

Here  $M_r' = (1/M_X + 1/M_A)^{-1}$  is the reduced mass of the final state system. The missing invariant mass is always less than the mass of the free  $\eta_c$  :

$$M_X = M_{\eta_c} - \epsilon - \frac{\vec{p}^2}{2M_r'} \quad (5)$$

thus the invariant mass varies with the recoil momentum. The mass deficit can be understood as the result of the fact that the  $\eta_c$  decays off its energy shell when bound to the nucleus.

More information is obtained by studying completely specified final states— exclusive channels such as  $pd \rightarrow \gamma\gamma He^3$ . Observation of the two-photon decay of the  $\eta_c$  would be a decisive signal for nuclear-bound quarkonia. The position of the bound  $c\bar{c}$  at the instant of its decay is distributed in the nuclear volume according to the eigen-wavefunction  $\psi(\vec{r})$ . Thus the hadronic decays of the  $c\bar{c}$  system allows the study of the propagation of hadrons through the nucleus starting from a wave-packet centered on the nucleus, a novel initial condition. In each case, the initial state condition for the decay is specified by the Schrödinger wavefunction with specific orbital and spin quantum numbers. Consider, then, the decay  $\eta_c \rightarrow p\bar{p}$ . As the nucleons transit the nuclear medium, their outgoing wave will be modified by nuclear final state interactions. The differential between the energy and momentum spectrum of the proton and anti-proton should be a sensitive measure of the hadronic amplitudes. More interesting is the fact that the nucleons are initially formed from the  $c\bar{c} \rightarrow gg$  decay amplitude. The size

of the production region is of the order of the charm Compton length  $\ell \sim 1/m_c$ . The proton and anti-proton thus interact in the nucleus as a small color singlet state before they are asymptotic hadron states. The distortion of the outgoing hadron momenta thus tests formation zone physics<sup>84</sup> and color transparency.<sup>29</sup>

#### 24. POSSIBILITY OF $J/\psi$ -NUCLEUS BOUND STATES

The interactions of the  $J/\psi$  and other excited states of charmonium in nuclear matter are more complicated than the  $\eta_c$  interaction because of the possibility of spin-exchange interactions which allow the  $c\bar{c}$  system to couple to the  $\eta_c$ . This effect, illustrated in Fig. 30, adds inelasticity to the effective  $c\bar{c}$  nuclear potential. In effect the bound  $J/\psi - He^3$  can decay to  $\eta_c d p$  and its width will change from tens of  $KeV$  to  $MeV$ . However if the  $J/\psi$ -nucleus binding is sufficiently strong, then the  $\eta_c$  plus nuclear continuum states may not be allowed kinematically, and the bound  $J/\psi$  could then retain its narrow width,  $\simeq 70 KeV$ . As seen in Table I this appears to be the case for the  $J/\psi - He^4$  system. An important signature for the bound vector charmonium state will be the exclusive  $\ell^+\ell^-$  plus nucleus final state.

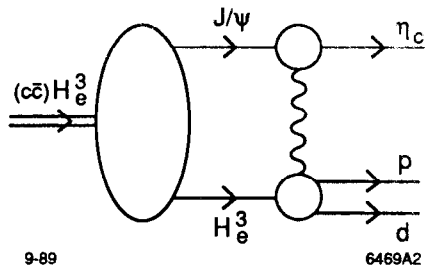


Figure 30. Decay of the  $J/\psi - He^3$  bound state into  $\eta_c pd$ .

The narrowness of the charmonium states implies that the charmonium-nucleus bound state is formed at a sharp distinct cm energy, spread by the total width  $\Gamma$  and the much smaller probability that it will decay back to the initial state. By duality the product of the cross section peak times its width should be roughly a constant. Thus the narrowness of the resonant energy leads to a large multiple of the peak cross section, favoring experiments with good incident energy resolution.

The formation cross section is thus characterized by a series of narrow spikes corresponding to the binding of the various  $c\bar{c}$  states. In principle there could be higher orbital or higher angular momentum bound state excitations of the quarkonium-nuclear system. In the case of  $J/\psi$  bound to spin-half nuclei, we predict a hyperfine separation of the  $L = 0$  ground state corresponding to states of total spin  $J = 3/2$  and  $J = 1/2$ .

This separation will measure the gluonic magnetic moment of the nucleus and that of the  $J/\psi$ . Measurements of the binding energies could in principle be done with excellent precision, thus determining fundamental hadronic measures with high accuracy.

## 25. STOPPING FACTOR

The production cross section for creating the quarkonium-nucleus bound state is suppressed by a dynamical “stopping” factor representing the probability that the nucleons and nuclei in the final state convert their kinetic energy to the heavy quark pair and are all brought to approximately zero relative velocity. For example, in the reaction  $pd \rightarrow (c\bar{c})He^3$  the initial proton and deuteron must each change momentum from  $p_{\text{cm}}$  to zero momentum in the center of mass. The probability for a nucleon or nucleus to change momentum and stay intact is given by the square of its form factor  $F_A^2(q_A^2)$ , where  $q_A^2 = [(M_A^2 + p_{\text{cm}}^2)^{1/2} - M_A]^2 - p_{\text{cm}}^2$ . We can use as a reference cross section the  $pp \rightarrow c\bar{c}pp$  cross section above threshold, which was estimated in Ref. 30 to be of order  $\sim 1\mu b$ . Then

$$\sigma(A_1 A_2 \rightarrow c\bar{c} A_{12}) = \sigma(pp \rightarrow c\bar{c}pp) \frac{F_{A_1}^2(q_{A_1}^2) F_{A_2}^2(q_{A_2}^2)}{F_N^4(q_N^2)}. \quad (6)$$

For the  $pd \rightarrow c\bar{c}He^3$  channel, we thus obtain a suppression factor relative to the  $pp$  channel of  $F_d^2(4.6 \text{ GeV}^2) F_p^2(3.2 \text{ GeV}^2) / F_N^4(2.8 \text{ GeV}^2) \sim 10^{-5}$  giving a cross section which may be as large as  $10^{-35} \text{ cm}^2$ . Considering the uniqueness of the signal and the extra enhancement at the resonance energy, this appears to be a viable experimental cross section.

## 26. CONCLUSIONS ON NUCLEAR-BOUND QUARKONIUM

In QCD, the nuclear forces are identified with the residual strong color interactions due to quark interchange and multiple-gluon exchange.<sup>88</sup> Because of the identity of the quark constituents of nucleons, a short-range repulsive component is also present (Pauli-blocking). From this perspective, the study of heavy quarkonium interactions in nuclear matter is particularly interesting: due to the distinct flavors of the quarks involved in the quarkonium-nucleon interaction there is no quark exchange to first order in elastic processes, and thus no one-meson-exchange potential from which to build a standard nuclear potential. For the same reason, there is no Pauli-blocking and consequently no short-range nuclear repulsion. The nuclear interaction in this case is purely gluonic and thus of a different nature from the usual nuclear forces.

We have discussed the signals for recognizing quarkonium bound in nuclei. The production of nuclear-bound quarkonium would be the first realization of hadronic nuclei with exotic components bound by a purely gluonic potential. Furthermore, the charmonium-nucleon interaction would provide the dynamical basis for understanding the spin-spin correlation anomaly in high energy  $p-p$  elastic scattering.<sup>30</sup> In this case, the interaction is not strong enough to produce a bound state, but it can provide a strong enough enhancement at the heavy-quark threshold characteristic of an almost-bound system.<sup>89</sup>

## 27. NUCLEAR EFFECTS IN QCD

The study of electroproduction and other hard-scattering processes in nuclear targets gives the experimentalist the extraordinary ability to modify the environment in which hadronization occurs. The essential question is how the nucleus changes or influences the mechanism in which the struck quark and the spectator system of the target nucleon form final state hadrons. The nucleus acts as a background field modifying the dynamics in interesting, though possibly subtle, ways. In particular, the observation of non-additivity of the nuclear structure functions as measured by the EMC and SLAC/American University collaborations have opened up a whole range of new physics questions:

1. What is the effect of simple potential-model nuclear binding, as predicted, for example, by the shell model? What is the associated modification of meson distributions required by momentum sum rules?
2. Is there a physical change in the nucleon size, and hence the shape of quark momentum distributions?
3. Are there nuclear modifications of the nucleonic and mesonic degrees of freedom, such as induced mesonic currents, isobars, six-quark states, or even "hidden color" degrees of freedom?
4. Does the nuclear environment modify the starting momentum scale evolution scale for gluonic radiative corrections?
5. What are the effects of diffractive contributions to deep inelastic structure functions which leave the nucleon or nuclear target intact?
6. Are there shadowing and possibly anti-shadowing coherence effects influencing the propagation of virtual photons or redistributing the nuclear constituents? Do these appear at leading twist?

7. How important are interference effects between quark currents in different nucleons?<sup>90</sup>

It seems likely that all of these non-additive effects occur at some level in the nuclear environment. In particular it will be important to examine the  $A$ -dependence of each reaction channel by channel.

The use of nuclear targets in electroproduction allows one to probe effects specific to the physics of the nucleus itself such as the short-distance structure of the deuteron, high momentum nucleon-nucleon components, and coherent effects such as shadowing, anti-shadowing, and  $x > 1$  behavior. However, perhaps the most interesting aspect for high energy physics is the use of the nucleus to modify the environment for quark hadronization and particle formation.

There are several general properties of the effect of the nuclear environment which follow from quantum mechanics and the structure of gauge theory. The first effect is the "formation zone" which reflects the principle that a quark or hadron can change state only after a finite intrinsic time in its rest system. This implies that the scattered quark in electroproduction cannot suffer an inelastic reaction with mass squared change  $\Delta M^2$  while propagating a distance  $L$  if its laboratory energy is greater than  $\Delta M^2 L$ . Thus at high energies, the quark jet does not change its state or hadronize over a distance scale proportional to its energy; inelastic or absorptive processes cannot occur inside a nucleus—at least for the very fast hadronic fragments. The energy condition is called the target length condition<sup>91,92</sup> However the outgoing quark can still scatter elastically as it traverses the nuclear volume, thus spreading its transverse momentum due to multiple scattering. Recently Bodwin and Lepage and I have explained the quantum mechanical origin of formation zone physics in terms of the destructive interference of inelastic amplitudes that occur on two different scattering centers in the nuclear target.<sup>93</sup> The discussion in that paper for the suppression of inelastic interactions of the incoming anti-quark in Drell-Yan massive lepton pair reactions can be carried over directly to the suppression of final state interactions of the struck quark in electroproduction.

As I have discussed in previous sections, one can also use a nuclear target to test another important principle of gauge theory controlling quark hadronization into exclusive channels inside nuclei: "color transparency".<sup>29</sup> Suppose that a hadronic state has a small transverse size  $b_{\perp}$ . Because of the cancellation of gluonic interactions with wavelength smaller than  $b_{\perp}$ , such a small color-singlet hadronic state will propagate through the nucleus with a small cross section for interacting in either elastically or inelastically. In particular, the recoil proton in large momentum transfer electron-proton scattering is produced initially as a small color singlet three-quark state of

transverse size  $b_{\perp} \sim 1/Q$ . If the electron-proton scattering occurs inside a nuclear target (quasi-elastic scattering) then the recoil nucleon can propagate through the nuclear volume without significant final-state interactions. This perturbative QCD prediction is in striking contrast to standard treatments of quasi-elastic scattering which predict significant final state scattering and absorption in the nucleus due to large elastic and inelastic nucleon-nucleon cross sections. The theoretical calculations of the color transparency effect must also take into account the expansion of the state as it evolves to a normal proton of normal transverse size while it traverses the nucleus.

## 28. SHADOWING AND ANTI-SHADOWING OF NUCLEAR STRUCTURE FUNCTIONS

One of the most striking nuclear effects seen in the deep inelastic structure functions is the depletion of the effective number of nucleons  $F_2^A/F_2^N$  in the region of low  $x$ . The results from the EMC collaboration<sup>94,95</sup> indicate that the effect is roughly  $Q^2$ -independent; i.e. shadowing is a leading twist in the operator product analysis. In contrast, the shadowing of the real photo-absorption cross section due to  $\rho$ -dominance<sup>96-99</sup> falls away as an inverse power of  $Q^2$ .

Shadowing is a destructive interference effect which causes a diminished flux and interactions in the interior and back face of the nucleus. The Glauber analysis<sup>100</sup> corresponds of hadron-nucleus scattering to the following: the incident hadron scatters elastically on a nucleon  $N_1$  on the front face of the nucleus. At high energies the phase of the amplitude is imaginary. The hadron then propagates through the nucleus to nucleon  $N_2$  where it interacts inelastically. The accumulated phase of the hadron propagator is also imaginary, so that this two-step amplitude is coherent and opposite in phase to the one-step amplitude where the beam hadron interacts directly on  $N_2$  without initial-state interactions. Thus the target nucleon  $N_2$  sees less incoming flux: it is shadowed by elastic interactions on the front face of the nucleus. If the hadron-nucleon cross section is large, then for large  $A$  the effective number of nucleons participating in the inelastic interactions is reduced to  $\sim A^{2/3}$ , the number of surface nucleons.

In the case of virtual photo-absorption, the photon converts to a  $q\bar{q}$  pair at a distance before the target proportional to  $\omega = x^{-1} = 2p \cdot q/Q^2$  in the laboratory frame.<sup>101</sup> In a physical gauge, such as the light-cone  $A^+ = 0$  gauge, the final-state interactions of the quark can be neglected in the Bjorken limit, and effectively only the anti-quark interacts. The nuclear structure function  $F_2^A$  producing quark  $q$  can then be written as an integral<sup>102,103</sup> over the inelastic cross section  $\sigma_{\bar{q}A}(s')$  where  $s'$  grows as  $1/x$  for fixed space-like anti-quark mass. Thus the  $A$ -dependence of the cross

section mimics the  $A$ -dependence of the  $\bar{q}$  cross section in the nucleus. Hung Jung Lu and I<sup>104</sup> have thus applied the standard Glauber multi-scattering theory, to  $\sigma_{\bar{q}A}$  assuming that formalism can be taken over to off-shell  $\bar{q}$  interactions (the shadowing mechanism is illustrated in Fig. 31). Our results show that for reasonable values of the  $\bar{q}$ -nucleon cross section, one can understand the magnitude of the shadowing effect at small  $x$ . Moreover, if one introduces an  $\alpha_R \simeq 1/2$  Reggeon contribution to the  $\bar{q}N$  amplitude, the real phase introduced by such a contribution automatically leads to “anti-shadowing” (effective number of nucleons  $F_2^A(x, Q^2)/F_2^N(x, Q^2) > A$ ) at  $x \simeq 0.15$  of the few percent magnitude seen by the SLAC and EMC experiments.<sup>94,95</sup>

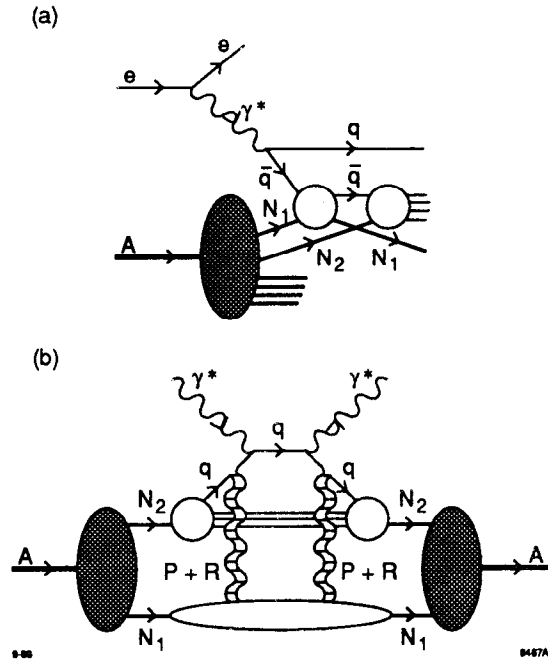


Figure 31. (a) The double-scattering amplitude that shadows the direct interaction of the anti-quark with  $N_2$ . (b) The same mechanism as in (a), drawn in the traditional “hand-bag” form. The Pomeron and Reggeon exchanges between the quark line and  $N_1$  are explicitly illustrated.

Our analysis provides the input or starting point for the  $\log Q^2$  evolution of the deep inelastic structure functions, as given for example by Mueller and Qiu.<sup>105</sup> The parameters for the effective  $\bar{q}$ -nucleon cross section required to understand shadowing phenomena provide important information on the interactions of quarks in nuclear matter.

Our analysis also has implications of the nature of particle production for virtual photo-absorption in nuclei. At high  $Q^2$  and  $x > 0.3$ , hadron production should be uniform throughout the nucleus. At low  $x$  or at low  $Q^2$ , where shadowing occurs, the inelastic reaction occurs mainly at the front surface. These features can be examined

in detail by studying non-additive multi-particle correlations in both the target and current fragmentation region.

Recently Frankfurt and Strikman have proposed a model for the shadowing and anti-shadowing of the leading-twist nuclear structure function in the small  $x$  region.<sup>106</sup> Their approach differs with ours in two ways: 1) They apply the Glauber's formula in the spirit of a vector meson dominance calculation in an aligned jet model, hence their analysis essentially aims toward the lower  $Q^2$  region ( $Q^2 \leq 4 \text{ GeV}^2$ ). 2) The anti-shadowing effect is required on the basis of the momentum sum rule rather than attributed to any particular dynamical mechanism.

We neglect the quark spin degrees of freedom in our analysis. The distribution functions of spinless partons in the nucleon and nucleus are respectively:<sup>102,103</sup>

$$x f^N(x) = \frac{2}{(2\pi)^3} \frac{C x^2}{1-x} \int ds d^2 k_{\perp} \text{Im} T_R^N(s, \mu^2) \quad (3)$$

and

$$x f^A(x) = \frac{2}{(2\pi)^3} \frac{C x^2}{1-x} \int ds d^2 k_{\perp} \text{Im} T_R^A(s, \mu^2) \quad (4)$$

where the integral is over the right-hand cut of the forward  $\bar{q}$ -nucleon ( or  $\bar{q}$ -nucleus) scattering amplitude  $\text{Im} T_R^N(s, \mu^2)$  ( $\text{Im} T_R^A(s, \mu^2)$ ), which includes the propagators of the partons. We will assume the amplitudes vanish as  $\mu^2 \rightarrow -\infty$ , where

$$\mu^2 = -x(s + k_{\perp}^2)/(1-x) + xM^2 - k_{\perp}^2 \quad (5)$$

is the invariant four-momentum squared of the interacting parton. The constant  $C$  incorporates the parton wavefunction renormalization constant,<sup>103</sup>  $M$  is the mass of nucleon, and  $k_{\perp}$  is the parton's transverse momentum.

The scaled effective number of nucleons for fixed  $x$  is defined as ( $\nu^2 = -\mu^2$ )

$$\begin{aligned} A_{eff}(x)/A &= F_2^A(x)/AF_2^N(x) = x f^A(x) / A x f^N(x) \\ &= \int ds d^2 k_{\perp} \text{Im} T_R^A(s, \nu^2) / A \int ds d^2 k_{\perp} \text{Im} T_R^N(s, \nu^2) \end{aligned} \quad (6)$$

We have implicitly considered an "average parton", that is,  $f^A(x)$  and  $f^N(x)$  are the distribution functions averaged over all the quark and anti-quark flavors. The region of integration transformed onto the  $s - \nu^2$  plane is indicated in Fig. 32, where  $\bar{\nu}^2$  represents the typical cut-off in the  $\nu^2$  dependence of the amplitude  $T_R^N$  (or  $T_R^A$ ) and  $s^*$  is the first threshold in the  $s$ -cut of the amplitude  $T_R^N$ . Observe that when  $x \rightarrow 0$

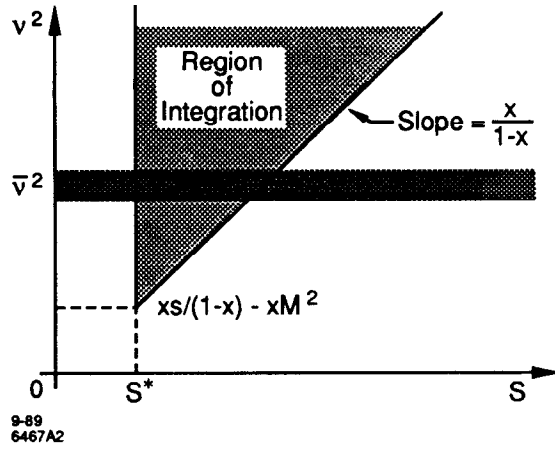


Figure 32. The region of integration of the amplitudes  $T_R^N$  and  $T_R^A$  in the  $s - \nu^2$  plane

the main contribution to the integrals comes from the region of large  $s$  and finite  $\nu^2$ , whereas the case  $x \rightarrow 1$  probes into the low- $s$  and large- $\nu^2$  sector.

In general we expect, that even for colored partons, the  $\bar{q} - A$  scattering amplitude can be obtained from the  $\bar{q} - N$  amplitude via Glauber's theory<sup>107</sup> For our model we also include  $\alpha_R = 1/2$  and  $\alpha_R = -1$  Reggeon terms in addition to the Pomeron exchange term ( the diagram corresponding to these contributions is shown on Fig. 31 (b) ):

$$T_{\bar{q}N}(s, \nu^2) = \sigma [is\beta_1(\nu^2) + (1 - i)s^{1/2}\beta_{1/2}(\nu^2) + is^{-1}\beta_{-1}(\nu^2)] \quad (7)$$

(Note this is the amputated  $\bar{q} - N$  amplitude, i.e. by attaching the external parton propagators to  $T_{\bar{q}N}$  we recover the non-amputated amplitude  $T_R^N$ .) For large  $s$ , the Pomeron term dominates and  $T_{\bar{q}N}$  becomes imaginary, thus leading to the shadowing effect for small  $x$ . However, at lower values of  $s$  the real part is important, and we shall see this leads to an anti-shadowing enhancement of the  $\bar{q} - A$  amplitude. The main role of the  $\alpha_R = -1$  "Reggeon" in the parametrization (5) is to simulate the valence quark contribution in the low  $x$  domain. Further terms can be added, but these three terms reflect the essential properties of parton distribution functions needed here to study the low  $x$  region (see Fig. 33).

We assume a Gaussian wavefunction for the nucleons in the nucleus<sup>108-110</sup>

$$|\Psi(\mathbf{r}_1, \dots, \mathbf{r}_A)|^2 = \prod_{j=1}^A (\pi R^2)^{3/2} \exp(-\mathbf{r}_j^2/R^2) \quad (8)$$

$$R^2 = \frac{2}{3}R_0^2; \quad R_0 = 1.123A^{1/3} \text{ fm}$$

and adopt the usual parametrization for the high energy particle-nucleon scattering

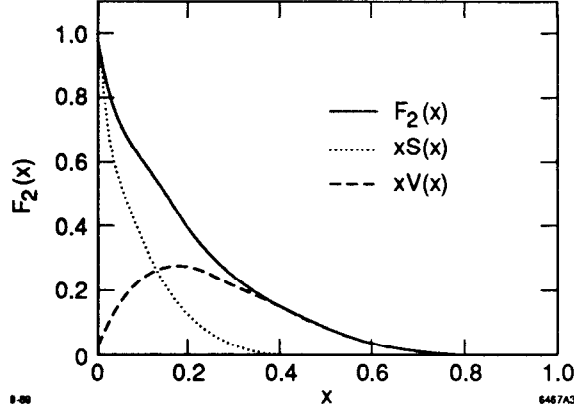


Figure 33. The computed nucleon structure function  $F_2(x)$  assuming the set of parameters in Table I and normalized such that  $F_2(0) = 1$ . In order to show separate sea distribution  $xS(x)$  and valence distribution  $xV(x)$ , we have assumed the parametrization:

$$\begin{aligned} T_{\bar{q}N}^{sea}(s, \nu^2) &= \sigma[is\beta_1(\nu^2) + 1.2(1-i)s^{1/2}\beta_{1/2}(\nu^2)] \\ T_{\bar{q}N}^{valence}(s, \nu^2) &= \sigma[-0.2(1-i)s^{1/2}\beta_{1/2}(\nu^2) + is^{-1}\beta_{-1}(\nu^2)] \end{aligned}$$

amplitude

$$T_{\bar{q}N}(s, \nu^2, \mathbf{q}) = T_{\bar{q}N}(s, \nu^2) \exp\left(-\frac{1}{2}b\mathbf{q}^2\right) \quad (9)$$

where  $\mathbf{q}^2 \simeq -q^2$  is the square of the transferred momentum in the lab frame.

Glauber's analysis<sup>108,109,110</sup> then yields:

$$T_{\bar{q}A}(s, \nu^2) = T_{\bar{q}N}(s, \nu^2) \sum_{j=1}^A \frac{1}{j} \binom{A}{j} \left\{ \frac{iT_{\bar{q}N}(s, \nu^2)}{4\pi p_{cm} s^{1/2} (R^2 + 2b)} \right\}^{j-1} \quad (10)$$

After attaching the propagators to the amplitudes in (7) and (10), the ratio

$$\frac{A_{eff}(x)}{A} = \frac{\int ds d^2k_{\perp} \text{Im} T_{\bar{q}A}(s, \nu^2) \Delta_F^2(\nu^2)}{A \int ds d^2k_{\perp} \text{Im} T_{\bar{q}N}(s, \nu^2) \Delta_F^2(\nu^2)} \quad (11)$$

can be evaluated numerically.

We will assume that  $T_{\bar{q}N}(s, \nu^2)$  vanishes as inverse power of  $\nu^2$  at large space-like quark mass. We take:

$$\beta_{\alpha}(\nu^2) = \frac{f_{\alpha}}{1 + (\nu^2/\bar{\nu}_{\alpha}^2)^{n_{\alpha}}} \quad (12)$$

where  $\alpha = 1, 1/2, -1$ . The characteristic scale for the Pomeron and the  $\alpha_R = 1/2$  Reggeon is taken to be:  $\bar{\nu}_1^2, \bar{\nu}_{1/2}^2 \simeq 0.30 \text{ GeV}^2$ . The  $\alpha_R = -1$  valence term is assumed to fall-off at the nucleon mass scale:  $\bar{\nu}_{-1}^2 \simeq 1 \text{ GeV}^2$ . In order to give a short momentum range behavior to the Pomeron and the  $\alpha_T = 1/2$  Reggeon we fix  $n_1 = 4$ , and we

assign  $n_{-1} = 2$  to provide the long tail necessary for larger  $x$  behavior of the valence quark distribution function. By definition  $f_1 = 1$ , whereas  $f_{1/2}$  and  $f_{-1}$  are adjusted consistently with the shape of the nucleon structure function at low  $x$ . The propagator of the anti-quark lines in the non-amputated amplitudes is assumed to have a monopole form on the space-like quark mass:

$$i\Delta_F(\nu^2) \propto \frac{1}{\bar{\nu}_p^2 + \nu^2} \quad (13)$$

A summary of the set of parameters used is given in Table III.

Table III

$\sigma$	30 mb	$f_{1/2}$	0.90 GeV
$\bar{\nu}_1^2, \bar{\nu}_{1/2}^2, \bar{\nu}_p^2$	0.30 (GeV) <sup>2</sup>	$f_{-1}$	0.20 (GeV) <sup>4</sup>
$\bar{\nu}_{-1}^2$	1.00 (GeV) <sup>2</sup>	$M^2$	0.88 (GeV) <sup>2</sup>
$n_1, n_{1/2}$	4	$s^*$	1.52 (GeV) <sup>2</sup>
$n_{-1}$	2	$b$	10 (GeV/c) <sup>-2</sup>

The resulting nucleon structure function computed from equation (1) is shown in Fig. 33. The parametrization used for  $T_{\bar{q}N}$  gives a reasonable description of the components of  $F_2^N$  at low  $x$ . We can now compute the nuclear structure function and the ratio  $A_{eff}(x)/A$  from equation (9). The results are given in Fig. 34 for  $A = 12, 64,$  and 238. One observes shadowing below  $x \simeq 0.1$  and an anti-shadowing peak around  $x \simeq 0.15$ . The shadowing effects are roughly logarithmic on the mass number  $A$ . The magnitude of shadowing predicted by the model is consistent with the data for  $x > 0.01$ ; below this region, one expects higher-twist and vector-meson dominance shadowing to contribute. For  $x > 0.2$  other nuclear effects must be taken into account. Most of the parameters used in the model are assigned typical hadronic values, but  $\sigma$  and  $f_{1/2}$  deserve more explanation.  $\sigma$  controls the magnitude of shadowing effect near  $x = 0$ : a larger value of  $\sigma$  implies a larger  $\bar{q}^*N$  cross section and thus more shadowing. Notice that  $\sigma$  is the effective cross section at zero  $\bar{q}$  virtuality, thus the typical value  $\langle\sigma\rangle$  entering the calculation is somewhat smaller. A variation in the parameter  $f_{1/2}$  modifies the amount of anti-shadowing by altering the real-to-imaginary-part ratio of the scattering amplitude.

Our semi-quantitative analysis shows that parton multiple-scattering process provides a mechanism for explaining the observed shadowing at low  $x$  in the EMC-SLAC

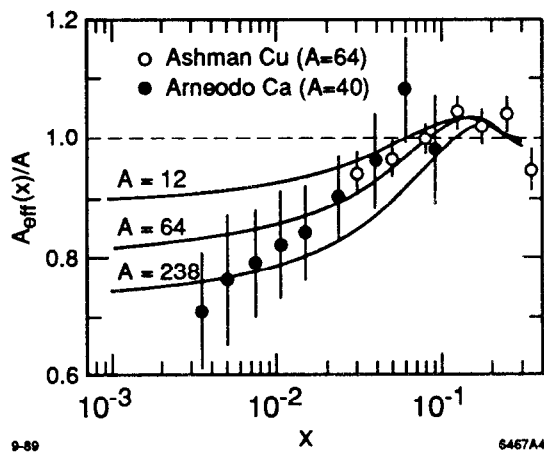


Figure 34. The predicted ratio of  $A_{eff}(x)/A$  of the multi-scattering model in the low  $x$  region for different nuclear mass number. The data points are results from the EMC experiment for  $Cu$  and  $Ca$ .

data. The existence of anti-shadowing requires the presence of regions where the real part of the  $\bar{q} - N$  amplitude dominates over the imaginary part.

Finally we note that due to the perturbative QCD factorization theorem for inclusive reactions, the same analysis can be extended to Drell-Yan processes. Thus shadowing and anti-shadowing should also be observable in the nuclear structure function  $F_2^A(x_2, Q^2)$  extracted from massive lepton pair production on nuclear target at low  $x_2$ .<sup>111</sup>

## 29. THE NUCLEUS AS A COLOR FILTER IN QCD: HADRON PRODUCTION IN NUCLEI

The data on hadron production in nuclei exhibit two striking regularities which are not readily explained by conventional hadron dynamics:

1. The nuclear number dependence  $A^{\alpha(x_F)}$  of inclusive production cross sections has a universal power  $\alpha(x_F)$ , which is independent of the produced hadron.
2. The  $A$ -dependence of  $J/\psi$  production in nuclei has two distinct components: an  $A^1$  contribution at low  $x_F$  and an anomalous  $A^{2/3}$  contribution which dominates at large  $x_F$ . Recently Paul Hoyer and I<sup>112</sup> have shown that both phenomena can be understood in QCD as a consequence of the nucleus filtering out small, color-singlet Fock state components of the incident hadron wavefunction.

In high energy hadron-nucleus collisions the nucleus may be regarded as a "filter" of the hadronic wave function.<sup>113</sup> The argument, which relies only on general features such as time dilation, goes as follows. Consider the equal-time Fock state expansion of a hadron, in terms of its quark and gluon constituents. E.g., for a meson,

$$|h\rangle = |q\bar{q}\rangle + |q\bar{q}g\rangle + |q\bar{q}q\bar{q}\rangle + \dots \quad (1)$$

The various Fock components will mix with each other during their time evolution. However, at sufficiently high hadron energies  $E_h$ , and during short times  $t$ , the mixing is negligible. Specifically, the relative phase  $\exp[-i(E - E_h)t]$  of a given term in Eq. (1) is proportional to the energy difference

$$E - E_h = \left[ \sum_i \frac{m_i^2 + \mathbf{P}_{Ti}^2}{x_i} - M_h^2 \right] / (2E_h) \quad (2)$$

which vanishes for  $E_h \rightarrow \infty$ . Hence the time evolution of the Fock expansion (1) is, at high energies, diagonal during the time  $\sim 1/R$  it takes for the hadron to cross a nucleus of radius  $R$ .

The diagonal time development means that it is possible to describe the scattering of a hadron in a nucleus in terms of the scattering of its individual Fock components. Here we shall explore the consequences for typical, soft collisions characterized by momentum transfers  $q_T \simeq \Lambda_{QCD}$ . The partons of a given Fock state will then scatter independently of each other if their transverse separation is  $r_T \geq 1/\Lambda_{QCD}$ ; i.e., if the state is of typical hadronic size. Conversely, the nuclear scattering will be coherent over the partons in Fock states having  $r_T \ll 1/\Lambda_{QCD}$  since  $e^{iq_T \cdot r_T} \simeq 1$ . For color-singlet clusters, the interference between the different parton amplitudes interacting with the nuclear gluonic field is destructive. Thus the nucleus will appear nearly transparent to small, color-singlet Fock states.<sup>29</sup>

The momenta of the produced secondary hadrons depend on how the Fock state scatters. A large Fock state will tend to produce slow hadrons, since its momentum is shared by the partons which scatter, and hence also fragment, independently of each other. A small, color-singlet Fock state can transport the entire hadron momentum through the nucleus, and then convert back to one, or several, fast hadrons. In an experiment detecting fast secondary hadrons the nucleus indeed serves, then, as a filter that selects the small Fock components in the incident hadrons.

For ordinary, light hadrons the small Fock components typically constitute some fraction of the valence quark state (i.e., of  $|q\bar{q}\rangle$ ). However, if the hadron has an intrinsic heavy quark Fock state<sup>114,115</sup> then this non-valence state can be important in processes with fast, heavy hadrons in the final state. Consider the intrinsic charm state  $|u\bar{d}c\bar{c}\rangle$  of a  $|\pi^+\rangle$ . Because of the large charm mass  $m_c$ , the energy difference will be minimized when the charm quarks have large  $x$ , i.e., when they carry most of the longitudinal momentum. Moreover, because  $m_c$  is large, the transverse momenta  $p_{Tc}$  of the charm quarks range up to  $\mathcal{O}(m_c)$ , implying that the transverse size of the  $c\bar{c}$  system is  $\mathcal{O}(1/m_c)$ . Hence, provided only that the  $c\bar{c}$  forms a color singlet, it can penetrate the nucleus with little energy loss. In effect, the nucleus is transparent to the heavy quark pair component of the intrinsic state. The light quark pair of the intrinsic state typically is of hadronic size and thus is absorbed by the nucleus.

### 31. UNIVERSAL A-DEPENDENCE OF HADROPRODUCTION

The experimental results on particle production in hadron-nucleus collisions show a remarkable regularity.<sup>116</sup> When the  $A$ -dependence is parametrized as

$$\frac{d\sigma}{dx_h}(p + A \rightarrow h + X) = A^\alpha \frac{d\sigma_N}{dx_h} \quad (3)$$

where  $d\sigma_N/dx_h$  is independent of  $A$ , it is found that the exponent  $\alpha(x_h)$  is the same for all hadrons  $h = \pi^\pm, K^\pm, p, n, \Lambda, \bar{\Lambda}$ . Thus at a given momentum fraction  $x_h$ , the ratios of the production of the various types of hadrons  $h$  are independent of the nucleus (and also of the beam energy). The exponent  $\alpha$  decreases smoothly from  $\alpha(x = 0.1) \simeq 0.7$  to  $\alpha(x = 0.9) \simeq 0.45$ .

It is perhaps even more remarkable that a parametrization of the above form gives an  $x_h$ -dependent  $\alpha$  even in the case of charm production ( $h = D, \Lambda_c, J/\psi, \dots$ ). According to the hard scattering picture of QCD,  $\alpha = 1$  for all  $x_h$  would be expected. In the Drell-Yan process of large mass muon pair production  $\alpha \simeq 1$  for all  $x_h$  is indeed observed.<sup>117</sup> However, several experiments on open charm production show<sup>118</sup> that  $\alpha(x \geq 0.2) \simeq 0.7 \dots 0.8$ . For small  $x_h$ , an indirect analysis<sup>119</sup> comparing different measurements of the total charm production cross section indicates  $\alpha(x \simeq 0) \simeq 1$ . More detailed data on the nuclear dependence of charm production is available from the hadroproduction of  $J/\psi$ . Here a decrease of  $\alpha$  from  $\alpha(x \simeq 0) \simeq 1$  to  $\alpha(x \simeq 0.8) \simeq 0.8$  has been seen by several groups.<sup>120</sup> Particularly interesting from our present point of view is the analysis of Badier, et al.<sup>120</sup> They noted that the production of  $J/\psi$  at large Feynman  $x_h$  (up to  $x_h \simeq 0.8$ ) cannot be explained only by the gluon and light quark

fusion mechanisms of perturbative QCD, due to the anomalous  $A$ -dependence. However, their  $\pi^- A \rightarrow J/\psi + X$  data was well reproduced if, in addition to hard QCD fusion (with  $\alpha = 0.97$ ), they included a “diffractive” component of  $J/\psi$  production having  $\alpha = 0.77$ . Using the measured  $A$ -dependence to extract the “diffractive” component, they found that (for a pion beam) it peaks at  $x \simeq 0.5$  and dominates the hard scattering  $A^1$  component for  $x \geq 0.6$ .

### 32. HADROPRODUCTION BY PENETRATING FOCK STATES: LIGHT HADRON PRODUCTION IN NUCLEI

The simple qualitative features of the data on light hadron production in nuclei follow in a straightforward way from the picture of a nuclear filter described above. The fast hadrons are fragments of the small, color-singlet, penetrating valence quark Fock states. Due to time dilation, the Fock state fragments only after passing through the nucleus.<sup>121</sup> Since it carries the quantum numbers of the beam hadron, it is natural that the ratios of the  $x_h$ -distributions of the various secondary hadrons  $h$  in (3) will be independent of the size of the nuclear target.

To illustrate our ideas, let us assume that a penetrating Fock state suffers an energy loss in the nucleus which is proportional to its transverse area,

$$\frac{dE}{d\ell} = -\rho r_T^2 E \quad (4)$$

where  $\rho$  is an effective nuclear density. Thus in the average nuclear distance  $\frac{4}{3}R$  the state retains a fraction  $z$  of its energy,

$$z(r_T) = E_{out}/E_{in} = \exp\left(-\frac{4}{3}R\rho r_T^2\right) \quad (5)$$

The inclusive hadron distribution (3) derived from the penetrating state is then

$$\frac{d\sigma}{dx_h} = \pi R^2 \int d^2r_T |\psi(r_T)|^2 \frac{1}{z} f_h(x_h/z) \quad (6)$$

If we parametrize the incident hadron wave function  $\psi(r_T)$  by a gaussian,

$$|\psi(r_T)|^2 = \frac{1}{\pi \langle r_T^2 \rangle} \exp(-r_T^2 / \langle r_T^2 \rangle) \quad (7)$$

and describe the inclusive fragmentation function  $f_h(x)$  of the final Fock state into

hadrons  $h$  as

$$f_h(x) = \frac{C_h}{x} (1-x)^n, \quad (8)$$

then the inclusive cross section (6) is

$$\frac{d\sigma}{dx_h} = \frac{3\pi C_h R}{4\rho \langle r_T^2 \rangle x_h} \int_{x_h}^1 \frac{dz}{z} z^{\beta/R} \left(1 - \frac{x_h}{z}\right)^n \quad (9)$$

where  $\beta = 3/(4\rho \langle r_T^2 \rangle)$ .

The  $A$ -dependence of  $d\sigma/dx_h$  now follows from  $R \propto A^{1/3}$ . For  $x_h \simeq 1$  we have  $z \simeq 1$  in the integral (9) and consequently  $d\sigma/dx_h \propto A^{1/3}$  for all values of  $n$ , i.e., independently of the shape of the fragmentation function  $f_h(x)$  in (8). For  $x_h \simeq 0$  the integral in (9) is seen to give  $d\sigma/dx_h \propto A^{2/3}$ , again for all values of  $n$ . These scaling laws follow from our general picture of the nucleus as a filter of the incident Fock states, and are thus independent of the specific model considered here. They are also in good accord with the trend of the data.<sup>116</sup>

For intermediate values of  $x_h$  the effective power  $\alpha(x_h)$  in (3) can be estimated from

$$\alpha(x_h) = \frac{1}{3} R \frac{d}{dR} \left( \frac{d\sigma}{dx_h} \right) / \frac{d\sigma}{dx_h} \quad (10)$$

The value of  $\alpha(x_h)$  depends in our model on the parameter  $\beta/R$ , and also on  $n$ . In practice the  $n$ -dependence can be relatively weak. For example, taking  $\beta/R = 10$  we find that the  $\alpha(x_h)$  calculated from (10) differs from the experimental parametrization of Barton, et al.<sup>116</sup> by less than 0.07 as  $n$  ranges from 2 to 8, for all  $x_h$  between 0.1 and 0.8. At this value of  $\beta/R$  a penetrating Fock state with  $r_T^2 = \langle r_T^2 \rangle$  loses, according to (5), 10 % of its energy in the nucleus.

At very small  $x_h$  our independent Fock state scattering picture breaks down. The hadronization begins to occur already inside the nucleus, resulting in a hadronic cascade. A simple empirical characterization<sup>122</sup> of the  $A$ -dependence of soft hadron production is  $d\sigma/dx \simeq \frac{1}{2} (1 + \bar{\nu}) \sigma \propto A^1$ , where  $\bar{\nu} \propto A^{1/3}$  is the mean number of collisions and  $\sigma \propto A^{2/3}$  is the geometric cross section.

### 33. HEAVY QUARKONIUM PRODUCTION IN NUCLEI

In heavy quark production on nuclei, the experimental evidence that the exponent  $\alpha$  in Eq. (3) is  $x_h$ -dependent requires a non-perturbative contribution to charm production. The usual QCD factorization formula always gives an  $x_h$ -independent  $\alpha$  in the scaling (energy-independent) region, regardless of the form of the nuclear structure function.<sup>123</sup> In fact, the  $A$ -dependence indicated by the data on open charm,<sup>118,119</sup> and also measured in  $J/\psi$ -production,<sup>120</sup> can be readily understood if the incident hadron has Fock states with intrinsic charm.<sup>114</sup>

According to our earlier discussion, the  $c\bar{c}$  pair in the intrinsic charm Fock state carries most of the momentum and has a small transverse extent,  $\langle r_T \rangle \sim 1/m_c$ . For such separations the nucleus is practically transparent, i.e.,  $z \simeq 1$  in (5). Thus the  $c\bar{c}$  color-singlet cluster in the incident hadron passes through the nucleus undeflected; it can then evolve into charmonium states after transiting the nucleus.<sup>124</sup> The remaining cluster of light quarks in the intrinsic charm Fock state is typically of hadronic size and will interact strongly on the front surface of the nucleus. Consequently, the  $A$ -dependence of the cross section (6) is given by the geometrical factor,  $\alpha \simeq 2/3$ . This justifies the analysis of Badier et al,<sup>120</sup> in which the perturbative and non-perturbative charm production mechanisms were separated on the basis of their different  $A$ -dependence ( $\alpha = 0.97$  and  $\alpha = 0.77$  for a pion beam, respectively). The effective  $x_h$ -dependence of  $\alpha$  seen in charm production is explained by the different characteristics of the two production mechanisms. Hard, gluon fusion production dominates at small  $x_h$ , due to the steeply falling gluon structure function. The contribution from intrinsic charm Fock states in the beam peaks at higher  $x_h$ , due to the large momentum carried by the charm quarks.

An important consequence of our picture is that all final states produced by a penetrating intrinsic  $c\bar{c}$  component will have the same  $A$ -dependence. Thus, in particular, the  $\psi(2S)$  radially excited state will behave in the same way as the  $J/\psi$ , in spite of its larger size. The nucleus cannot influence the quark hadronization which (at high energies) takes place outside the nuclear environment.

Quarkonium production due to the intrinsic heavy quark state will fall off rapidly for  $p_T$  greater than  $M_Q$ , reflecting the fast-falling transverse momentum dependence of the higher Fock state wavefunction. Thus we expect the conventional fusion contributions to dominate in the large  $p_T$  region. The data are in fact consistent with a simple  $A^1$  law for  $J/\psi$  production at large  $p_T$ . The CERN experiment of Badier et al.<sup>120</sup> finds that the ratio of nuclear cross sections is close to additive in  $A$  for all  $x_F$

when  $p_T$  is between 2 and 3 GeV. The data of the FermiLab experiment of Katsanevas et al.<sup>120</sup> shows consistency with additivity for  $p_T$  ranging from 1.2 to 3 GeV.

The probability for intrinsic heavy quark states in a light hadron wave function is expected<sup>114,125</sup> to scale with the heavy quark mass  $M_Q$  as  $1/M_Q^2$ . This implies a production cross section proportional to  $1/M_Q^4$ . The total rate of heavy quark production by the intrinsic mechanism therefore decreases with quark mass, compared to the perturbative cross section which is proportional to  $1/M_Q^2$ . At large  $x$  the intrinsic production should still dominate, however, implying a nuclear dependence in this region characterized by  $\alpha \simeq 0.7 \dots 0.8$  in Eq. (3). Experimental measurements of beauty hadroproduction in nuclei over the whole range of  $x$  will be essential for unraveling the two components of the cross section.

#### 34. COHERENCE AND HADRON PRODUCTION IN NUCLEI

The coherent scattering of quark systems has largely been neglected in earlier treatments of hadroproduction on nuclei, as for example in the additive quark model.<sup>126</sup> For light hadron production, the  $x_h$ -dependence of  $\alpha$  in Eq. (3) has often been assumed<sup>127</sup> to result from a dominantly peripheral production mode for fast hadrons. In such a picture, the nucleus is taken to be nearly opaque to hadrons, which consequently lose most of their momentum in central collisions. However, if this were the case it would also imply that  $\alpha < 1$  in the Drell–Yan process: The incoming hadron could not interact as effectively with the quarks on the back side of the nucleus. The experimental proof<sup>117</sup> that  $\alpha \simeq 1$  in large mass muon pair production requires the nucleus to be nearly transparent to the individual quarks of the beam hadron. The coherence of the hadronic wave function is nevertheless destroyed by the nuclear interactions – only the small Fock components can penetrate coherently and produce fast hadrons even in central collisions.

The Fock state picture discussed above will cease to be useful at low energies, when the Fock states no longer evolve independently over nuclear distances. According to Eq. (2), the required beam energy is higher for heavy quark states and, more generally, for states with small transverse size. At low energies hadrons will form, and may re-interact, inside the nucleus. This implies a breakdown of Feynman scaling, which could thus be used as an experimental signal for the transition to the low energy region.

Thus the qualitative characteristics of both light and heavy particle production on nuclei can be understood in terms of the nucleus acting as a filter for the incident Fock states. The picture we have presented, which is consistent with the general principles

of gauge theory, immediately accounts for the gross features of the data. By contrast, it is difficult to find simple explanations of those features in other models. For charm production, there is no way of understanding the  $x_h$ -dependence of  $\alpha$  purely within perturbative QCD.

### 35. EXCLUSIVE NUCLEAR REACTIONS — REDUCED AMPLITUDES

The nucleus is itself an interesting QCD structure. At short distances nuclear wavefunctions and nuclear interactions necessarily involve *hidden color*, degrees of freedom orthogonal to the channels described by the usual nucleon or isobar degrees of freedom. At asymptotic momentum transfer, the deuteron form factor and distribution amplitude are rigorously calculable. One can also derive new types of testable scaling laws for exclusive nuclear amplitudes in terms of the reduced amplitude formalism.

An ultimate goal of QCD phenomenology is to describe the nuclear force and the structure of nuclei in terms of quark and gluon degrees of freedom. Explicit signals of QCD in nuclei have been elusive, in part because of the fact that an effective Lagrangian containing meson and nucleon degrees of freedom must be in some sense equivalent to QCD if one is limited to low-energy probes. On the other hand, an effective local field theory of nucleon and meson fields cannot correctly describe the observed off-shell falloff of form factors, vertex amplitudes, Z-graph diagrams, etc. because hadron compositeness is not taken into account.

We have already mentioned the prediction  $F_d(Q^2) \sim 1/Q^{10}$  which comes from simple quark counting rules, as well as perturbative QCD. One cannot expect this asymptotic prediction to become accurate until very large  $Q^2$  is reached since the momentum transfer has to be shared by at least six constituents. However there is a simple way to isolate the QCD physics due to the compositeness of the nucleus, not the nucleons. The deuteron form factor is the probability amplitude for the deuteron to scatter from  $p$  to  $p + q$  but remain intact. Note that for vanishing nuclear binding energy  $\epsilon_d \rightarrow 0$ , the deuteron can be regarded as two nucleons sharing the deuteron four-momentum (see Fig. 35). The momentum  $\ell$  is limited by the binding and can thus be neglected. To first approximation the proton and neutron share the deuteron's momentum equally. Since the deuteron form factor contains the probability amplitudes for the proton and neutron to scatter from  $p/2$  to  $p/2 + q/2$ ; it is natural to define the reduced deuteron form factor

$$f_d(Q^2) \equiv \frac{F_d(Q^2)}{F_{1N}\left(\frac{Q^2}{4}\right) F_{1N}\left(\frac{Q^2}{4}\right)}.$$

The effect of nucleon compositeness is removed from the reduced form factor. QCD

then predicts the scaling

$$f_d(Q^2) \sim \frac{1}{Q^2}$$

i.e. the same scaling law as a meson form factor. Diagrammatically, the extra power of  $1/Q^2$  comes from the propagator of the struck quark line, the one propagator not contained in the nucleon form factors. Because of hadron helicity conservation, the prediction is for the leading helicity-conserving deuteron form factor ( $\lambda = \lambda' = 0$ .) As shown in Fig. 36, this scaling is consistent with experiment for  $Q = p_T \gtrsim 1 \text{ GeV}$ .<sup>129</sup>

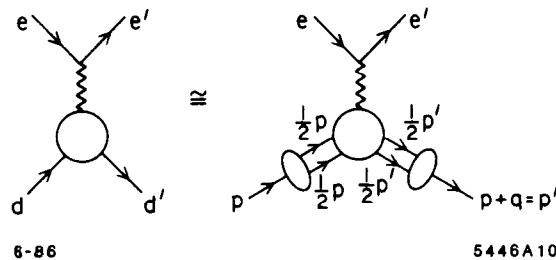


Figure 35. Application of the reduced amplitude formalism to the deuteron form factor at large momentum transfer.

The distinction between the QCD and other treatments of nuclear amplitudes is particularly clear in the reaction  $\gamma d \rightarrow np$ ; i.e. photodisintegration of the deuteron at fixed center-of-mass angle. Using dimensional counting, the leading power-law prediction from QCD is simply  $\frac{d\sigma}{d\Omega}(\gamma d \rightarrow np) \sim \frac{1}{s^{11}} F(\theta_{\text{cm}})$ . Again we note that the virtual momenta are partitioned among many quarks and gluons, so that finite mass corrections will be significant at low to medium energies. Nevertheless, one can test the basic QCD dynamics in these reactions taking into account much of the finite-mass, higher-twist corrections by using the “reduced amplitude” formalism. Thus the photodisintegration amplitude contains the probability amplitude (i.e. nucleon form factors) for the proton and neutron to each remain intact after absorbing momentum transfers  $p_p - 1/2p_d$  and  $p_n - 1/2p_d$ , respectively (see Fig. 37). After the form factors are removed, the remaining “reduced” amplitude should scale as  $F(\theta_{\text{cm}})/p_T$ . The single inverse power of transverse momentum  $p_T$  is the slowest conceivable in any theory, but it is the unique power predicted by PQCD.

The prediction that  $f(\theta_{\text{cm}})$  is energy dependent at high-momentum transfer is compared with experiment in Fig. 38. It is particularly striking to see the QCD prediction verified at incident photon lab energies as low as 1 GeV. A comparison with a standard nuclear physics model with exchange currents is also shown for comparison

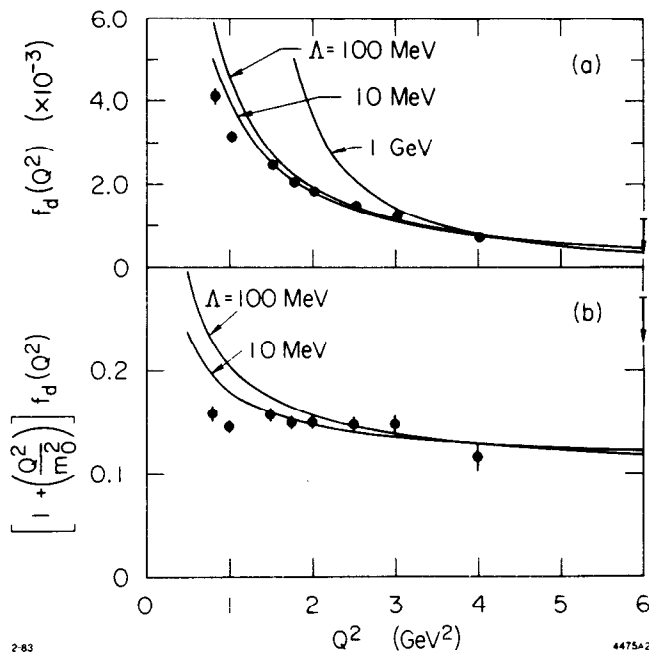


Figure 36. Scaling of the deuteron reduced form factor. The data are summarized in Ref. 128.

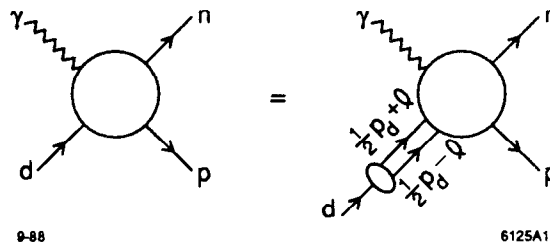


Figure 37. Construction of the reduced nuclear amplitude for two-body inelastic deuteron reactions.<sup>128</sup>

as the solid curve in Fig. 38(a). The fact that this prediction falls less fast than the data suggests that meson and nucleon compositeness are not taken into account correctly. An extension of these data to other angles and higher energy would clearly be very valuable.

An important question is whether the normalization of the  $\gamma d \rightarrow pn$  amplitude is correctly predicted by perturbative QCD. A recent analysis by Fujita<sup>130</sup> shows that mass corrections to the leading QCD prediction are not significant in the region in which the data show scaling. However Fujita also finds that in a model based on simple one-gluon plus quark-interchange mechanism, normalized to the nucleon-nucleon scattering amplitude, gives a photo-disintegration amplitude with a normalization an order of magnitude below the data. However this model only allows for diagrams in which the photon insertion acts only on the quark lines which couple to the exchanged gluon. It is expected that including other diagrams in which the photon couples to the current

of the other four quarks will increase the photo-disintegration amplitude by a large factor.

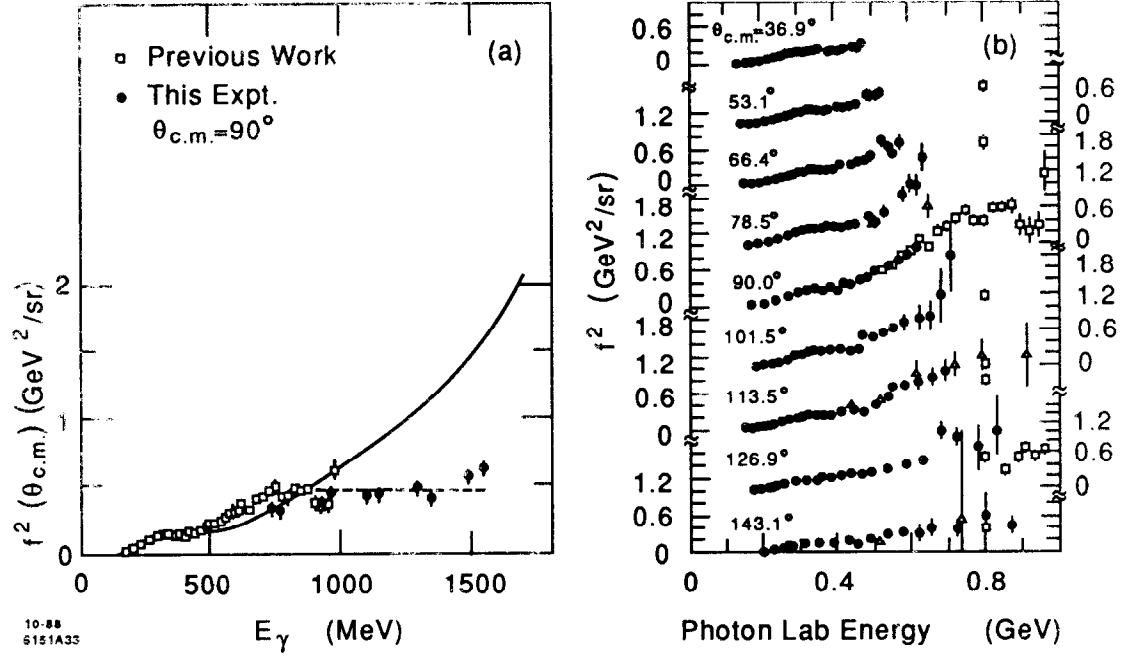


Figure 38. Comparison of deuteron photodisintegration data with the scaling prediction which requires  $f^2(\theta_{cm})$  to be at most logarithmically dependent on energy at large momentum transfer. The data in (a) are from the recent experiment of Ref. 132. The nuclear physics prediction shown in (a) is from Ref. 133. The data in (b) are from Ref. 134.

The derivation of the evolution equation for the deuteron and other multi-quark states is given in Ref. 131. In the case of the deuteron, the evolution equation couples five different color singlet states composed of the six quarks. The leading anomalous dimension for the deuteron distribution amplitude and the helicity-conserving deuteron form factor at asymptotic  $Q^2$  is given in Ref. 131.

There are a number of related tests of QCD and reduced amplitudes which require  $\bar{p}$  beams such as  $\bar{p}d \rightarrow \gamma n$  and  $\bar{p}d \rightarrow \pi^- p$  in the fixed  $\theta_{cm}$  region. These reactions are particularly interesting tests of QCD in nuclei. Dimensional counting rules predict the asymptotic behavior  $\frac{d\sigma}{dt}(\bar{p}d \rightarrow \pi^- p) \sim \frac{1}{(p_T^2)^{12}} f(\theta_{cm})$  since there are 14 initial and final quanta involved. Again one notes that the  $\bar{p}d \rightarrow \pi^- p$  amplitude contains a factor representing the probability amplitude (i.e. form factor) for the proton to remain intact after absorbing momentum transfer squared  $\hat{t} = (p - 1/2p_d)^2$  and the  $\bar{N}N$  time-like form factor at  $\hat{s} = (\bar{p} + 1/2p_d)^2$ . Thus  $\mathcal{M}_{\bar{p}d \rightarrow \pi^- p} \sim F_{1N}(\hat{t}) F_{1N}(\hat{s}) \mathcal{M}_r$ , where  $\mathcal{M}_r$  has the same QCD scaling properties as quark meson scattering. One thus predicts

$$\frac{\frac{d\sigma}{d\Omega}(\bar{p}d \rightarrow \pi^- p)}{F_{1N}^2(\hat{t}) F_{1N}^2(\hat{s})} \sim \frac{f(\Omega)}{p_T^2}$$

The reduced amplitude scaling for  $\gamma d \rightarrow pn$  at large angles and  $p_T \gtrsim 1$  GeV (see Fig. 38). One thus expects similar precocious scaling behavior to hold for  $\bar{p}d \rightarrow \pi^- p$  and other  $\bar{p}d$  exclusive reduced amplitudes. Recent analyses by Kondratyuk and Sapozhnikov<sup>135</sup> show that standard nuclear physics wavefunctions and interactions cannot explain the magnitude of the data for two-body anti-proton annihilation reactions such as  $\bar{p}d \rightarrow \pi^- p$ .

### 36. DISCRETIZED LIGHT-CONE QUANTIZATION

Only a small fraction of strong interaction and nuclear physics can be addressed by perturbative QCD analyses. The solution to the mass and wavefunction of the proton requires a solution to the QCD bound-state problem. Even with the simplicity of the  $e^+e^-$  and  $\gamma\gamma$  initial state, the full complexity of hadron dynamics is involved in understanding resonance production, exclusive channels near threshold, jet hadronization, the hadronic contribution to the photon structure function, and the total  $e^+e^-$  or  $\gamma\gamma$  annihilation cross section. A primary question is whether we can ever hope to confront QCD directly in its nonperturbative domain. Lattice gauge theory and effective Lagrangian methods such as the Skyrme model offer some hope in understanding the low-lying hadron spectrum but dynamical computations appear intractable. Considerable information<sup>21</sup> on the spectrum and the moments of hadron valence wavefunctions has been obtained using the ITEP QCD sum rule method, but the region of applicability of this method to dynamical problems appears limited.

Recently a new method for analysing QCD in the nonperturbative domain has been developed: discretized light-cone quantization (DLCQ).<sup>136</sup> The method has the potential for providing detailed information on all the hadron's Fock light-cone components. DLCQ has been used to obtain the complete spectrum of neutral states in QED<sup>3</sup> and QCD<sup>137</sup> in one space and one time for any mass and coupling constant. The QED results agree with the Schwinger solution at infinite coupling. We will review the QCD[1+1] results below. Studies of QED in 3+1 dimensions are now underway.<sup>138</sup> Thus one can envision a nonperturbative method which in principle could allow a quantitative confrontation of QCD with the data even at low energies and momentum transfer.

The basic idea of DLCQ is as follows: QCD dynamics takes a rather simple form when quantized at equal light-cone "time"  $\tau = t + z/c$ . In light-cone gauge  $A^+ = A^0 + A^z = 0$ , the QCD light-cone Hamiltonian

$$H_{\text{QCD}} = H_0 + gH_1 + g^2H_2$$

contains the usual 3-point and 4-point interactions plus induced terms from instantaneous gluon exchange and instantaneous quark exchange diagrams. The perturbative vacuum is an eigenstate of  $H_{\text{QCD}}$  and serves as the lowest state in constructing a complete basis set of color singlet Fock states of  $H_0$  in momentum space. Solving QCD is then equivalent to solving the eigenvalue problem:

$$H_{\text{QCD}}|\Psi\rangle = M^2|\Psi\rangle$$

as a matrix equation on the free Fock basis. The set of eigenvalues  $\{M^2\}$  represents the spectrum of the color-singlet states in QCD. The Fock projections of the eigenfunction corresponding to each hadron eigenvalue gives the quark and gluon Fock state wavefunctions  $\psi_n(x_i, k_{\perp i}, \lambda_i)$  required to compute structure functions, distribution amplitudes, decay amplitudes, etc. For example, as shown by Drell and Yan,<sup>139</sup> the form-factor of a hadron can be computed at any momentum transfer  $Q$  from an overlap integral of the  $\psi_n$  summed over particle number  $n$ . The  $e^+e^-$  annihilation cross section into a given  $J = 1$  hadronic channel can be computed directly from its  $\psi_{q\bar{q}}$  Fock state wavefunction.

The light-cone momentum space Fock basis becomes discrete and amenable to computer representation if one chooses (anti-)periodic boundary conditions for the quark and gluon fields along the  $z^- = z - ct$  and  $z_{\perp}$  directions. In the case of renormalizable theories, a covariant ultraviolet cutoff  $\Lambda$  is introduced which limits the maximum invariant mass of the particles in any Fock state. One thus obtains a finite matrix representation of  $H_{\text{QCD}}^{(\Lambda)}$  which has a straightforward continuum limit. The entire analysis is frame independent, and fermions present no special difficulties.

Since  $H_{LC}$ ,  $P^+$ ,  $\vec{P}_{\perp}$ , and the conserved charges all commute,  $H_{LC}$  is block diagonal. By choosing periodic (or anti-periodic) boundary conditions for the basis states along the negative light-cone  $\psi(z^- = +L) = \pm\psi(z^- = -L)$ , the Fock basis becomes restricted to finite dimensional representations. The eigenvalue problem thus reduces to the diagonalization of a finite Hermitian matrix. To see this, note that periodicity in  $z^-$  requires  $P^+ = \frac{2\pi}{L}K$ ,  $k_i^+ = \frac{2\pi}{L}n_i$ ,  $\sum_{i=1}^n n_i = K$ . The dimension of the representation corresponds to the number of partitions of the integer  $K$  as a sum of positive integers  $n$ . For a finite resolution  $K$ , the wavefunction is sampled at the discrete points

$$x_i = \frac{k_i^+}{P^+} = \frac{n_i}{K} = \left\{ \frac{1}{K}, \frac{2}{K}, \dots, \frac{K-1}{K} \right\}$$

The continuum limit is clearly  $K \rightarrow \infty$ .

One can easily show that  $P^-$  scales as  $L$ . One thus defines  $P^- \equiv \frac{L}{2\pi} H$ . The eigenstates with  $P^2 = M^2$  at fixed  $P^+$  and  $\vec{P}_\perp = 0$  thus satisfy  $H_{LC} |\Psi\rangle = KH |\Psi\rangle = M^2 |\Psi\rangle$ , independent of  $L$  (which corresponds to a Lorentz boost factor).

The basis of the DLCQ method is thus conceptually simple: one quantizes the independent fields at equal light-cone time  $\tau$  and requires them to be periodic or anti-periodic in light-cone space with period  $2L$ . The commuting operators, the light-cone momentum  $P^+ = \frac{2\pi}{L} K$  and the light cone energy  $P^- = \frac{L}{2\pi} H$  are constructed explicitly in a Fock space representation and diagonalized simultaneously. The eigenvalues give the physical spectrum: the invariant mass squared  $M^2 = P^\nu P_\nu$ . The eigenfunctions give the wavefunctions at equal  $\tau$  and allow one to compute the current matrix elements, structure functions, and distribution amplitudes required for physical processes. All of these quantities are manifestly independent of  $L$ , since  $M^2 = P^+ P^- = HK$ . Lorentz-invariance is violated by periodicity, but re-established at the end of the calculation by going to the continuum limit:  $L \rightarrow \infty$ ,  $K \rightarrow \infty$  with  $P^+$  finite. In the case of gauge theory, the use of the light-cone gauge  $A^+ = 0$  eliminates negative metric states in both Abelian and non-Abelian theories.

Since continuum as well as single hadron color singlet hadronic wavefunctions are obtained by the diagonalization of  $H_{LC}$ , one can also calculate scattering amplitudes as well as decay rates from overlap matrix elements of the interaction Hamiltonian for the weak or electromagnetic interactions. An important point is that all higher Fock amplitudes including spectator gluons are kept in the light-cone quantization approach; such contributions cannot generally be neglected in decay amplitudes involving light quarks.

The simplest application of DLCQ to local gauge theory is QED in one-space and one-time dimensions. Since  $A^+ = 0$  is a physical gauge there are no photon degrees of freedom. Explicit forms for the matrix representation of  $H_{QED}$  are given in Ref. 3.

The basic interactions which occur in  $H_{LC}(\text{QCD})$  are illustrated in Fig. 39. Recently Hornbostel<sup>137</sup> has used DLCQ to obtain the complete color-singlet spectrum of QCD in one space and one time dimension for  $N_C = 2, 3, 4$ . The hadronic spectra are obtained as a function of quark mass and QCD coupling constant (see Fig. 40).

Where they are available, the spectra agree with results obtained earlier; in particular, the lowest meson mass in SU(2) agrees within errors with lattice Hamiltonian results.<sup>140</sup> The meson mass at  $N_C = 4$  is close to the value obtained in the large  $N_C$  limit. The method also provides the first results for the baryon spectrum in a non-Abelian gauge theory. The lowest baryon mass is shown in Fig. 40 as a function of

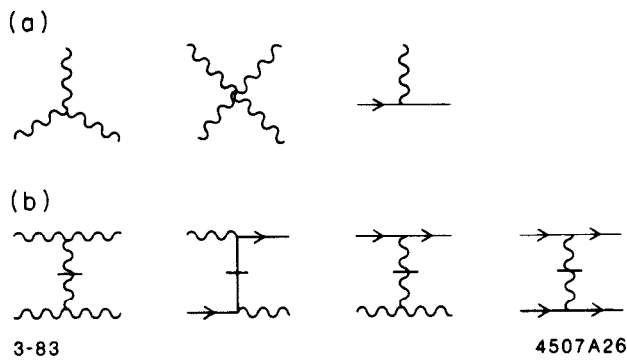


Figure 39. Diagrams which appear in the interaction Hamiltonian for QCD on the light cone. The propagators with horizontal bars represent "instantaneous" gluon and quark exchange which arise from reduction of the dependent fields in  $A^+ = 0$  gauge. (a) Basic interaction vertices in QCD. (b) "Instantaneous" contributions.

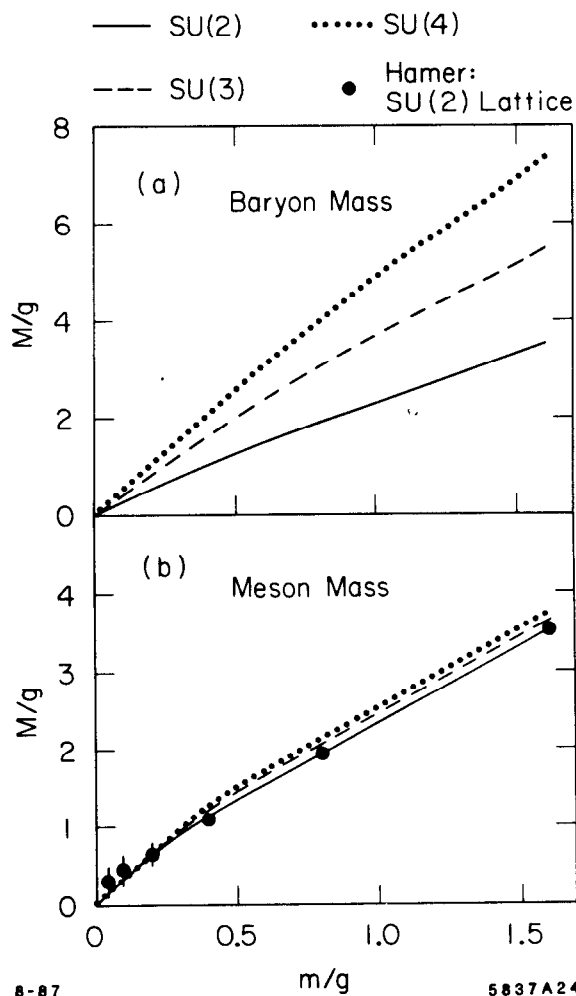


Figure 40. The lowest baryon and meson masses in QCD [1+1] computed in DLCQ for  $N_C = 2, 3, 4$  as a function of quark mass and coupling constant.<sup>137</sup>

coupling constant. The ratio of meson to baryon mass as a function of  $N_C$  also agrees at strong coupling with results obtained by Frishman and Sonnenschein.<sup>141</sup> Precise values for the mass eigenvalue can be obtained by extrapolation to large  $K$  since the

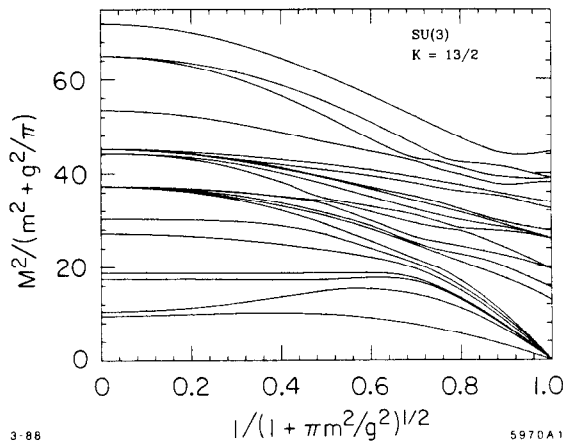


Figure 41. Representative baryon spectrum for QCD in one-space and one-time dimension.<sup>137</sup>

functional dependence in  $1/K$  is understood.

As emphasized above, when the light-cone Hamiltonian is diagonalized for a finite resolution  $K$ , one gets a complete set of eigenvalues corresponding to the total dimension of the Fock state basis. A representative example of the spectrum is shown in Fig. 41 for baryon states ( $B = 1$ ) as a function of the dimensionless variable  $\lambda = 1/(1 + \pi m^2/g^2)$ . Note that spectrum automatically includes continuum states with  $B = 1$ .

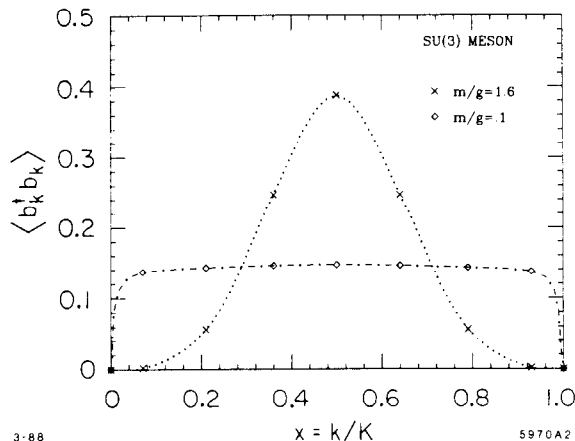


Figure 42. The meson quark momentum distribution in QCD[1+1] computed using DLCQ.<sup>137</sup>

The structure functions for the lowest meson and baryon states in SU(3) at two different coupling strengths  $m/g = 1.6$  and  $m/g = 0.1$  are shown in Figs. 42 and 43. Higher Fock states have a very small probability; representative contributions to the baryon structure functions are shown in Figs. 44 and 45. For comparison, the valence wavefunction of a higher mass state which can be identified as a composite of meson

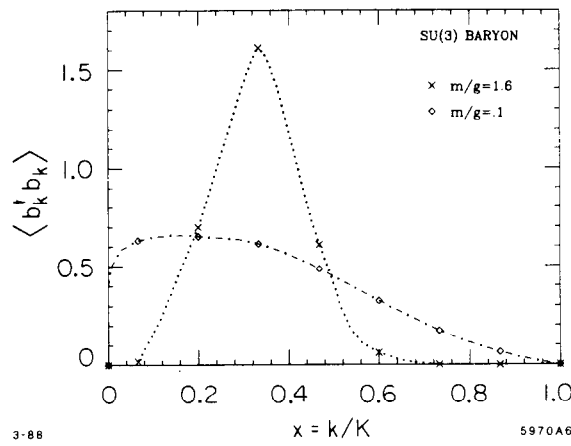


Figure 43. The baryon quark momentum distribution in QCD[1+1] computed using DLCQ.<sup>137</sup>

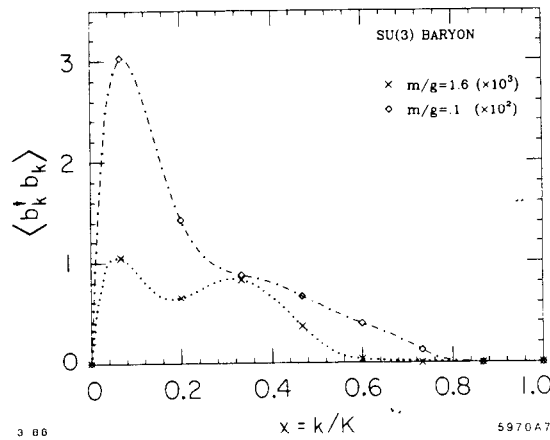


Figure 44. Contribution to the baryon quark momentum distribution from  $qqq\bar{q}$  states for QCD[1+1].<sup>137</sup>

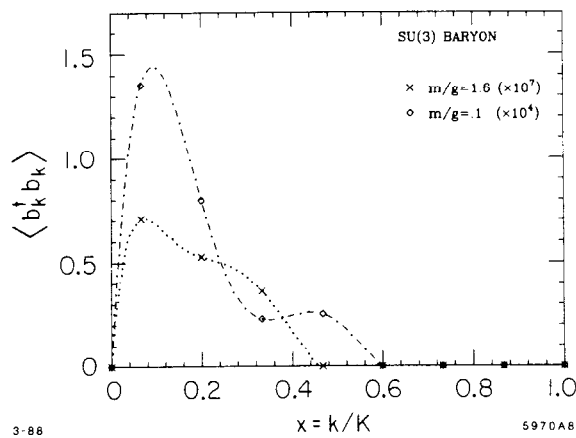


Figure 45. Contribution to the baryon quark momentum distribution from  $qqq\bar{q}q\bar{q}$  states for QCD[1+1].<sup>137</sup>

pairs (analogous to a nucleus) is shown in Fig. 46. The interactions of the quarks in the pair state produce Fermi motion beyond  $x = 0.5$ . Although these results are for

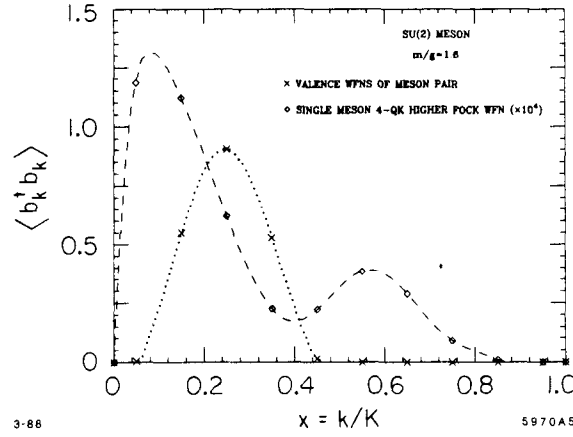


Figure 46. Comparison of the meson quark distributions in the  $qq\bar{q}\bar{q}$  Fock state with that of a continuum meson pair state. The structure in the former may be due to the fact that these four-particle wavefunctions are orthogonal.<sup>137</sup>

one time one space theory they do suggest that the sea quark distributions in physical hadrons may be highly structured.

In the case of gauge theory in 3+1 dimensions, one also takes the  $k_{\perp}^i = (2\pi/L_{\perp})n_{\perp}^i$  as discrete variables on a finite cartesian basis. The theory is covariantly regulated if one restricts states by the condition

$$\sum_i \frac{k_{\perp i}^2 + m_i^2}{x_i} \leq \Lambda^2,$$

where  $\Lambda$  is the ultraviolet cutoff. In effect, states with total light-cone kinetic energy beyond  $\Lambda^2$  are cut off. In a renormalizable theory physical quantities are independent of physics beyond the ultraviolet regulator; the only dependence on  $\Lambda$  appears in the coupling constant and mass parameters of the Hamiltonian, consistent with the renormalization group.<sup>142</sup> The resolution parameters need to be taken sufficiently large such that the theory is controlled by the continuum regulator  $\Lambda$ , rather than the discrete scales of the momentum space basis.

There are a number of important advantages of the DLCQ method which have emerged from this study of two-dimensional field theories:

1. The Fock space is denumerable and finite in particle number for any fixed resolution  $K$ . In the case of gauge theory in 3+1 dimensions, one expects that photon or gluon quanta with zero four-momentum decouple from neutral or color-singlet bound states, and thus need not be included in the Fock basis.
2. Because one is using a discrete momentum space representation, rather than a space-time lattice, there are no special difficulties with fermions: e.g. no fermion

doubling, fermion determinants, or necessity for a quenched approximation. Furthermore, the discretized theory has basically the same ultraviolet structure as the continuum theory. It should be emphasized that unlike lattice calculations, there is no constraint or relationship between the physical size of the bound state and the length scale  $L$ .

3. The DLCQ method has the remarkable feature of generating the complete spectrum of the theory; bound states and continuum states alike. These can be separated by tracing their minimum Fock state content down to small coupling constant since the continuum states have higher particle number content. In lattice gauge theory it appears intractable to obtain information on excited or scattering states or their correlations. The wavefunctions generated at equal light cone time have the immediate form required for relativistic scattering problems. In particular one can calculate the relativistic form factor from the matrix element of currents.
4. DLCQ is basically a relativistic many-body theory, including particle number creation and destruction, and is thus a basis for relativistic nuclear and atomic problems. In the nonrelativistic limit the theory is equivalent to the many-body Schrödinger theory.

Whether QCD can be solved using DLCQ -- considering its large number of degrees of freedom is unclear. The studies for Abelian and non-Abelian gauge theory carried out so far in 1+1 dimensions give grounds for optimism.

### 37. OTHER APPLICATIONS OF LIGHT-CONE QUANTIZATION

In the discretized light-cone quantization method, one can construct an explicit matrix representation of the QCD Hamiltonian on the light-cone momentum space Fock representation. The kinetic energy operator in this representation is diagonal. In principle one can diagonalize the total Hamiltonian on this representation to obtain not only the discrete and continuum eigenvalues, but also the corresponding light-cone wavefunctions required to compute intrinsic structure functions and distribution amplitudes. Since we are primarily interested in the lowest mass eigenstates of the hadron spectrum, we can use the variational method and simply minimize the expectation value of the light-cone Hamiltonian. This is currently being carried out by Tang<sup>138</sup> for the study of positronium at large  $\alpha$ . The evaluation of the Fock state sum can be made highly efficient by using vectorized code and importance sampling algorithms such as Lepage's program *VEGAS*. On the other hand if the total Hamiltonian could be diagonalized, one could immediately construct the resolvent, and thus the  $T$ -matrix for

scattering problems. The fractional experimental resolution in center-of-mass energy squared  $\delta s/s$  can be matched to the a corresponding resolution  $1/K$ .

The light-cone Fock state representation can also be used advantageously in perturbation theory. For example, one can calculate any scattering amplitude in terms of the usual Lippman-Schwinger series:

$$T = H_I + H_I \frac{1}{P^- - H_0 + i\epsilon} H_I + \dots$$

Langnau and I are currently applying this method to the higher order calculation of the electron's anomalous magnetic moment in quantum electrodynamics. The sum over intermediate Fock states is equivalent to summing all  $\tau$ -ordered diagrams and integrating over the transverse momentum and light-cone fractions  $x$ . Because of the restriction to positive  $x$ , diagrams corresponding to vacuum fluctuations or those containing backward-moving lines are eliminated. The amplitudes are regulated in the infrared and ultraviolet by cutting off the invariant mass. The ultraviolet regularization and renormalization of the perturbative contributions may be carried out by using the "alternating denominator method"<sup>143</sup> which yields an automatic construction of mass renormalization counter-terms.

The same method can also be used to compute perturbative contributions to the annihilation ratio  $R_{e^+e^-} = \sigma(e^+e^- \rightarrow \text{hadrons})/\sigma(e^+e^- \rightarrow \mu^+\mu^-)$  as well as the quark and gluon jet distribution. The results are obtained in the light-cone variables,  $x$ ,  $k_\perp$ ,  $\lambda$ , which are the natural covariant variables for this problem. Since there are no Faddeev-Popov or Gupta-Bleuler ghost fields in the light-cone gauge  $A^+ = 0$ , the calculations are explicitly unitary. It is hoped that one can in this way check the three-loop calculation of Gorishny, et al.<sup>144</sup> who found a surprisingly large value of 64.9 for the coefficient of  $(\alpha_s/\pi)^3$  of  $R_{e^+e^-}$  in the  $\overline{MS}$  scheme.

### 38. CONCLUSIONS

In these lectures I have emphasized several novel features of quantum chromodynamics, features which lead to new insights into the structure of the hadrons and their interactions. Among the highlights:

1. The structure of the proton now appears both theoretically and experimentally to be surprisingly complex, often at variance with intuition based on non-relativistic quark model. The most convenient covariant representation of the hadron in QCD is given by the light-cone Fock basis. According to QCD sum rules, the valence Fock state wavefunction of the proton turns out to be highly structured

and asymmetric between the valence  $u$  and  $d$  quarks. Polarized deep inelastic structure function measurements by the SLAC-Yale and CERN-EMC collaborations show that the gluons and strange quarks have strong spin correlations with the proton spin. There is even the possibility of a small admixture of hidden charm in the nucleon wavefunction. I have also discussed the distinctions between intrinsic (bound state) versus extrinsic (collision-induced) contributions to the proton structure functions, and a new approach to understanding the non-additive shadowing and anti-shadowing features of the leading twist nuclear structure functions.

2. The perturbative QCD analysis of exclusive amplitudes has now become a highly-developed field, based on all-orders factorization theorems, evolution equations, Sudakov-regulated pinch contributions, etc. The application to experiment has been highly successful; the recent confirmation by the TPC-  $\gamma\gamma$  experiment of the PQCD predictions for the photon- $\eta$  transition form factor is an important verification of the theory, as significant as Bjorken scaling in deep inelastic inclusive reactions. The recent observation at SLAC of reduced-amplitude scaling for large angle photo-disintegration provides a striking demonstration of the dominance of simple quark-gluon degrees of freedom in nuclear amplitudes at the few GeV scale. The observation at BNL of increasing color transparency of quasi-elastic  $pp$  scattering in nuclei has confirmed perhaps the most novel feature of perturbative QCD. The experimental results contradict the standard Glauber treatment of initial and final state interactions but support the PQCD prediction that large-angle  $pp$  scattering involves only the small color-dipole moment configurations of the proton Fock state. The observation of color transparency rules against a description of large momentum exclusive amplitudes in terms of the convolution of soft hadronic wavefunctions. It is clearly essential that color transparency be tested in other channels, particularly quasi-elastic  $e - p$  scattering.
3. It should be emphasized that experimental and theoretical studies of exclusive amplitudes are necessary for the fundamental understanding of the structure of the hadronic wavefunctions. Exclusive amplitudes provide a testing ground for hadronization in the simplest, most controlled amplitudes. These tests are essential if we are ever able to understand coherence and coalescence phenomena in the hadronization of QCD jets. The calculation of weak decay matrix elements and the extraction of quark mixing parameters of electro-weak theory also require a detailed understanding of hadronic wavefunctions.
4. I have described a new approach to the problem of solving QCD in the non-

perturbative domain–discretized light-cone quantization. The application of the method to QCD in one-space and one-time has been very encouraging. The challenge now is to apply this method to obtain the mass spectrum and light-cone Fock wave functions of the hadrons in QCD[3+1]. A very interesting feature of the DLCQ results for QCD[1+1] are the oscillations which emerge in the higher Fock state contributions to the hadron structure functions. The DLCQ method also leads naturally to a perturbative method for computing  $R_{e^+e^-}$  as well as coherent contributions to jet observables at the amplitude rather than probabilistic level.

5. One of the most important challenges to the PQCD analysis of exclusive reactions is the striking behavior observed in the spin-spin correlation  $A_{NN}$  in large-angle  $pp$  scattering at  $E_{cm} \sim 5 \text{ GeV}$ . As I have discussed in these lectures, this phenomena can be interpreted as due to a threshold enhancement or resonance due to open charm production in the intermediate state. This explanation also naturally accounts for the observed diminishing of color transparency seen in the BNL experiment at the same kinematic domain. A corollary of this explanation is the prediction of new bound states of charmonium with nucleons or nuclei, just below the production threshold for open charm.

Quantum Chromodynamics has now emerged as a science in itself, unifying hadron and nuclear physics in terms of a common set of fundamental degrees of freedom. It is clear that we have only begun the study its novel perturbative and non-perturbative features.

#### ACKNOWLEDGEMENTS

Some of the material presented here is based on collaborations with others, particularly G. de Teramond, J. F. Gunion, J. R. Hiller, K. Hornbostel, G. P. Lepage, A. H. Mueller, H. C. Pauli, I. Schmidt, D. F. Soper, A. Tang, and S. F. Tuan.

## REFERENCES

1. For general reviews of QCD see J. C. Collins and D. E. Soper, *Ann. Rev. Nucl. Part. Sci.*, **37**, 383 (1987); E. Reya, *Phys. Rept.* **69**, 195 (1981); A.H. Mueller, Lectures on perturbative QCD given at the Theoretical Advanced Study Inst., New Haven, 1985; *Quarks and Gluons in Particle and Nuclei*, Proc. of the UCSB Institute for Theoretical Physics Workshop on Nuclear Chromodynamics, eds., S.J. Brodsky and E. Moniz (World Scientific, 1985). For a detailed discussion of exclusive processes in QCD, see S. J. Brodsky and G. P. Lepage, SLAC-PUB-4947 (1989), published in *Perturbative Quantum Chromodynamics*, World Scientific, edited by A. Mueller, 1989.
2. P.A.M. Dirac, *Rev. Mod. Phys.* **21**, 392 (1949). Further references to light-cone quantization are given in Ref. 3.
3. T. Eller, H. C. Pauli and S. J. Brodsky, *Phys. Rev.* **D35**, 1493 (1987).
4. See e.g. S. J. Brodsky, J. Ellis and M. Karliner, *Phys. Lett.* **206B**, 309 (1988).
5. S. J. Brodsky and I. Schmidt, SLAC-PUB-5036 (1989).
6. V. N. Gribov and L. N. Lipatov, *Sov. J. Nucl. Phys.* **15**, 438 and 675 (1972).
7. P. Aurenche, R. Baier, M. Fontannaz, J. F. Owens and M. Werlen, *Phys. Rev.* **D39**, 3275 (1989).
8. Further discussion will appear in S. J. Brodsky and I. Schmidt, to be published. For a corresponding example in atomic physics see M. L. Goldberger and F. E. Low, *Phys. Rev.* **176**, 1778 (1968).
9. For a general review of the PQCD analysis of exclusive processes and for further reference, see S. J. Brodsky and G. P. Lepage, SLAC-PUB-4947 (1989), to be published in "Perturbative Quantum Chromodynamics", ed. A. H. Mueller, World Scientific (1989).
10. S.J. Brodsky and G.R. Farrar, *Phys. Rev. Lett.* **31**, 1153 (1973); *Phys. Rev.* **D11**, 1309 (1975). V. A. Matveev, R. M. Muradyan and A. V. Tavkheldize, *Lett. Nuovo Cimento* **7**, 719 (1973).
11. A. H. Mueller, *Phys. Rept.* **73**, 237 (1981). J. Botts, and G. Sterman, *Phys. Lett.* **B224**, 201 (1989); Stony Brook preprints ITP-SB-89-7, 44.
12. S. Dubnicka and E. Etim, Frascati preprint, LNF-89/013-PT, presented at Nucleon Structure Workshop: FENICE Experiment and Investigation of the Neutron Form-Factor, Frascati, Italy, October 1988.
13. S. J. Brodsky SLAC-PUB-4648, 8th Int. Workshop on Photon-Photon Collisions, Jerusalem, Israel, (1988.)
14. G. P. Lepage and S. J. Brodsky, *Phys. Rev.* **D22**, 2157 (1980); *Phys. Lett.* **87B**,

- 359 (1979); Phys. Rev. Lett. 43, 545, 1625(E) (1979).
15. S. J. Brodsky and G. P. Lepage, Phys. Rev. D24, 2848 (1981).
  16. V. D. Burkert, CEBAF-PR-87-006.
  17. See also G. R. Farrar, presented to the Workshop on Quantum Chromodynamics at Santa Barbara, 1988.
  18. V. L. Chernyak, A. A. Ogloblin and I. R. Zhitnitskii, Novosibirsk preprints INP 87-135,136, and references therein. See also Xiao-Duang Xiang, Wang Xin-Nian, and Huang Tao, BIHEP-TH-84, 23 and 29, 1984, and M. J. Lavelle, ICTP-84-85-12; Nucl. Phys. B260, 323 (1985).
  19. N. Isgur and C.H. Llewellyn Smith, Phys. Rev. Lett. 52, 1080 (1984). G. P. Korchemskii, A. V. Radyushkin, Sov. J. Nucl. Phys. 45, 910 (1987) and refs. therein.
  20. Z. Dziembowski, G. Farrar, H. Zhang, and L. Mankiewicz, contribution to the 12th Int. Conf. on Few Body Problems in Physics, Vancouver, 1989.
  21. V.L. Chernyak and A.R. Zhitnitskii, Phys. Rept. 112, 173 (1984). See also Xiao-Duang Xiang, Wang Xin-Nian, and Huang Tao, BIHEP-TH-84, 23 and 29 (1984).
  22. Z. Dziembowski and J. Franklin, contribution to the 12th Int. Conf. on Few Body Problems in Physics, Vancouver, 1989.
  23. S. J. Brodsky, T. Huang, G. P. Lepage, published in the proceedings of the SLAC Summer Institute 1981:87.
  24. C. Carlson and F. Gross, Phys. Rev. Lett. 53, 127 (1984); Phys. Rev. D36, 2060 (1987).
  25. O. C. Jacob and L. S. Kisslinger, Phys. Rev. Lett. 56, 225 (1986).
  26. Z. Dziembowski and L. Mankiewicz, Phys. Rev. Lett. 58 2175 (1987); Z. Dziembowski, Phys. Rev. D37, 768, 778, 2030 (1988).
  27. T. Huang, Q.-X. Shen, and P. Kroll, to be published.
  28. R. G. Arnold et al., Phys. Rev. Lett. 57, 174 (1986).
  29. A. H. Mueller, Proc. XVII Recontre de Moriond (1982); S. J. Brodsky, Proc. XIII Int. Symp. on Multiparticle Dynamics, Volendam (1982). See also G. Bertsch, A. S. Goldhaber, and J. F. Gunion, Phys. Rev. Lett. 47, 297 (1981); G. R. Farrar, H. Liu, L. L. Frankfurt, M. J. Strikmann, Phys. Rev. Lett. 61, 686 (1988); A. H. Mueller, CU-TP-415, talk given at the DPF meeting, Storrs, Conn (1988), and CU-TP-412 talk given at the Workshop on Nuclear and Particle Physics on the Light-Cone, Los Alamos, (1988).
  30. S. J. Brodsky and G. de Teramond, Phys. Rev. Lett. 60, 1924 (1988).
  31. I. Peruzzi et al., Phys. Rev. D17, 2901 (1978).

32. Unless otherwise noted, the data used here is from the compilation of the Particle Data Group, Phys. Lett. B, 204, 1988.
33. M. E. B. Franklin, Ph.D Thesis (1982), SLAC-254, UC-34d; M. E. B. Franklin et al., Phys. Rev. Lett. 51, 963 (1983); G. Trilling, in the Proceedings of the Twenty-First International Conference on High Energy Physics, Paris, July 26-31, 1982; E. Bloom, *ibid.*
34. S. J. Brodsky, G. P. Lepage and San Fu Tuan, Phys. Rev. Lett. 59, 621 (1987).
35. M. Chaichian and N. A. Tornqvist, Nucl. Phys. B323, 75 (1989).
36. Wei-Shou Hou and A. Soni, Phys. Rev. Lett. 50, 569 (1983).
37. P. G. O. Freund and Y. Nambu, Phys. Rev. Lett. 34, 1645 (1975).
38. S. J. Brodsky and C. R. Ji, Phys. Rev. Lett. 55, 2257 (1985).
39. For general discussions of  $\gamma\gamma$  annihilation in  $e^+e^- \rightarrow e^+e^-X$  reactions, see S. J. Brodsky, T. Kinoshita, and H. Terazawa, Phys. Rev. Lett. 25, 972 (1970), Phys. Rev. D4, 1532 (1971), V. E. Balakin, V. M. Budnev, and I. F. Ginzburg, JETP Lett. 11, 388 (1970), N. Arteaga-Romero, A. Jaccarini, and P. Kessler, Phys. Rev. D3, 1569 (1971), R. W. Brown and I. J. Muzinich, Phys. Rev. D4, 1496 (1971), and C. E. Carlson and W.-K. Tung, Phys. Rev. D4, 2873 (1971). Reviews and further references are given in H. Kolanoski and P. M. Zerwas, DESY 87-175 (1987), H. Kolanoski, in "Two-Photon Physics in  $e^+e^-$  Storage Rings," Springer-Verlag (1984), and Ch. Berger and W. Wagner, Phys. Rep. 136 (1987); J. H. Field, University of Paris Preprint LPNHE 84-04 (1984).
40. G. Köpp, T. F. Walsh, and P. Zerwas, Nucl. Phys. B70, 461 (1974). F. M. Renard, Proc. of the Vth International Workshop on  $\gamma\gamma$  Interactions, and Nuovo Cim. 80, 1 (1984). Backgrounds to the  $C = +, J = 1$  signal can occur from tagged  $e^+e^- \rightarrow e^+e^-X$  events which produce  $C = -$  resonances.
41. H. Aihara et al., Phys. Rev. Lett. 57, 51, 404 (1986). Mark II data for combined charged meson pair production are also in good agreement with the PQCD predictions. See J. Boyer et al., Phys. Rev. Lett. 56, 207 (1986).
42. S.J. Brodsky and G.P. Lepage, Phys. Rev. D24, 1808 (1981).
43. H. Suura, T. F. Walsh, and B. L. Young, Lett. Nuovo Cimento 4, 505 (1972) See also M. K. Chase, Nucl. Phys. B167, 125 (1980).
44. G. W. Atkinson, J. Sucher, and K. Tsokos, Phys. Lett. 137B, 407 (1984); G. R. Farrar, E. Maina, and F. Neri, Nucl. Phys. B259, 702 (1985) Err.-*ibid.* B263, 746 (1986).; E. Maina, Rutgers Ph.D. Thesis (1985); J. F. Gunion, D. Millers, and K. Sparks, Phys. Rev. D33, 689 (1986); P. H. Damgaard, Nucl. Phys. B211, 435,(1983); B. Nizic, Ph.D. Thesis, Cornell University (1985); D. Millers and J. F. Gunion, Phys. Rev D34, 2657 (1986).

45. J. Boyer et al., Ref. 41; TPC/Two Gamma Collaboration (H. Aihara et al.), Phys. Rev. Lett. 57, 404 (1986).
46. M. Benayoun and V. L. Chernyak, College de France preprint LPC 89 01 (1989).
47. B. Nizic Phys. Rev. D35, 80 (1987)
48. G. R. Farrar RU-88-47, Invited talk given at Workshop on Particle and Nuclear Physics on the Light Cone, Los Alamos, New Mexico, 1988; G. R. Farrar, H. Zhang, A. A. Globlin and I. R. Zhitnitskii, Nucl. Phys. B311, 585 (1989); G. R. Farrar, E. Maina, and F. Neri, Phys. Rev. Lett. 53, 28 and, 742 (1984).
49. A simple method for estimating hadron pair production cross sections near threshold in  $\gamma\gamma$  collisions is given by S. J. Brodsky, G. Kopp, and P. Zerwas, Phys. Rev. Lett. 58, 443 (1987).
50. C. Avilez, E. Ley Koo, M. Moreno, Phys. Rev. D19, 2214 (1979). C. Avilez, R. Montemayor, M. Moreno, Nuovo Cim. Lett. 21, 301 (1978). M. B. Voloshin, unpublished.
51. J. Schwinger, in "Particles, Sources and Fields," Addison-Wesley, New York, 1973. Vol II.
52. For a review and references, see R. M. Barnett, M. Dine, L. McLerran, Phys. Rev. D22, 594 (1980).
53. I. D. King and C. T. Sachrajda, Nucl. Phys. B279, 785 (1987).
54. G. P. Lepage, S. J. Brodsky, Tao Huang and P. B. Mackenzie, published in the *Proceedings of the Banff Summer Institute*, 1981.
55. S.J. Brodsky and B.T. Chertok, Phys. Rev. Lett. 37, 269 (1976); Phys. Rev. D114, 3003 (1976).
56. M. Gari and N. Stefanis, Phys. Lett. B175, 462 (1986), M. Gari and N. Stefanis, Phys. Lett. 187B, 401 (1987).
57. C-R Ji, A. F. Sill and R. M. Lombard-Nelsen, Phys. Rev. D36, 165 (1987).
58. S. Gottlieb and A. S. Kronfeld, CLNS-85/646, June 1985.
59. G. Martinelli and C. T. Sachrajda, Phys. Lett. 190B, 151, 196B, 184, (1987); Phys. Lett. B217, 319, (1989).
60. A. S. Carroll, et al., Phys. Rev. Lett. 61, 1698 (1988).
61. G. R. Court et al., Phys. Rev. Lett. 57, 507 (1986).
62. R. Blankenbecler and S. J. Brodsky, Phys. Rev. D10, 2973 (1974).
63. I.A. Schmidt and R. Blankenbecler, Phys. Rev. D15, 3321 (1977).
64. For other attempts to explain the spin correlation data, see C. Avilez, G. Cocho and M. Moreno, Phys. Rev. D24, 634 (1981); G. R. Farrar, Phys. Rev. Lett. 56, 1643 (1986), Err-ibid. 56, 2771 (1986); H. J. Lipkin, Nature 324, 14 (1986); S. M. Troshin and N. E. Tyurin, JETP Lett. 44, 149 (1986) [Pisma Zh. Eksp.

- Teor. Fiz. 44, 117 (1986)]; G. Preparata and J. Soffer, Phys. Lett. 180B, 281 (1986); S. V. Goloskokov, S. P. Kuleshov and O. V. Seljugin, *Proceedings of the VII International Symposium on High Energy Spin Physics*, Protvino (1986); C. Bourrely and J. Soffer, Phys. Rev. D35, 145 (1987).
65. See Ref. 61; T. S. Bhatia et al., Phys. Rev. Lett. 49, 1135 (1982); E. A. Crosbie et al., Phys. Rev. D23, 600 (1981); A. Lin et al., Phys. Lett. 74B, 273 (1978); D. G. Crabb et al., Phys. Rev. Lett. 41, 1257 (1978); J. R. O'Fallon et al., Phys. Rev. Lett. 39, 733 (1977); For a review, see A. D. Krisch, *Proceedings of the VII International Symposium on High Energy Spin Physics*, Protvino (1986) p. 272.
66. General QCD analyses of exclusive processes are given in Ref. 14, S. J. Brodsky and G. P. Lepage, SLAC-PUB-2294, presented at the Workshop on Current Topics in High Energy Physics, Cal Tech (Feb. 1979), S. J. Brodsky, in the Proc. of the La Jolla Inst. Summer Workshop on QCD, La Jolla (1978), A. V. Efremov and A. V. Radyushkin, Phys. Lett. B94, 245 (1980), V. L. Chernyak, V. G. Serbo, and A. R. Zhitnitskii, Yad. Fiz. 31, 1069 (1980), S. J. Brodsky, Y. Frishman, G. P. Lepage, and C. Sachrajda, Phys. Lett. 91B, 239 (1980), and A. Duncan and A. H. Mueller, Phys. Rev. D21, 1636 (1980).
67. There are five different combinations of six quarks which yield a color singlet  $B=2$  state. It is expected that these QCD degrees of freedom should be expressed as  $B=2$  resonances. See, e.g. C. R. Ji and S. J. Brodsky, Phys. Rev. D34, 1460 (1986); D33, 1951, 1406, 2653, (1986). For a review of multi-quark evolution, see S. J. Brodsky, C.-R. Ji, SLAC-PUB-3747, (1985).
68. For other examples of threshold enhancements in QCD, see S. J. Brodsky, J. F. Gunion and D. E. Soper, S. J. Brodsky, J. F. Gunion and D. E. Soper, Phys. Rev. D36, 2710 (1987) and also Ref. 49. Resonances are often associated with the onset of a new threshold. For a discussion, see D. Bugg, Presented at the IV LEAR Workshop, Villars-Sur-Ollon, Switzerland, September 6-13, 1987.
69. G. C. Blazey et al., Phys. Rev. Lett. 55, 1820 (1985); G. C. Blazey, Ph.D. Thesis, University of Minnesota (1987); B. R. Baller, Ph.D. Thesis, University of Minnesota (1987); D. S. Barton, et al., J. de Phys. 46, C2, Supp. 2 (1985). For a review, see D. Sivers, S. J. Brodsky and R. Blankenbecler, Phys. Reports 23C, 1 (1976).
70. J. F. Gunion, R. Blankenbecler and S. J. Brodsky, Phys. Rev. D6, 2652 (1972).
71. S. J. Brodsky, C. E. Carlson and H. J. Lipkin, Phys. Rev. D20, 2278 (1979); G. R. Farrar, S. Gottlieb, D. Sivers and G. Thomas, Phys. Rev. D20, 202 (1979).
72. With the above normalization, the unpolarized  $pp$  elastic cross section is  $d\sigma/dt =$

- $\Sigma_{i=1,2,\dots,5} |\phi_i^2| / (128\pi s p_{\text{cm}}^2)$ .
73. J. P. Ralston and B. Pire, Phys. Rev. Lett. 57, 2330 (1986); Phys. Lett. 117B, 233 (1982).
  74. At low momentum transfers one expects the presence of both helicity-conserving and helicity non-conserving pomeron amplitudes. It is possible that the data for  $A_N$  at  $p_{\text{lab}} = 11.75$  GeV/c can be understood over the full angular range in these terms. The large value of  $A_N = 24 \pm 8\%$  at  $p_{\text{lab}} = 28$  GeV/c and  $p_T^2 = 6.5$  GeV<sup>2</sup> remains an open problem. See P. R. Cameron et al., Phys. Rev. D32, 3070 (1985).
  75. K. Abe et al., Phys. Rev. D12, 1 (1975), and references therein. The high energy data for  $d\sigma/dt$  at  $\theta_{\text{cm}} = \pi/2$  are from C. W. Akerlof et al., Phys. Rev. 159, 1138 (1967); G. Cocconi et al., Phys. Rev. Lett. 11, 499 (1963); J. V. Allaby et al., Phys. Lett. 23, 389 (1966).
  76. I. P. Auer et al., Phys. Rev. Lett. 52, 808 (1984). Comparison with the low energy data for  $A_{LL}$  at  $\theta_{\text{cm}} = \pi/2$  suggests that the resonant amplitude below  $p_{\text{lab}} = 5.5$  GeV/c has more structure than the single resonance form adopted here. See I. P. Auer et al., Phys. Rev. Lett. 48, 1150 (1982).
  77. A. W. Hendry, Phys. Rev. D10, 2300 (1974); N. Jahren and J. Hiller, University of Minnesota preprint, 1987.
  78. The neutral strange inclusive  $pp$  cross section measured at  $p_{\text{lab}} = 5.5$  GeV/c is  $0.45 \pm 0.04$  mb; see G. Alexander et al., Phys. Rev. 154, 1284 (1967).
  79. G. R. Court et al., Phys. Rev. Lett. 57, 507 (1986); for a review, see A. D. Krisch, University of Michigan Report No. UM-HE-86-39, 1987 (unpublished).
  80. S. J. Brodsky, G. de Teramond, and I. Schmidt, SLAC-PUB 5102 (1989).
  81. See, for example, T. Appelquist and W. Fischler, Phys. Lett. 77B, 405 (1978).
  82. Due to the vector-like gluonic nature of the QCD van der Waals interaction, the pomeron scattering amplitude can be extrapolated to small  $s$  yielding a nuclear potential which incorporates multiple-gluon exchange. In principle, we could use such a procedure to evaluate the isospin-zero vector component of the low energy nucleon-nucleon potential. However, this extrapolation is not completely unambiguous if quark interchange is the dominant component, since multiple gluon exchange is difficult to distinguish from effective  $\omega$  exchange. Nevertheless, in principle, the QCD van der Waals interaction provides an attractive vector-like isospin-zero potential which should be added to the usual meson-exchange potential, and this may have implications for low energy nuclear physics studies, such as nucleon-nucleon scattering and binding.
  83. A. Donnachie and P. V. Landshoff, Nucl. Phys. B244, 322 (1984). P. V. Landshoff and O. Nachtmann, Zeit. Phys. C35, 405 (1987).

84. It should be noted that the absorptive cross section deduced from the  $A$ -dependence of  $J/\psi$  photoproduction in nuclei underestimates the true cross section since the  $J/\psi$  is typically formed outside the nucleus; see S. J. Brodsky and A. H. Mueller, Phys. Lett. 206B, 685 (1988).
85. For discussions of the possibility of bound states of strange particles with nuclei, see R. E. Chrien et al., Phys. Rev. Lett. 60, 2595 (1988), and refs. therein; and J. L. Rosen, Northwestern University preprint, submitted to the BNL Workshop on Glueballs, Hybrids, and Exotic Hadrons (1988).
86. R. Hofstadter, Ann. Rev. of Nuclear Science 7, 231 (1957). The  $He^3$  and  $He^4$  data are from J. S. McCarthy et al., Phys. Rev. C15, 1396 (1977).
87. D. B. Lichtenberg and J. G. Wills, Nuovo Cimento 47A, 483 (1978).
88. See, for example, S. A. Williams et al., Phys. Rev. Lett. 49, 771 (1982).
89. The signal for the production of almost-bound nucleon (or nuclear) charmonium systems near threshold such as in  $\gamma p \rightarrow (c\bar{c})p$  is the isotropic production of the recoil nucleon (or nucleus) at large invariant mass  $M_X \simeq M_{\eta_c}, M_{J/\psi}$ .
90. P. Hoodbhoy and R.L. Jaffe, Phys. Rev. D35, 113 (1987); R.L. Jaffe, CTP #1315 (1985).
91. S.J. Brodsky, G.T. Bodwin and G.P. Lepage, in the Proc. of the Volendam Multipart. Dyn. Conf., 1982, p. 841; Proc. of the Banff Summer Inst., 1981, p. 513. This effect is related to the formation zone principle of L. Landau and I. Pomeranchuk, Dok. Akademii Nauk SSSR 92, 535,735 (1953).
92. G.T. Bodwin, Phys. Rev. D31, 2616 (1985); G.T. Bodwin, S.J. Brodsky and G.P. Lepage, ANL-HEP-CP-85-32-mc (1985), presented at 20th Rencontre de Moriond, Les Arcs, France, March 10-17, 1985.
93. G. T. Bodwin, S. J. Brodsky, and G. P. Lepage, Phys. Rev. D39, 3287 (1989).
94. J. Ashman et al., Phys. Lett. 202B, 603 (1988) and CERN-EP/88-06 (1988)  
M. Arneodo et al., Phys. Lett. 211B, 493 (1988)
95. R. G. Arnold et al., Phys. Rev. Lett. 52, 727 (1984) and SLAC-PUB-3257 (1983)
96. J. S. Bell, Phys. Rev. Lett. 13, 57 (1964)
97. L. Stodolsky, Phys. Rev. Lett. 18, 135 (1967)
98. S. J. Brodsky and J. Pumplin, Phys. Rev. 182, 1794 (1969)
99. J. J. Sakurai and D. Schildknecht, Phys. Lett. 40B, 121 (1972); Phys. Lett. 41B, 489 (1972); Phys. Lett. 42B, 216 (1972)
100. R. J. Glauber, in *Lectures in Theoretical Physics*, edited by W. E. Brittin et al. (Interscience, New York, 1959), vol. I
101. T. H. Bauer, R. D. Spital, D. R. Yennie and F. M. Pipkin, Rev. Mod. Phys. 50, 261 (1978)

102. P. V. Landshoff, J. C. Polkinghorne and R. D. Short, Nucl. Phys. B28, 225 (1971)
103. S. J. Brodsky, F. E. Close and J. F. Gunion, Phys. Rev. D 5, 1384 (1972)
104. S. J. Brodsky and H. J. Lu, SLAC-PUB-5098 (1989).
105. A. H. Mueller and J. Qiu, Nucl. Phys. B268, 427 (1986)  
J. Qiu, Nucl. Phys. B291, 746 (1987)
106. L. L. Frankfurt and M. I. Strikman, Nucl. Phys. B316, 340 (1988) and  
Phys. Rep. 160, 235 (1988)
107. Rigorously we should also include the effect due to shadowing of the gluon structure function of the nucleus. A more detailed analysis may be able to distinguish quark and gluon shadowing effects.
108. V. Franco, Phys. Rev. Lett. 24, 1452 (1970) and Phys. Rev. C 6, 748 (1972)
109. A. Y. Abul-Magd, Nucl. Phys. B8, 638 (1968)
110. R. A. Rudin, Phys. Lett. 30B, 357 (1969)
111. E. L. Berger, Nucl. Phys. B267, 231 (1986)
112. S. J. Brodsky and P. Hoyer, SLAC-PUB-4978 (1989).
113. G. Bertsch, S. J. Brodsky, A. S. Goldhaber, and J. F. Gunion, Phys. Rev. Lett. 47, 297 (1981). In this paper the "color filter" argument was used to predict the production in nuclei of diffractive high mass multi-jet final states with momentum distributions controlled by the structure of the valence Fock state of the incident hadrons.
114. S. J. Brodsky, P. Hoyer, C. Peterson, and N. Sakai, Phys. Lett. 93B, 451 (1980);  
S. J. Brodsky, C. Peterson, and N. Sakai, Phys. Rev. D23, 2745 (1981).
115. Detailed predictions for the contribution of intrinsic charm to the nucleon charmed quark structure functions and comparisons with existing lepto-production data are given by E. Hoffmann and R. Moore Z. Phys. C20, 71 (1983).
116. T. Eichten, et al., Nucl. Phys. B44, 333 (1978); P. Skubic, et al., Phys. Rev. D18, 3115 (1978); D. S. Barton, et al., Phys. Rev. D27, 2580 (1983); W. Busza, Proc. XIII Int. Symp. on Multiparticle Dynamics, Volendam (1982);  
L. G. Pondrom, Phys. Rep. 122, 57 (1985).
117. K. J. Anderson, et al., Phys. Rev. Lett. 42, 944 (1979); A. S. Ito, et al.,  
Phys. Rev. D23, 604 (1981); J. Badier, et al., Phys. Lett. 104B, 335 (1981);  
P. Bordalo, et al., Phys. Lett. 193B, 368 (1987).
118. S. P. K. Tavernier, Rep. Prog. Phys. 50, 1439 (1987); U. Gasparini, Proc. XXIV  
Int. Conf. on High Energy Physics, (R. Kotthaus and J. H. Kühn, Eds., Springer  
1989), p. 971.
119. M. MacDermott and S. Reucroft, Phys. Lett. 184B, 108 (1987).

120. Yu. M. Antipov, et al., Phys. Lett. 76B, 235 (1978); M. J. Corden, et al., Phys. Lett. 110B, 415 (1982); J. Badier, et al., Z. Phys. C20, 101 (1983); S. Katsanevas, et al., Phys. Rev. Lett. 60, 2121 (1988).
121. The condition for no inelastic rescattering of a high energy particle in a nucleus of length  $L_A$  is  $E_h > \mu^2 L_A$ . Here  $\mu^2$  is the change in the square of the invariant mass occurring in the rescattering. For a recent discussion of formation zone conditions in gauge theory see G. T. Bodwin, S. J. Brodsky, and G. P. Lepage, Phys. Rev. D39, 3287 (1989).
122. W. Busza et al., Acta Phys. Polon. B8, 333 (1977), and Proc. of the 7th Int. Colloquium on Multiparticle Reactions, Tutzing, Germany, 1976 (publ. by Max Planck Inst., Munich 1976).
123. P. Hoyer, B. P. Mahapatra, K. Sridhar, and U. Sukhatme, Working Group Report, Workshop on High Energy Physics Phenomenology, T. I. F. R., Bombay (1989). (To be published in the Proceedings.)
124. Alternatively, the individual charmed quarks can fragment into final state charmed hadrons either by hadronization or by coalescing with co-moving light quark spectators from the beam. See S. J. Brodsky and A. H. Mueller, Phys. Lett. B206, 685 (1988). Mueller and I have also used this coalescence mechanism to explain the suppression of  $J/\psi$  production in heavy ion collisions at high transverse energy  $E_T$
125. S. J. Brodsky, H. E. Haber, and J. F. Gunion, in *Anti-pp Options for the Supercollider*, Division of Particles and Fields Workshop, Chicago, IL, 1984. edited by J. E. Pilcher and A. R. White (SSC-ANL Report No. 84/01/13, Argonne, IL, 1984), p. 100. S. J. Brodsky, J. C. Collins, S. D. Ellis, J. F. Gunion, and A. H. Mueller, published in Snowmass Summer Study 1984, p. 227.
126. A. Białas and W. Czyż, Nucl. Phys. B194, 21 (1982).
127. H. E. Miettinen and P. M. Stevenson, Phys. Lett. B199, 591 (1987)
128. See Ref. 55 and S. J. Brodsky and J. R. Hiller, Phys. Rev. C28, 475 (1983).
129. The data are compiled in Brodsky and Hiller, Ref. 128.
130. T. Fujita, MPI-Heidelberg preprint, 1989.
131. S. J. Brodsky, C.-R. Ji, G. P. Lepage, Phys. Rev. Lett. 51, 83 (1983).
132. J. Napolitano et al., ANL preprint PHY-5265-ME-88 (1988).
133. T. S.-H. Lee, ANL preprint (1988).
134. H. Myers et al., Phys. Rev. 121, 630 (1961); R. Ching and C. Schaerf, Phys. Rev. 141, 1320 (1966); P. Dougan et al., Z. Phys. A 276, 55 (1976).
135. L. A. Kondratyuk and M. G. Sapozhnikov, Phys. Lett. B220, 333 (1989).
136. H. C. Pauli and S. J. Brodsky, Phys. Rev. D32, 1993, 2001 (1985) and Ref. 3.

137. K. Hornbostel, SLAC-0333, Dec 1988; K. Hornbostel, S. J. Brodsky, and H. C. Pauli, SLAC-PUB-4678, Talk presented to Workshop on Relativistic Many Body Physics, Columbus, Ohio, June, 1988.
138. S. J. Brodsky, H. C. Pauli, and A. Tang, in preparation.
139. S. D. Drell and T. M. Yan, Phys. Rev. Lett. 24, 181 (1970).
140. C. J. Burden and C. J. Hamer, Phys. Rev. D37, 479 (1988), and references therein.
141. Y. Frishman and J. Sonnenschein, Nucl. Phys. B294, 801 (1987), and Nucl. Phys. B301, 346 (1988).
142. For a discussion of renormalization in light-cone perturbation theory, see Ref. 143 and also Ref. 14.
143. S. J. Brodsky, R. Suaya, and R. Roskies, Phys. Rev. D8, 4574 (1973).
144. S. G. Gorishny, A. L. Kataev, and S. A. Larin, Phys. Lett. B212, 238 (1988).